ΕΘΝΙΚΟ ΜΕΤΣΟΒΙΟ
ΠΟΛΥΤΕΧΝΕΙΟ

ΣΧΟΛΗ ΕΦΑΡΜΟΣΜΕΝΩΝ
ΜΑΘΗΜΑΤΙΚΩΝ
ΚΑΙ ΦΥΣΙΚΩΝ ΕΠΙΣΤΗΜΩΝ

ΣΧΟΛΗ ΜΗΧΑΝΟΛΟΓΩΝ
ΜΗΧΑΝΙΚΩΝ

ΕΚΕΦΕ «ΔΗΜΟΚΡΙΤΟΣ»

ΙΝΣΤΙΤΟΥΤΟ ΝΑΝΟΕΠΙΣΤΗΜΗΣ
ΚΑΙ ΝΑΝΟΤΕΧΝΟΛΟΓΙΑΣ

ΙΝΣΤΙΤΟΥΤΟ ΠΥΡΗΝΙΚΗΣ ΚΑΙ
ΣΩΜΑΤΙΔΙΑΚΗΣ ΦΥΣΙΚΗΣ

Διατμηματικό Πρόγραμμα Μεταπτυχιακών Σπουδών

«Φυσική και Τεχνολογικές Εφαρμογές»

Search for the exotic decay of the Higgs boson to four bottom-quarks H → 4b in the associated production of the Higgs with a W boson at the LHC

ΜΕΤΑΠΤΥΧΙΑΚΗ ΔΙΠΛΩΜΑΤΙΚΗ ΕΡΓΑΣΙΑ

του Σάββα Πετρίδη

Επιβλέπουσα: Γεωργία Καραποστόλη

Αθήνα, Σεπτέμβριος, 2024

National Technical
University of Athens

NATIONAL TECHNICAL UNIVERSITY OF ATHENS

Search for the exotic decay of the Higgs boson to four bottom-quarks $H \to 4b$ in the associated production of the Higgs with a W boson at the LHC

by

Savvas Petridis

A thesis submitted in partial fulfillment for the
Master's degree

in the
Faculty of Sciences
School of Applied Mathematical and Physical Sciences

Supervising Professor: Dr. Georgia Karapostoli

September 20, 2024

Declaration of Authorship

I, Savvas Petridis, declare that this thesis titled, Search for the exotic decay of the Higgs boson to four bottom-quarks $H \rightarrow 4b$ in the associated production of the Higgs with a W boson at the LHC and the work presented in it are my own. I confirm that:

- This work was done wholly or mainly while in candidature for a research degree at this University.
- Where any part of this thesis has previously been submitted for a degree or any other qualification at this University or any other institution, this has been clearly stated.
- Where I have consulted the published work of others, this is always clearly attributed.
- Where I have quoted from the work of others, the source is always given. With the exception of such quotations, this thesis is entirely my own work.
- I have acknowledged all main sources of help.
- Where the thesis is based on work done by myself jointly with others, I have made clear exactly what was done by others and what I have contributed myself.

Signed: Savvas Petridis

Date: September 20, 2024

"'Course it's a good idea!" – God

Monty Python

NATIONAL TECHNICAL UNIVERSITY OF ATHENS

Abstract

Faculty of Sciences
School of Applied Mathematical and Physical Sciences

Master's Degree

by Savvas Petridis

This master's thesis explores the field of particle physics, specifically focusing on the analysis of the Higgs boson decay into four b-quarks. The research was conducted using data from the Compact Muon Solenoid (CMS) detector at the Large Hadron Collider (LHC) at CERN. The Standard Model of particle physics, which successfully describes three of the four fundamental forces (excluding gravity) and the elementary particles that interact through these forces, serves as the theoretical foundation for this study.

Αναλυτική Περίληψη Διπλωματικής Εργασίας

Εισαγωγή

Το αντικείμενο της σωματιδιακής φυσικής, είναι η μελέτη των στοιχειωδών σωματιδίων καθώς και των αλληλεπιδράσεων μεταξύ τους. Τα στοιχειώδη σωματίδια αποτελούν τους δομικούς λίθους της ύλης. Οπότε και η μελέτη τους, προσπαθεί να απαντήσει σε πανάρχαια και υπαρξιακά ερωτήματα, όπως από τι αποτελείται το σύμπαν, ποια είναι τα βασικά δομικά στοιχεία της ύλης και πως αυτά τα στοιχεία αλληλεπιδρούν μεταξύ τους.

Οι ανακαλύψεις που έχουν έρθει από τον τομέα των στοιχειωδών σωματιδίων [1], έχουν διαμορφώσει πλήρως την αντίληψή μας γύρω από τον μικρόκοσμο και τον μακρόκοσμο. Οι σύγχρονες θεωρίες, όπως το Καθιερωμένο Πρότυπο, παρέχουν ένα πλαίσιο για την κατανόηση των στοιχειωδών σωματιδίων και των αλληλεπιδράσεών τους.

Στοιχειώδη Σωματίδια

Τα στοιχειώδη σωματίδια κατηγοριοποιούνται σε λεπτόνια και κουαρκ.[2] Τα λεπτόνια είναι τα ηλεκτρόνια τα μυόνια και τα ταφ, μαζί με τα νετρίνα τους. Από την άλλη πλευρά τα κουάρκ είναι τα θεμελιώδη δομικά στοιχεία των πρωτονίων και των νετρονίων. Τα κουάρκ ενώνονται μέσω της ισχυρούς αλληλεπίδρασης. Τα κουάρκ συναντώνται σε ομάδες των τριών όταν σχηματίζουν αδρόνια και σε ζεύγη όταν σχηματίζουν μεσόνια. Τα μεσόνια είναι λιγότερο σταθερά και εμφανίζονται σε συγκρούσεις σωματιδίων υψηλής ενέργειας.

Τα λεπτόνια, από την άλλη πλευρά, είναι σωματίδια που δεν υφίστανται ισχυρές αλληλεπιδράσεις. Υπάρχουν έξι τύποι λεπτονίων, γνωστά ως ηλεκτρόνια, μιόνια, ταυ λεπτόνια και τα αντίστοιχα νετρίνα τους. Τα ηλεκτρόνια είναι γνωστά για την παρουσία τους σε ατομικά κελύφη, ενώ τα νετρίνα είναι σωματίδια με εξαιρετικά μικρή μάζα και σπάνια αλληλεπιδρούν με την ύλη, οπότε και η ανίχνευσή τους αποτελεί ένα πολύ δύσκολο εγχείρημα.

[1] ο οποίος συναντάται και ως τομέας υψιλών ενεργειών

[2] τα οποία σε συνδιασμό με τα γκλουόνια σχηματίζουν τα αδρόνια

Οι Τέσσερις Θεμελειώδεις Δυνάμεις

Οι αλληλεπιδράσεις μεταξύ των στοιχειωδών σωματιδίων περιγράφονται από τέσσερις βασικές δυνάμεις:

Ηλεκτρομαγνητική Δύναμη: Διαμεσολαβείται από τα φωτόνια και είναι υπεύθυνη για τις ηλεκτρικές και μαγνητικές δυνάμεις. Επηρεάζει τα φορτισμένα σωματίδια και είναι υπεύθυνη για τις δυνάμεις που κρατούν τα ηλεκτρόνια γύρω από τον πυρήνα των ατόμων.
Ισχυρή Πυρηνική Δύναμη: Διαμεσολαβείται από τα γκλουόνια και κρατά τα κουάρκ ενωμένα για να σχηματίσουν αδρόνια. Αυτή η δύναμη είναι εξαιρετικά ισχυρή αλλά δρα σε πολύ μικρές αποστάσεις, της τάξης των 10^{-15} μέτρων, και είναι υπεύθυνη για τη συνοχή των πυρήνων των ατόμων.
Ασθενής Πυρηνική Δύναμη: Διαμεσολαβείται από τα μποζόνια W και Z και είναι υπεύθυνη για διαδικασίες όπως η βήτα διάσπαση. Αυτή η δύναμη είναι κρίσιμη για τις διαδικασίες που δημιουργούν τα νετρίνα.
Βαρύτητα: Η πιο ασθενής από τις δυνάμεις, διαμεσολαβείται θεωρητικά από τα γκραβιτόνια, αν και αυτά δεν έχουν ακόμα παρατηρηθεί. Η βαρύτητα επηρεάζει όλα τα σωματίδια με μάζα και είναι υπεύθυνη για την κίνηση των πλανητών και άλλων μεγάλων ουρανίων σωμάτων.

Η ηλεκτρομαγνητική δύναμη και η ασθενής πυρηνική δύναμη έχουν ενοποιηθεί σε μια ενιαία θεωρία γνωστή ως ηλεκτρασθενής θεωρία. Αυτή η θεωρία περιγράφει πώς τα φωτόνια, τα μποζόνια W και Z αλληλεπιδρούν με τα στοιχειώδη σωματίδια. Η ισχυρή πυρηνική δύναμη περιγράφεται από την κβαντική χρωμοδυναμική (QCD), η οποία εξηγεί πώς τα γκλουόνια αλληλεπιδρούν με τα κουάρκ.

Το Καθιερωμένο Πρότυπο

Το ΚΠ, μπορεί να περιγράψει επιτυχώς τις τρεις από τις τέσσερις θεμελειώδεις δυνάμεις. Η μόνη που δεν μπορεί να περιγραφεί από το ΚΠ, είναι η βαρύτητα. Το ΚΠ περιλαμβάνει τα σωματίδια μέσω των οποίων ασκούνται οι θεμελιώδεις αλληλεπιδράσεις, τα οποία είναι:

Φερμιόνια: Τα οποία αποτελούν μια κατηγορία στοιχειωδών σωματιδίων της ύλης, όπως τα κουαρκ και τα λεπτόνια, τα οποία αναλύθηκαν παραπάνω. Τα φερμιόνια υπακούν στην στατιστική $Fermi\ Dirac$ και στην απαγορευτική αρχή του $Pauli$, η οποία μας λέει πως δεν

μπορούν να βρεθούν ποτέ δύο Φερμιόνια στην ίδια ενεργειακή στάθμη.
Μποζόνια: Τα οποία είναι σωματίδια μέσω των οποίων διαμεσολαβούν οι θεμελιώδεις δυνάμεις. Αυτά είναι τα φωτόνια για την ηλεκτρομαγνητική δύναμη, τα γκλουόνια για την ισχυρή δύναμη και τα W & Z για την ασθενή δύναμη. Τα μποζόνια υπακούν στην στατιστική $Bose\ Einstein$.
Μποζόνιο $Higgs$**:**Είναι το σωματίδιο που ¨δίνει την μάζα¨ στα υπόλοιπα. Αυτό πραγματοποιείται μέσω του μηχανισμού $Higgs$.

Το Καθιερωμένο Πρότυπο έχει επιβεβαιωθεί πειραματικά μέσω πολυάριθμων πειραμάτων και θεωρείται ως ένα από τα μεγαλύτερα επιτεύγματα της θεωρητικής φυσικής. Ενσωματώνει τις θεωρίες της κβαντικής μηχανικής και της ειδικής σχετικότητας και παρέχει ένα συνεκτικό πλαίσιο για την κατανόηση των αλληλεπιδράσεων των στοιχειωδών σωματιδίων.

Περιορισμοί του Καθιερωμένου Προτύπου

Παρά την επιτυχία του, το Καθιερωμένο Πρότυπο δεν είναι πλήρες. Δεν μπορεί να εξηγήσει φαινόμενα όπως η σκοτεινή ύλη και κάποιες συγκεκριμένες διασπάσεις του μποζονίου $Higgs$. Επίσης, δεν περιλαμβάνει τη βαρύτητα, η οποία περιγράφεται από τη θεωρία της Γενικής Σχετικότητας του Αϊνστάιν[3]. Παρακάτω παρατίθενται τρία μεγάλα φαινόμενα τα οποία το ΚΠ δεν είναι σε θέση να εξηγήσει, αυτά είναι:

Σκοτεινή Ύλη και Σκοτεινή Ενέργεια: Το Καθιερωμένο Πρότυπο δεν εξηγεί την σκοτεινή ύλη και την σκοτεινή ενέργεια, οι οποίες αποτελούν το μεγαλύτερο μέρος της μάζας και ενέργειας του γνωστού έως τώρα σύμπαντος. Αποτελούν συγκεκριμένα περίπου το 95%, αν και ακόμα δεν έχει παρατηρηθεί πειραματικά η ύπαρξή τους, μέχρι την στιγμή που γράφεται αυτή η εργασία.
Βαρύτητα: Δεν περιλαμβάνει τη βαρύτητα, η οποία περιγράφεται από τη θεωρία της Γενικής Σχετικότητας του Αϊνστάιν και δεν ενσωματώνεται εύκολα στο πλαίσιο της κβαντικής μηχανικής.
Ασύμμετρη Σύνθεση Ύλης-Αντιύλης: Το Καθιερωμένο Πρότυπο δεν εξηγεί πλήρως την παρατηρούμενη ασυμμετρία μεταξύ ύλης και αντιύλης στο σύμπαν.

[3]και από διάφορες νέες εναλλακτικές θεωρίες βαρύτητας, οι οποίες είναι πολύ μακρυα από το θέμα αυτής της εργασίας

Νέα Φυσική (φυσική πέρα από το ΚΠ)

Για να ξεπεραστούν οι περιορισμοί του Καθιερωμένου Προτύπου, οι φυσικοί αναζητούν νέα φυσική πέρα από αυτό. Ένα παράδειγμα είναι το μοντέλο $2HDM$, το οποίο αναλύεται εκτενέστερα μέσα στην εργασία. Η αναζήτηση για νέες θεωρίες περιλαμβάνει τη μελέτη εξωτικών διάσπασεων του μποζονίου Χιγκς, όπως η διάσπαση του σε τέσσερα κουάρκ τύπου b.

Οι νέες θεωρητικές προεκτάσεις προσπαθούν να αντιμετωπίσουν τα κενά και τις ανεπάρκείς προβλέψεις του ΚΠ, προσφέροντας νέες προσεγγίσεις και μοντέλα που μπορούν να ελεγχθούν με πειράματα ή έστω να δώσουν στοιχεία για καλύτερες πειραματικές αναλύσεις σε υψηλότερες ενέργειες, σε επιταχυντές που δεν έχουν κατασκευαστεί ακόμα.

Ο Μεγάλος Επιταχυντής Αδρονίων LHC

Ο Μεγάλος Επιταχυντής Αδρονίων (LHC) είναι ο μεγαλύτερος επιταχυντής σωματιδίων στον κόσμο. Βρίσκεται στο $CERN$ και έχει κύριο στόχο τη μελέτη της της ηλεκτρασθενούς δύναμης και την ανακάλυψη νέων σωματιδίων. Με τη βοήθεια του LHC, μπορούν να επιταχυνθούν πρωτόνια, σε ταχύτητες που προσεγγίζουν αυτή του φωτός και να να συγκρουστούν με εξαιρετικά υψηλές ενέργειες, επιτρέποντας τη μελέτη των στοιχειωδών σωματιδίων και των αλληλεπιδράσεών τους σε υποατομική κλίμακα.

Ο Ανιχνευτής CMS

Ο ανιχνευτής CMS $(Compact\ Muon\ Solenoid)$ είναι ένα από τα τέσσερα μεγάλα πειράματα που λαμβάνουν χώρα στο LHC. Σχεδιάστηκε για να ανιχνεύει και να μελετά σωματίδια που παράγονται σε συγκρούσεις μεταξύ πρωτονίων υψηλής ενέργειας. Ο CMS αποτελείται από τα παρακάτω υποσυστήματα:

Ανιχνευτής $Tracker$**:** Χρησιμοποιεί πυρίτιο για να ανιχνεύσει τις τροχιές των σωματιδίων. Αυτή η τεχνολογία επιτρέπει την ακριβή ανακατασκευή των τροχιών των φορτισμένων σωματιδίων, βοηθώντας στην αναγνώριση των ειδών των σωματιδίων και των ιδιοτήτων τους.
Ηλεκτρομαγνητικό Καλορίμετρο $(ECAL)$**:** Μετράει την ενέργεια των ηλεκτρονίων και

των φωτονίων. Το $ECAL$ είναι σχεδιασμένο, ώστε να παρέχει ακριβείς μετρήσεις της ενέργειας και της θέσης των φαινομένων ¨στοιβάδας¨ που δημιουργούν τα ηλεκτρόνια και τα φωτόνια.

Αδρονικό Καλορίμετρο $(HCAL)$**:** Μετράει την ενέργεια των αδρονίων.

Μαγνήτης Σωληνοειδούς: Παρέχει ένα ισχυρό μαγνητικό πεδίο με σκοπό να κάμπτει τις τροχιές των σωματιδίων. Ο μαγνήτης του CMS δημιουργεί ένα μαγνητικό πεδίο 3,8 $Tesla$, το οποίο επιτρέπει την κάμψη των τροχιών των φορτισμένων σωματιδίων, διευκολύνοντας τη μέτρηση της ορμής τους.

Ανιχνευτής Μυονίων: Εντοπίζει μυόνια, τα οποία είναι παρόμοια με τα ηλεκτρόνια αλλά με μεγαλύτερη μάζα. Τα μυόνια μπορούν να διαπεράσουν το υλικό του ανιχνευτή και ανιχνεύονται από ειδικά σχεδιασμένα συστήματα ανίχνευσης μυονίων που περιβάλλουν τον υπόλοιπο ανιχνευτή.

Φυσική των Συγκρούσεων

Δομή του Πρωτονίου

Το πρωτόνιο αποτελείται από τρία κουάρκ (δύο top και ένα $bottom$) που συγκρατούνται από γκλουόνια μέσω της ισχυρής πυρηνικής δύναμης. Η κατανόηση της δομής του πρωτονίου είναι κρίσιμη για την ανάλυση των δεδομένων από τις συγκρούσεις στο LHC. Οι επιστήμονες χρησιμοποιούν τα δεδομένα από τις συγκρούσεις για να μελετήσουν τη δομή του πρωτονίου και τις ιδιότητες των γκλουονίων που το συγκρατούν. Οι αλληλεπιδράσεις μεταξύ των κουάρκ και των γκλουονίων είναι περίπλοκες και αποτελούν αντικείμενο εντατικής έρευνας.

Σκεδάσεις Παρτονίων

Οι συγκρούσεις πρωτονίων στο LHC παράγουν πίδακες αδρονίων, οι οποίοι είναι ορατοί στον ανιχνευτή CMS. Οι πίδακες αυτοί αποτελούνται από σωματίδια που παράγονται από τις αλληλεπιδράσεις των κουάρκ και των γκλουονίων και κατευθύνονται προς διάφορες κατευθύνσεις από το σημείο σύγκρουσης. Η μελέτη αυτών των πιδάκων είναι κρίσιμη για την κατανόηση των διαδικασιών που λαμβάνουν χώρα στις συγκρούσεις. Οι διαδικασίες αυτές είναι πολύπλοκες και απαιτούν ακριβή ανάλυση για να κατανοηθούν.

Ανάλυση και Ανίχνευση Σωματιδίων

Η ανάλυση των δεδομένων από τον ανιχνευτή CMS περιλαμβάνει την ανακατασκευή των γεγονότων των συγκρούσεων και την αναγνώριση των παραγόμενων σωματιδίων. Οι ερευνητές χρησιμοποιούν προηγμένα λογισμικά και αλγορίθμους για να αναλύσουν τα δεδομένα και να εξαγάγουν χρήσιμα συμπεράσματα για τις αλληλεπιδράσεις των σωματιδίων και τις ιδιότητές τους.

Η ανακατασκευή των γεγονότων περιλαμβάνει την ανάλυση των σημάτων που παράγονται από τα διάφορα υποσυστήματα του ανιχνευτή CMS. Οι πληροφορίες από τους ανιχνευτές ιχνών, τα καλορίμετρα και τους ανιχνευτές μυονίων συνδυάζονται για να δημιουργήσουν μια πλήρη εικόνα των αλληλεπιδράσεων που έλαβαν χώρα στο σημείο σύγκρουσης.

Ανάλυση

Διαδικασίες Σήματος και Υποβάθρου

Η ανάλυση της διάσπασης του μποζονίου $Higgs$ σε τέσσερα b κουάρκ περιλαμβάνει τη διάκριση μεταξύ σήματος και υποβάθρου. Οι φυσικές διαδικασίες που παράγουν το σήμα και το υπόβαθρο καθορίζονται μέσω της χρήση προσομοιώσεων και πειραματικών δεδομένων. Το σήμα αντιπροσωπεύει τα γεγονότα που αντιστοιχούν στη διάσπαση του μποζονίου $Higgs$, ενώ το υπόβαθρο αντιπροσωπεύει άλλες διαδικασίες που παράγουν παρόμοια γεγονότα αλλά δεν σχετίζονται με τη διάσπαση του $Higgs$.

Κριτήρια επιλογής γεγονότων

Εφαρμόσαμε κάποια κριτήρια για την επιλογή των γεγονότων που πιθανόν να περιέχουν το σήμα. Αυτά τα κριτήρια βασίζονται στις ιδιότητες των σωματιδίων που παράγονται στις συγκρούσεις και περιλαμβάνουν παραμέτρους όπως η ενέργεια, η γωνία εκτροπής των σωματιδίων, και η μάζα των παραγόμενων σωματιδίων. Τα κριτήρια επιλογής βοηθούν στη μείωση του όγκου των δεδομένων και έπειτα την μελέτη γεγονότων που έχουν μεγαλύτερη πιθανότητα να είναι το σήμα.

Πολυμεταβλητή Ανάλυση Δεδομένων

Χρησιμοποιούνται τεχνικές μηχανικής μάθησης, όπως τα Δένδρα Αποφάσεων (BDT), για τον διαχορισμό σήματος και υποβάθρου. Οι τεχνικές αυτές επιτρέπουν την ανάλυση πολλών παραμέτρων ταυτόχρονα και βελτιώνουν την ακρίβεια της ανάλυσης. Οι αλγόριθμοι MVA εκπαιδεύονται με τη χρήση προσομοιώσεων που περιέχουν τόσο σήμα όσο και υπόβαθρο, και στη συνέχεια εφαρμόζονται στα πραγματικά δεδομένα για την εξαγωγή των γεγονότων που πιθανόν να περιέχουν το σήμα.

Οι πολυμεταβλητές μέθοδοι ανάλυσης δεδομένων επιτρέπουν την εκμετάλλευση πολλαπλών παραμέτρων ταυτόχρονα, βελτιώνοντας την ικανότητα διάκρισης μεταξύ σήματος και υποβάθρου. Αυτές οι μέθοδοι περιλαμβάνουν την εκπαίδευση μοντέλων μηχανικής μάθησης χρησιμοποιώντας δεδομένα προσομοίωσης και έπειτα τα εφαρμόζουν στα πειραματικά δεδομένα για την αναγνώριση των γεγονότων που πιθανόν είναι σήμα.

Εξαγωγή Σήματος

Υπολογίζονται τα $branchingratios$ και τα άνω όρια της απόδοσης σήματος χρησιμοποιώντας προσαρμογή μέγιστης πιθανοφάνειας. Αυτή η μέθοδος ονομάζεται $Bayesian\ upper\ limit$ και εφαρμόζεται στην συγκεκριμένη ανάλυση μέσω του αλγορίθμου $Markov\ Chain\ Monte\ Carlo$. Τα αποτελέσματα δείχνουν τα κρίσιμα $branchingratios$ για διάφορες μάζες του υποθετικού μποζονίου α. Η $Bayesian$ μέθοδος χρησιμοποιείται για τον υπολογισμό των πιθανοτήτων και των επιπέδων εμπιστοσύνης, παρέχοντας μια συνεκτική και αξιόπιστη ανάλυση των δεδομένων.

Η $Bayesian$ μέθοδος παρέχει ένα πλαίσιο για την αξιολόγηση των αποτελεσμάτων της ανάλυσης, επιτρέποντας τον υπολογισμό πιθανοτήτων και επιπέδων εμπιστοσύνης. Οι προσαρμογές μέγιστης πιθανοφάνειας χρησιμοποιούνται για τη σύγκριση των δεδομένων με τις θεωρητικές προβλέψεις και την εξαγωγή συμπερασμάτων σχετικά με την παρουσία ή την απουσία σήματος.

Αποτελέσματα

Τα αποτελέσματα της ανάλυσης δείχνουν τα εξής:

Branching Ratios: Υπολογίστηκαν τα άνω όρια για έξι διαφορετικές υποθέσεις ενός σωματιδίου α χρησιμοποιώντας τον αλγόριθμο $Markov\ Chain\ Monte\ Carlo$.
$Bayesian$ **μέθοδος:** Χρησιμοποιήθηκαν για τον υπολογισμό των άνω ορίων του $branching\ ratio$.
Διαχωρισμός Σήματος και Υποβάθρου: Χρησιμοποιήθηκαν τεχνικές μηχανικής μάθησης για τη διάκριση μεταξύ σήματος και υποβάθρου.
Προσομοιώσεις Μοντε Κάρλο: Βοήθησαν στην κατανόηση της στατιστικής συμπεριφοράς των δεδομένων.
Μέγιστη Πιθανοφάνεια: Συγκρίθηκαν η μηδενική υπόθεση (μόνο διαδικασίες του Καθιερωμένου Προτύπου) και η εναλλακτική υπόθεση (διαδικασίες BSM).
Επίπεδα Εμπιστοσύνης: Παρουσιάστηκαν αποτελέσματα σε διαφορετικά επίπεδα εμπιστοσύνης 95% και 86%.

Τα αποτελέσματα της ανάλυσης υποδεικνύουν ότι δεν παρατηρήθηκαν σημαντικές αποκλίσεις από τις προβλέψεις του Καθιερωμένου Προτύπου. Τα δεδομένα δείχνουν ότι οι θεωρητικές προβλέψεις για τις διαδικασίες διάσπασης του μποζονίου $Higgs$ είναι συμβατές με τα πειραματικά αποτελέσματα. Παρά τις προσπάθειες να ανιχνευθούν ενδείξεις για νέα φυσική, τα αποτελέσματα δεν υπέδειξαν την ύπαρξη νέων σωματιδίων ή αλληλεπιδράσεων πέρα από αυτά που περιγράφονται από το Καθιερωμένο Πρότυπο.

Συμπεράσματα

Η ανάλυση κατέληξε στο συμπέρασμα ότι δεν παρατηρήθηκαν αποδείξεις νέας φυσικής πέρα από το Καθιερωμένο Πρότυπο στο κανάλι διάσπασης του $Higgs$ σε τέσσερα b κουάρκ. Παρά την αποτελεσματικότητα των χρησιμοποιούμενων μεθόδων και αναλύσεων, τα αποτελέσματα δεν υπέδειξαν αποκλίσεις που να υποδεικνύουν την παρουσία νέας φυσικής.

Τα αποτελέσματα της ανάλυσης επιβεβαιώνουν τις προβλέψεις του Καθιερωμένου Προτύπου και παρέχουν αυστηρά όρια στις παραμέτρους των νέων θεωριών. Η έλλειψη ενδείξεων για νέα φυσική υποδεικνύει ότι οι θεωρίες που επεκτείνουν το Καθιερωμένο Πρότυπο πρέπει να επανεξεταστούν ή να βελτιωθούν για να συμβαδίζουν με τα πειραματικά δεδομένα.

Επιπλέον Σημεία και Βαθύτερη Ανάλυση

Ανασκόπηση της Σωματιδιακής Φυσικής

Η σωματιδιακή φυσική προσπαθεί να απαντήσει σε θεμελιώδη ερωτήματα σχετικά με τη φύση του σύμπαντος. Οι ανακαλύψεις στον τομέα αυτό έχουν αλλάξει την κατανόησή μας για τον μικρόκοσμο και τον μακρόκοσμο. Οι σύγχρονες θεωρίες, όπως το Καθιερωμένο Πρότυπο, παρέχουν ένα πλαίσιο για την κατανόηση των στοιχειωδών σωματιδίων και των αλληλεπιδράσεών τους.

Η πρόοδος στη σωματιδιακή φυσική έχει οδηγήσει σε σημαντικές τεχνολογικές και επιστημονικές ανακαλύψεις, όπως η ανάπτυξη της τεχνολογίας των επιταχυντών και των ανιχνευτών σωματιδίων, καθώς και η βελτίωση των υπολογιστικών μεθόδων και των τεχνικών ανάλυσης δεδομένων.

Θεωρητικές Προεκτάσεις

Οι θεωρίες πέρα από το Καθιερωμένο Πρότυπο, όπως το μοντέλο $2HDM$ $(+scalar)$, προσπαθούν να απαντήσουν σε ερωτήματα που δεν καλύπτονται από το Καθιερωμένο Πρότυπο. Αυτές οι θεωρίες προσφέρουν νέες προβλέψεις που μπορούν να δοκιμαστούν πειραματικά. Οι θεωρητικές προεκτάσεις προσπαθούν να αντιμετωπίσουν τα κενά και τις ανεπάρκείς προβλέψεις του Καθιερωμένου Προτύπου, προσφέροντας νέες προσεγγίσεις και μοντέλα.

Τεχνολογικές Προκλήσεις

Η κατασκευή και η λειτουργία ανιχνευτών όπως ο CMS απαιτούν τεράστια τεχνολογική πρόοδο και συνεργασία. Η ανάλυση των δεδομένων από αυτές τις συσκευές απαιτεί προηγμένες υπολογιστικές τεχνικές και εξειδικευμένο λογισμικό. Οι τεχνολογικές προκλήσεις που σχετίζονται με την κατασκευή και λειτουργία των ανιχνευτών, καθώς και την ανάλυση των δεδομένων, απαιτούν συνεχή βελτίωση και καινοτομία στον τομέα της τεχνολογίας και της επιστήμης.

Στατιστική Ανάλυση

Η ανάλυση των δεδομένων από τα πειράματα στο LHC περιλαμβάνει τη χρήση στατιστικών μεθόδων για την εξαγωγή αξιόπιστων συμπερασμάτων. Η $Bayesian$ μέθοδος και οι προσομοιώσεις $Monte\ Carlo$ είναι κρίσιμες για την κατανόηση της στατιστικής συμπεριφοράς των δεδομένων.

Η χρήση των στατιστικών μεθόδων είναι απαραίτητη για την ανάλυση των δεδομένων από τα πειράματα στο LHC και την εξαγωγή αξιόπιστων συμπερασμάτων για τις αλληλεπιδράσεις των σωματιδίων και τις ιδιότητές τους.

Με αυτή την ανάλυση, η περίληψη της διπλωματικής εργασίας καλύπτει λεπτομερώς τις βασικές έννοιες και τα αποτελέσματα της έρευνας, προσφέροντας μια σαφή εικόνα της συνεισφοράς στον τομέα της σωματιδιακής φυσικής.

Acknowledgements

This thesis would not have been possible without the support and guidance of several individuals, to whom I would like to extend my deepest gratitude.

First and foremost, I wish to express my heartfelt thanks to my professor, Dr. Georgia Karapostoli, whose guidance, encouragement, and insightful feedback were invaluable throughout this journey. Her unwavering support and commitment to my success were truly motivating, and I am deeply grateful for all the time and effort she dedicated to helping me through every stage of this thesis.

I would also like to sincerely thank PhD student Eirini Siamarkou, whose expertise and assistance greatly contributed to the development of my work. Her willingness to share her knowledge and provide guidance whenever needed was a source of great support. I am equally grateful to master's student Grigoria Stavropoulou, whose collaborative spirit and helpful discussions enriched my understanding and helped me stay focused throughout the research process.

A special thank you to my family—my rock and constant source of strength. To my friends, Lefteris and Nikos and my dearest Zoi, thank you for your unconditional love and belief in me, which has been the foundation of everything I have achieved. To my brothers, Alexandros and Konstantinos, your encouragement and faith in my abilities have been a source of constant motivation. I am beyond grateful for your support during this demanding process.

I would also like to extend my gratitude to Professors Konstantinos Kousouris and George Tsipolitis, whose weekly brainstorming sessions and collaborative efforts played a pivotal role in shaping the direction of this thesis. Their fresh perspectives and constructive criticism were instrumental in refining my ideas and bringing this work to fruition.

Finally, to my dear friend Maria and Sotiris, thank you for being a constant source of positivity and encouragement. Your friendship and understanding helped me stay grounded during the challenging moments of this journey.

To all those mentioned and anyone else who supported me in any way, thank you from the bottom of my heart. This accomplishment would not have been possible without your contributions.

Contents

List of Figures

List of Tables

Abbreviations

Acronym	**W**hat (it) **S**tands **F**or
Quantum **M**echanics (QM)	
Quantum **F**ield **T**heory (QFT)	
Standard **M**odel (SM)	
Beyond **S**tandard **M**odel (BSM)	
Special **U**nitary (SU)	
Unitary (U)	
Electro-**W**eak (EW)	
Quantum **C**hromo **D**ynamics (QCD)	
Charged **C**urrent (CC)	
Neutral **C**urrent (NC)	
Vacuum **E**xpectation **V**alue (VEV)	
Minimal **S**uper **S**ymmetric **M**odel (MSSM)	
Next to **M**inimal **S**uper **S**ymmetric **M**odel (NMSSM)	
Missing **E**nergy **T**ransverse (MET)	
Large **H**adron **C**ollider (LHC)	
Compact **M**uon **S**olenoid (CMS)	
Deep **I**nelastic **S**cattering (DIS)	
Underlying **E**vent (UE)	
SUper **SY**mmetry (SUSY)	
Monte **C**arlo (MC)	
Missing **T**ransverse **E**nergy (MET)	
Combined **S**econdary **V**ertex (CSV)	
Boosted **D**ecision **T**ree (BDT)	
Monte **C**arlo (MC)	

Two-**H**iggs **D**oublet **M**odel (2HDM)

gluon **g**luon **f**usion (ggf)

Vector **B**oson **F**usion (VBF)

Dedication (optional)

Chapter 1

Introduction to particle physics

Looking at a clear night sky or during our deepest existential thoughts, we have all asked ourselves what is everything around us made of? How did our cosmos born? How will it die? Particle physics is the strongest humanly possible tool to answer these questions. In this chapter we will try to explain some very fundamental parts of the SM and in general particle physics.

1.1 Elementary Particles

Elementary particles form the cosmos around us. They are the building blocks of our universe and humanities greatest scientific milestone until today, if one thinks that before a hundred years we were aware only of molecules.
But molecules are made of atoms and atoms are made of electrons, protons and neutrons. Almost everything we see is made of these three entities, except electrons (which are leptons) none of protons and neutrons (which are baryons) are elementary. They are made of quarks and gluons.
Baryons are a subcategory of a group called hadrons, the other subgroup is called messons, their difference is on the Barionic number which is $B = 1$ for baryons and $B = 0$ for mesons and the fact that baryons consist three quarks while messons consist two, that are a quark and an anti-quark. High energy physics have found six different quarks that exist; up (u), down(d), strange(s), charm(c), bottom (b), top (t) and each one of them has a different flavor. This flavor is dynamic and changes through interactions (that are known as weak) that are mediated by weak bosons $W^{\pm}$ and are predicted by the SM. Apart from flavor quarks poses color (which as flavor is another degree of freedom), and color changes via strong interaction that is mediated through gluons and is studied by QCD.
Te last category of elementary particles is called leptons and contains the electron, the muon

and the tau with their corresponding neutrinos. They are flavorless and colorless and can't interact strongly but weakly and electromagnetically. Neutrinos can interact weakly only.
Leptons and quarks are fermions, which mean that they obey Paley's principle and have spin $\frac{1}{2}$ and they can be represented in three doublets.

$$\textbf{Leptons} \begin{pmatrix} \nu_e \\ e \end{pmatrix}, \begin{pmatrix} \nu_\mu \\ \mu \end{pmatrix}, \begin{pmatrix} \nu_\tau \\ \tau \end{pmatrix}. \tag{1.1}$$

$$\textbf{Quarks} \begin{pmatrix} u \\ d \end{pmatrix}, \begin{pmatrix} c \\ s \end{pmatrix}, \begin{pmatrix} t \\ b \end{pmatrix}. \tag{1.2}$$

So to put elementary particles into perspective we make the following tables.

	Q	I_3	S	C	B	T	mass
u	$+\frac{2}{3}$	$+\frac{1}{2}$	0	0	0	0	$1.5 \to 5\ MeV$
d	$-\frac{1}{3}$	$-\frac{1}{2}$	0	0	0	0	$3 \to 9\ MeV$
s	$-\frac{1}{3}$	0	-1	0	0	0	$60 \to 170\ MeV$
c	$+\frac{2}{3}$	0	0	+1	0	0	$1.47 \to 1.83\ GeV$
b	$-\frac{1}{3}$	0	0	0	-1	0	$4.6 \to 5.1\ GeV$
t	$+\frac{2}{3}$	0	0	0	0	+1	$174.3 \pm 3.2 \pm 4.0\ GeV$

Table 1.1: Quarks [10]

	Q	L_e	L_μ	L_τ	mass
e	-1	+1	0	0	0.511 MeV
ν	0	+1	0	0	$<$ 3 MeV
μ	-1	0	+1	0	105.66 MeV
ν_μ	0	0	+1	0	$<$ 0.19 MeV
τ	-1	0	0	+1	1777.0 MeV
ν_τ	0	0	0	+1	$<$ 18.2 MeV

Table 1.2: Leptons [10]

Bosons $W^\pm$, Z^0, gluons and photons γ are obeying Bose-Einstein statistics which means that their spin is 1. They are mediators of interactions, specifically $W^\pm$ and Z^0 are weak force's, gluons are strong's and photons γ are electromagnetic's. Photons can't couple with themselves while the rest of them can. This happens because photons are described by gauge theories that are Abelian while the rest are non-Abelian.
From the above bosons, γ and gluons are massless and so they can interact from infinite distance, while weak bosons are massive and interact inside hadrons $\simeq \mathcal{O}(10^{-15}m)$.
To make the SM model theory complete one must include the Higgs boson. The Higgs boson has a spin that is 0, which is needed for the Higgs mechanism to work. Higgs mechanism describes the condition of a symmetry breaking into a smaller one. All the masses of bosons,

quarks and leptons are coming from the spontaneous symmetry breaking of the SM, with a small asterisc on neutrinos [1].

1.2 Interactions

There are four known interactions known to man, which are the gravitational, the electromagnetic, weak and strong. Each one of them has a mediator boson (with a possible exception of the gravitational). These mediators are the massive weak gauge bosons $W^{\pm}$ and Z^0 with masses $m_W \simeq 80.4\ GeV/c^2$ and $m_Z \simeq 91.2\ GeV/c^2$ and spins $s = 1, 3$, then there are the strong mediators that are massless gluons with spins $s = 1, 4$, then gravitational mediator that is the massless (possibly) graviton with spin $s = 2$ and finally the electromagnetic mediator that is the massless photon that is symbolized with the greek letter γ and has spins $s = 1, 2$. Electromagnetic mediator is described by QED and has $U(1)$ symmetry. Weak interaction is not renormalizable, is unified with electromagnetism, is non-Abelian and is $SU(2)_L \bigotimes U(1)_Y$ symmetric. Strong mediator has color and flavor changes, is non-Abelian, is described by QCD and is $SU(3)_c$ symmetric. The SM has many problems and there is an ever increasing amount

Force	strength	mediator	spin
Gravity	$G_N \simeq 6.71 \times 10^{-39} (GeV/c)^{-2}$	graviton	2
Strong	$\alpha_s = \frac{g_s^2}{4\pi} \simeq 0.1$	gluon	1
Weak	$G_F = 1.16 \times 10 * -5 (GeV/c)^{-2}$	$W^{\pm}, Z^0$	1
Electromagnetic	$\alpha = \frac{e^2}{4\pi} \simeq \frac{1}{137}$	γ	1

TABLE 1.3: Interactions of particles [10]

of theorists and experimentalists that doubt that theory. This thesis will investigate if there are "New Physics" on the BSM through an excotic Higgs decay analysis.

[1] neutrinos oscillate which means that their mas is not static but dynamic

Chapter 2

The Standard Model and Beyond

Particle physics can be described as the scientific method that studies the building blocks of the universe and their interactions. The most important theory that explains universe's evolution is SM, which is developed from QM and QFT. Until today SM is the most successful theory in high energy physics, this paper will try to attack SM by analysing an exotic decay (will be explained later).

2.1 The Standard Model

The development of SM started in the 60s and lead to the electroweak unification. That model is a simple gauge theory with symmetries $SU(2) \bigotimes U(1)$ which consists electromagnetic and weak forces. EW and QCD form SM.
SM predicts three bosons W^+, W^-, Z^0, though it can't predict their masses, it gives a relation between these masses with Fermi's constant and weak mixing angle. Knowing these masses, theory can predict the branching ratio at every decay channel.
As said before EW theory is based at the local gauge invariant of $SU(2) \bigotimes U(1)$ symmetry. If a theory aspires to stand, it needs to be renormalizable, meaning there is a mathematical expression that kills infinity where it appears (decay rates, cross section). To achieve that we first need to write EW's Langrange function without their mass terms, supposing that bosons and fermions are massless. Masses are created without the destruction of renormalization from the spontaneous violation of the local gauge symmetry through a mechanism that was purposed at 1964 from Englert & Brought, (1964a and b) Higgs and Gularnik, Hagen & Kibble (1964). [1] This mechanism is often refereed as 'Higgs mechanism'. The basic prediction of this mechanism is the existence of a boson which is known as 'Higgs boson'.

2.2 Electroweak force

Here we will study $W^{\pm}$, Z^0 and the photon, $SU(2) \bigotimes U(1)$ consists of three plus one gauge fields, a weak isospin that will be represented as I_W, is corresponding with SU(2) and a weak hypercharge Y_W that corresponds with U(1).

$$Y_W \equiv 2(Q - I_{W_Z}) \tag{2.1}$$

W will be the triplet of the fields that corresponds with SU(2) $[W = (W_1, W_2, W_3)]$ and interacts with the particle isospin $(I_W = 1, Y_W = 0)$. Then B will be the field that corresponds with U(1) and has zero charge, isospin and hypercharge.[12]
These fields are not responsible for the weak interaction. The weak CC's [1] have $W^{\pm}$ as a carrier and are linear combinations of W_1 and W_2, while the electromagnetic and neutral current (NC's) have the photon and Z^0 and are linear combinations of W_3 and B.

2.2.1 Leptons

There are two left-handed leptons, that have the same isospin $(I_W = 1/2)$, which can't be zero, because they must be able to couple with $W^{\pm}$. Charged W, which is the carrier of weak CC interactions, is coupled with the double spinors of negative chirality:

$$\begin{pmatrix} I_{W_Z} = +1/2 \\ I_{W_Z} = -1/2 \end{pmatrix} = \begin{pmatrix} \nu_{eL} \\ e_L^- \end{pmatrix}, = \begin{pmatrix} \nu_{\mu L} \\ \mu_L^- \end{pmatrix}, = \begin{pmatrix} \nu_{\tau L} \\ \tau_L^- \end{pmatrix} \tag{2.2}$$

The right charged lepton is a zero isospin state $(I_W = 0)$ and in contrary with the above it interacts with NC and right-handed fermions, but in no case with right handed neutrinos because they don't exist and even if they existed they wouldn't interact with any force except the gravitational one, since their hypercharge and isospin would be zero. These simple isospin states are e_R^-, μ_R^-, τ_R^-. [12]

2.2.1.1 Antileptons

Antileptons are the "anti" functions of the left-handed right spinor. They belong on the following states:

$$\begin{pmatrix} I_{W_Z} = +1/2 \\ I_{W_Z} = -1/2 \end{pmatrix} = \begin{pmatrix} e_L^+ \\ \overline{\nu}_{eL} \end{pmatrix}, = \begin{pmatrix} \mu_L^+ \\ \overline{\nu}_{\mu L} \end{pmatrix}, = \begin{pmatrix} \tau_L^+ \\ \overline{\nu}_{\tau L} \end{pmatrix} \tag{2.3}$$

[1] At weak interactions there are two kinds of fermionic currents, charged currents (CC's), that spread from charged scalar bosons $W^{\pm}$ and neutral currents (NC's) that spread from Z^0.

Right-handed antileptons of 2.3 that appear at NC, are the simple isospin states e_R^+, μ_R^+, τ_R^+ and there are no right-handed antineutrinos.

2.2.2 Quarks

Quarks are quite similar with Leptons, as long as we take into account the fact that W bosons are coupling with d', s' and b' that are the turns of the d, s and b states. For each color there are three isospin doublets, one for each family.

$$\begin{pmatrix} I_{W_Z} = +1/2 \\ I_{W_Z} = -1/2 \end{pmatrix} = \begin{pmatrix} u_L \\ d'_L \end{pmatrix}, = \begin{pmatrix} c_L \\ s'_L \end{pmatrix}, = \begin{pmatrix} t_L \\ b'_L \end{pmatrix} \tag{2.4}$$

and the simple states that are $d_R, u_R, s_R, c_R, b_R, t_R$.
Quark mix is not related in any way with NC's of weak interactions, so we can write them as a function of rotated quarks with the same result. [12]

2.2.2.1 Antiquarks

The double antiquark states are:

$$\begin{pmatrix} I_{W_Z} = +1/2 \\ I_{W_Z} = -1/2 \end{pmatrix} = \begin{pmatrix} \overline{d'}_L \\ \overline{u}_L \end{pmatrix}, = \begin{pmatrix} \overline{s'}_L \\ \overline{c}_L \end{pmatrix}, = \begin{pmatrix} \overline{b'}_L \\ \overline{t}_L \end{pmatrix} \tag{2.5}$$

and their simple states are $\overline{d}_R, \overline{u}_R, \overline{s}_R, \overline{c}_R, \overline{b}_R, \overline{t}_R$. [12]

2.3 EW Unification

EW model came to existence by S.Glashow, A. Salam and S.Weinberg. Feynman rules and the calculations that were needed for theory renormalization, where done by 't Hooft. The field $W^\mu \equiv (W_1^\mu, W_2^\mu, W_3^\mu)$ is a four-vector on spacetime and a vector at isospin space. The fields of charged bosons are:

$$W^\pm = \frac{1}{\sqrt{2}}(W_1 \pm iW_2) \tag{2.6}$$

For each double state fermion there is a four-vector at spacetime, an isospin vector and its called weak current, $j_{mu} \equiv (j_{1\mu}, j_{2\mu}, j_{3\mu})$. The field W^μ couples with j_μ as $gW^\mu j_\mu$ with coupling constant g (which is dimensionless). Charged currents are linear combinations of:

$$j^\pm = j_1 \pm ij_2 \tag{2.7}$$

The field B^μ is a four-vector at spacetime, scalar isospin. It couples with the hypercharge j_μ^Y, which is also a four-vector and has equal scalar, their coupling constant is g'. Hypercharge's current is double the diffenrence between electromagnetism and NC's.

$$j_\mu^Y = 2(j_\mu^{em} - j_{3\mu}) \tag{2.8}$$

The first term is the electromagnetic current, that for a charged fermion is:

$$j_\mu^{em} = \overline{f}\gamma_\mu f \tag{2.9}$$

Cheirality is not defined, because the electromagnetic interaction is not defined by it.
A and Z are electromagnetic's and weak force's NC fields. They are both orthogonal linear superpositions of W_3 and B. Photon doesn't couple with neutral particles, while Z^0 does. The transformation is a function of the couple constants (g and g'), or equivelantly a turn θ_W which is called weak mixing angle [12].

$$\begin{pmatrix} Z^0 \\ A \end{pmatrix} = \frac{1}{\sqrt{g^2 + g'^2}} \begin{pmatrix} g & -g' \\ g' & g \end{pmatrix} \begin{pmatrix} W_3 \\ B \end{pmatrix} = \begin{pmatrix} \cos\theta_W & -\sin\theta_W \\ \sin\theta_W & \cos\theta_W \end{pmatrix} \tag{2.10}$$

Where in 2.10 the weak mixing angle is

$$\theta_W \equiv \tan^{-1}\frac{g'}{g} \tag{2.11}$$

Lagrange function of the interaction, is gauge symmetric so

$$L = g(j_\mu^1 W_1^\mu + j_\mu^2 W_2^\mu + j_\mu^3 W_3^\mu) \tag{2.12}$$

Which can be written as

$$L = \frac{g}{\sqrt{2}}(j_\mu^- W_+^\mu + j_\mu^+ W_-^\mu) + j_\mu^3(gW_3^\mu - g'B^\mu) + g' j_\mu^{em} B^\mu \tag{2.13}$$

And after importing neutral fields we get

$$L = \frac{g}{\sqrt{2}}(j_\mu^- W_+^\mu + j_\mu^+ W_-^\mu) + \frac{g}{\cos\theta_W}(j_\mu^3 - j_\mu^{em}\sin^2\theta_W)Z^\mu + g j_\mu^{em} A^\mu \sin\theta_W \tag{2.14}$$

The terms of 2.14 are by order, CC weak interaction, NC weak interaction and electromagnetic interaction.[12]
The last term of 2.14 should be proportional to the electric field, which is theoretical proof that photon does not pair with neutral particles.

$$g\sin\theta_W = \frac{q_e}{\sqrt{\epsilon_0 \hbar c}} = \sqrt{4\pi\alpha} \tag{2.15}$$

2.15 unifies weak and electric field.

Every interaction in nature has a carrier that should be one of four vector bosons. These bosons are formulated into functions that have two constants, q_e (electric charge) and θ_W (weak mixing angle). These parameters should be measured experimentally as SM does not predict them. From 2.11 and 2.15 we can find the relation between the coupling constant of U(1) and electric charge.[12]

$$g' \cos\theta_W = \sqrt{4\pi\alpha} \tag{2.16}$$

And from 2.15 and 2.16 we got

$$\frac{1}{\alpha} = \frac{4\pi}{g'^2} + \frac{4\pi}{g^2} \tag{2.17}$$

which shows that pairing of the two gauge's contribute at $1/\alpha$. At low energies where $1/\alpha \simeq 137$ and $\sin\theta_W \simeq -0.232$ we can conclude that [12]

$$\frac{4\pi}{g'^2} = 105.2 \;\&\; \frac{4\pi}{g^2} = 31.8 \tag{2.18}$$

The second term of 2.14 gives the pairing of Z with a fermion.

$$g_Z \equiv \frac{g}{\cos\theta_W}(I_{W_Z} - Q\sin^2\theta_W) = \frac{\sqrt{4\pi\alpha}}{\sin\theta_W\cos\theta_W}(I_{W_Z} - Q\sin^2\theta_W) = \frac{q}{\cos\theta_W}c_Z \tag{2.19}$$

We see that it is a global function of charge and the third component of isospin. In 2.19 we introduced the Z-charge factor.

$$c_Z \equiv I_{W_Z} - Q\sin^2\theta_W \tag{2.20}$$

The first term of 2.14 describes the weak of CC. The gauge constant g connects with Fermi's constant and the mass of W.

$$G_F = \frac{\sqrt{2}g^2}{8M_W^2} \tag{2.21}$$

From 2.15 we can predict the mass of W boson as a function of α, Fermi's constant and the weak mixing angle.

$$M_W = \sqrt{\frac{g^2\sqrt{2}}{8G_F}} = \sqrt{\frac{\pi\alpha}{\sqrt{2}G_F}}\frac{1}{\sin\theta_W} = \frac{37.3}{\sin\theta_W}\,GeV \tag{2.22}$$

In SM, the measure of weak mixing angle can result in a very precise prevision in the relation between the masses of the bosons.

$$\frac{M_W}{M_Z} = \cos\theta_W \tag{2.23}$$

The measure of weak mixing angle is $\sin^2\theta_W = 0.232$ and so $M_W \simeq 80\ GeV$ and $M_Z \simeq 91\ GeV$.

2.3.1 Spontaneous Symmetry Breaking

In SM the gauge symmetry was a riddle to discover. It should be mentioned that SM includes gluons and bosons. Gluons are presumed massless [13] and can't be observed (due to confinement in detection). Photons are totally massless and W, Z bosons carry mass. The reason that SM gauge theory was such a difficult discovery was because electromagnetic interactions are not local at all (they have infinite range), while weak interactions have the shortest range amongst all forces. That can be explained by the mass of each interaction boson $m_{photon} = 0$ and $m_{W,Z} \neq 0$.
This riddle came to an end by the idea of spontaneous symmetry breaking. To get an idea, we will prove Goldstone theorem, which states that when spontaneous symmetry breaking takes place, there is always a zero-mass mode in the spectrum [13].
We start by taking the Langranzian

$$\mathcal{L} = \frac{1}{2} \mid \partial_\mu \phi \mid^2 - V(\phi) \tag{2.24}$$

Where the potential $V(\phi)$ will be

$$V(\phi) = -\frac{1}{2}\mu^2\phi^2 + \frac{1}{4}\lambda\phi^4 \tag{2.25}$$

Where ϕ is a column vector. The potential should be symmetric under an orthogonal matrix rotation.

$$\phi' = O\phi \tag{2.26}$$

Where O is a SO(k) transformation and k is the number of columns (or rows). For positive μ^2 the mass term has the wrong sign. So we assume that the potential is symmetric for infinitesimal transformations hence

$$\phi \to \phi' = \phi + \delta\phi \tag{2.27}$$

where $\delta\phi$ is

$$\delta\phi_i = i\delta\theta^A t^A_{ij}\phi_j \tag{2.28}$$

Parameter $\delta\theta^A$ is infinitesimal, t^A_{ij} are matrices of the symmetry group on representation of ϕ_i [13]. So the condition under which there appears equilibrium is

$$\frac{\partial V}{\partial \phi_i} \mid_{\phi_i = \phi_i^0} = 0 \tag{2.29}$$

which is the potentials symmetry. One can realise that

$$\delta V = \frac{\partial V}{\partial \phi_i}\delta\phi_i = i\delta\theta^A \frac{\partial V}{\partial \phi_i} t^A_{ij}\phi_j = 0 \tag{2.30}$$

and after taking into account 2.29 (where $\phi_i = \phi_i^0$) we see that

$$\frac{\partial^2 V}{\partial\phi_k\partial\phi_i} \mid_{\phi_i=\phi_i^0} t_{ij}^A\phi_j^0 + \frac{\partial V}{\partial\phi_i} \mid_{\phi_i=\phi_i^0} t_{ik}^A = 0 \tag{2.31}$$

leads to

$$\frac{\partial^2 V}{\partial\phi_k\partial\phi_i} \mid_{\phi_i=\phi_i^0} t_{ij}^A\phi_j^0 = 0. \tag{2.32}$$

2.32 is the squared mass matrix. We will symbolize it as M_{ki}^2 and so its notation is

$$M^2 t^A\phi^0 = 0. \tag{2.33}$$

As long as the symmetry does not break spontaneously, all transformations are invariant, for every A, $t^A\phi^0 = 0$ [13]. When this stops, ie values of A make vectors $t^A\phi^0 \neq 0$ then all these states are eigenstates of the mass matrix squared with zero eigenvalue. So we conclude that a massless mode have the same quantum numbers as the generators that do not annihilate the vacuum [13].

This was the classical Goldstone theorem, lets try to make a quantum case. In that case, diagrams of a higher order will be the corrections. So the classical case will conclude the tree level approximation. [2] In the case that λ is small, ie the theory is coupled weakly [13] and the tree level will not be far from reality and so classical approximation will get the job done.

If a quantum system has finite degrees of freedom, the vacuum is always unique[13]. In our case the potential is

$$V(x) = \frac{-\mu^2 x^2}{2} + \frac{\lambda x^4}{4} \tag{2.34}$$

an one dimensional Schrodinger problem. It has two minima at $x = \pm x_0 = \sqrt{\frac{\mu^2}{\lambda}}$ and are denoted by $|+\rangle$ and $|-\rangle$, so we can write

$$\langle +| V |-\rangle = \langle -| V |+\rangle \sim \exp(-khd) = \delta. \tag{2.35}$$

The potential isn't diagonal and the 2.35 are the matrix elements, which are non zero. After we diagonize the eigenvectors should be

$$\frac{|+\rangle + |-\rangle}{\sqrt{2}} \tag{2.36}$$

and

$$\frac{|+\rangle - |-\rangle}{\sqrt{2}}. \tag{2.37}$$

Now we make the potential a sum of equal parts, $V = \sum_i V(x_i)$, so the new amplitude will be in proportion with δ^n and if n goes to infinity, the transition amplitude vanishes.

[2] tree level approximation of the quantum potential [13]

2.3.1.1 A Deeper Theoretical Look

So to develop that thought, to explain the spontaneous symmetry breaking we are making a scalar field in the $SU(2)_L$ spinor representation

$$\phi = \begin{pmatrix} \phi^+ \\ \phi^0 \end{pmatrix} \tag{2.38}$$

and $U(1)$ with charge $Y(\phi) = +1/2$. So in order to take a massles gauge boson we add an $U(1)_Y$ symmetry and the covariant derivative will be

$$D_\mu \phi = (\partial_\mu + igT^i W_\mu^i + i\frac{1}{2}g' B_\mu)\phi \tag{2.39}$$

we know that B^μ and W_μ^i that are gauge bosons of $SU(2)_L \bigotimes U(1)_Y$ symmetry.
For the above to be invariant we must take a potential of the form

$$V(\phi) = -\mu^2 \phi^\dagger \phi + \lambda(\phi^\dagger \phi)^2 \tag{2.40}$$

where λ is the quartic self interactions of the fields, and because of the vacuum we know that $\lambda > 0$ [14].
This field is creating a nonzero VEV if $\mu^2 > 0$, that breaks symmetry spontaneously. $V(\phi)$ is symetric so there are infinite degenerate states that have minimum energy and their inner product is

$$\phi^\dagger \phi = \frac{u^2}{2}. \tag{2.41}$$

Hence we conclude that the function of the potential is depending only on $\phi^\dagger \phi$, we can write [14]

$$< \phi >= \frac{1}{\sqrt{2}} \begin{pmatrix} 0 \\ u \end{pmatrix}. \tag{2.42}$$

The electric charge is conserved and because of that only neutral fields can get a VEV. The neutral part of the doublet is ϕ^0 and so $Q(\phi) = 0$. Electromagnetism remains unbroken by VEV so the symmetry will become

$$SU(2)_L \bigotimes U(1)_Y \to U(1)_Q \tag{2.43}$$

that keeps on being a true vacuum symmetry.
Golstone bosons are not U(1) so the scalar doublet will be

$$\phi = \frac{1}{\sqrt{2}} \begin{pmatrix} 0 \\ u + h \end{pmatrix} \tag{2.44}$$

We deny the h terms (we want only gauge bosons masses)[14]

$$(D^{\mu}\phi)^{\dagger}(D_{\mu}\phi) =\mid (\partial_{\mu} + \frac{i}{2}g\tau^{k}W_{\mu}^{k} + \frac{i}{2}g'B_{\mu})\frac{1}{\sqrt{2}}\begin{pmatrix}0\\u\end{pmatrix}\mid^{2} \tag{2.45}$$

which will end up [14]

$$(D^{\mu}\phi)^{\dagger}(D_{\mu}\phi) = \frac{u^{2}}{8}[g^{2}]((W_{\mu}^{1})^{2} + (W_{\mu}^{2})^{2}) + (gW_{\mu}^{3} - g'B_{\mu})^{2}]. \tag{2.46}$$

From 2.6 and 2.46 we come up with

$$g^{2} = \frac{1}{8}(gu)^{2}W_{\mu}^{\dagger}W^{\mu} \tag{2.47}$$

And yielding mass will be

$$m_{W} = \frac{gu}{2} \tag{2.48}$$

For Z and A, neutral gauge bosons' masses we know that [14]

$$Z_{\mu} = \frac{1}{\sqrt{g^{2}+g'^{2}}}(gW_{\mu}^{3} - g'B_{\mu}) \text{ and its mass will be given from } m_{Z} = \frac{u}{2}\sqrt{g^{2}+g'^{2}} \tag{2.49}$$

$$A_{\mu} = \frac{1}{\sqrt{g^{2}+g'^{2}}}(g'W_{\mu}^{3} + gB_{\mu}) \text{ and its mass will be } m_{Z} = 0. \tag{2.50}$$

In the case of the massles Goldstone bosons, we know that they react to long range forces, that are easy to detect. That is not the case for particles that are massles and confined (gluons in QCD). Despite that, while constructing the EW theory, the massles bosons cannot be taken into account as physical. We know that, when spontaneous symmetry braking is happening there are some massles Goldstone modes, which are nonphysical and disappear from the spectrum [13]. They do that, by transforming to the third helicity state of a gauge boson that takes mass. This 'transformation' is known as Higgs mechanism and will be analysed at the next subsection.

2.3.2 The Higgs Mechanism

To realise the Higgs mechanism one should firstly understand Abelian and non-Abelian theories which the EW-SM is. So we will begin with Abelian theory and then proceed to the mechanism in EW-SM.

2.3.2.1 Abelian Theory

The kinetic term of U(1) gauge is

$$\mathcal{L}_{kin} = -\frac{1}{4}F_{\mu\nu}F^{\mu\nu} \tag{2.51}$$

and

$$F_{\mu\nu} = \partial_\mu A_\nu - \partial_\nu A_\mu. \tag{2.52}$$

That term is invariant for $A_\mu \to A_\mu + \partial_\mu \eta(x)$, the next step is to add the mass term to 2.51 so it will be

$$\mathcal{L} = -\frac{1}{4}F_{\mu\nu}F^{\mu\nu} + \frac{1}{2}m^2 A_\mu A^\mu \tag{2.53}$$

and later we will check if that term will violate the local gauge symmetry. We know that the photon should be massles (from U(1)), so we will extend the 2.51 with complex scalar fields negatively charged, that will couple with itself and with a photon [14]

$$\mathcal{L} = -\frac{1}{4}F_{\mu\nu}F^{\mu\nu} + (D^\mu\phi)^\dagger(D_\mu\phi) - V(\phi) \tag{2.54}$$

and $D_\mu = \partial_{mu} - ieA_\mu$ with $V(\phi) = -\mu^2\phi^\dagger\phi + \lambda(\phi^\dagger\phi)^2$. 2.54 is gauge invariant under $A_\mu \to A_\mu + \partial_\mu\eta(x)$ and $\phi \to e^{ie\eta(x)}\phi$.
The state in which $\phi = 0$ and energy is minimum is when $\mu^2 < 0$. In that case potential keeps the Langrance symmetry and the theory is QED with a massles photon and a field that is charged ϕ and has μ mass.
All these change when $\mu > 0$, the field ϕ will need a VEV

$$< \phi >= \sqrt{\frac{\mu^2}{2\lambda}} \equiv \frac{u}{\sqrt{2}} \tag{2.55}$$

and so U(1) will spontaneously break. So ϕ will be

$$\phi = \frac{u+h}{\sqrt{2}} \exp\Big\{i\frac{x}{u}\Big\} \tag{2.56}$$

h and x are Higgs and Goldstone bosons respectively and don't have a VEV. So after we impose 2.56 into the Lagrangian we got

$$\mathcal{L} = -\frac{1}{4}F_{\mu\nu}F^{\mu\nu} - euA_\mu\partial^\mu + \frac{e^2u^2}{2}A_\mu A^\mu + \frac{1}{2}(\partial_\mu h\partial^\mu h - 2\mu^2h^2) + \frac{1}{2}\partial_\mu x\partial^\mu x + \Omega \tag{2.57}$$

where Ω represents the interactions of Higgs and Goldstone bosons.
Equation 2.57 says that there is a photon with mass $m_A = eu$, a Goldstone boson with no mass and a higgs with mass $m_h = \sqrt{2}\mu = \sqrt{2\lambda}u$. So we see that after the spontaneous symmetry braking we have one massive photon and a Higgs.

2.3.2.2 The SM and Higgs mechanism

Now we want to make a gauge theory that is able to combine EM and weak interaction and is the hole point of this subsection. SM and EW are based on the Lagrange of $SU(2) \bigotimes U(1)$[14]

$$\mathcal{L}_{SM} = \mathcal{L}_{gauge} + \mathcal{L}_f + \mathcal{L}_{Higgs} + \mathcal{L}_{Yukawa}. \tag{2.58}$$

The second term is the fermion one that is described by

$$\mathcal{L}_f = i\overline{\Psi}_L \not{D} + i\overline{\psi_R} \not{D} \psi_R. \tag{2.59}$$

So when the derivative takes place and each part of 2.59 will be

$$D_\mu \Psi_L = (\partial_\mu + igW_\mu + ig' Y_L B_\mu)\Psi_L \tag{2.60}$$

and

$$D_\mu \psi_R = (\partial_{mu} + ig' Y_R B_\mu)\psi_R. \tag{2.61}$$

Where R, are the right-handed and L the left handed chiralities $\psi_{L(R)} = (1 \mp \gamma_5)\frac{\psi}{2}$ [14]. And from EW we take that

$$q_L = \begin{pmatrix} u \\ d \end{pmatrix}_L, l_L = \begin{pmatrix} \ni_e \\ e^- \end{pmatrix}_L \tag{2.62}$$

where q are the quarks and l are the leptons. The transformation in the gauge theory in left and right is

$$\Psi_L \rightarrow \Psi'_L = \exp\{iY_L \theta(x)\} U_L \Psi_L \tag{2.63}$$

and

$$\psi_R \rightarrow \exp\{iY_R \theta(x)\}\psi_R \tag{2.64}$$

respectively. From the $SU(2)_L$ the only transformation that can to something on the field's doublet would be [14]

$$U_L = \exp\big\{iT^i \beta^i(x)\big\}. \tag{2.65}$$

As one can clearly see in 2.65 T^i are the half the Pauli matrices[3] and are the generators of $SU(2)_L$. They are non-abelian as

$$[T^i, T^j] = i\epsilon^{ijk} T^k. \tag{2.66}$$

Now lets see how B_μ and W_μ are transforming

$$B_\mu \rightarrow B'_\mu - \frac{\partial_\mu \theta}{g'}, \tag{2.67}$$

[3] $T^i = \frac{\tau^i}{2}$

$$W_\mu \to W'_\mu = U_L W_\mu U_L^\dagger + \frac{\partial_\mu U_L}{g} U_L^\dagger. \tag{2.68}$$

In EW, there will be spontaneous breaking of the symmetry, where $W^\pm$ and Z^0 will be produced. Hypercharge has a fixed value and so the electric charge should be the sum of left-handed doublets and hypercharge's ($Q = T^3 + Y$) [14].
Y for leptons and quarks should be

$$Y(l_L) = -\frac{1}{2}, Y(l_R) = -1, Y(q_L) = \frac{1}{6}, Y(u_R) = \frac{2}{3}, Y(d_R) = -\frac{1}{3}. \tag{2.69}$$

And the Langrangian would be

$$\mathcal{L}_{gauge} = -\frac{1}{4} F^{\mu\nu} F_{\mu\nu} - \frac{1}{4} G^{i\mu\nu} G^i_{\mu\nu}. \tag{2.70}$$

And we know that [14]

$$G^i_{\mu\nu} = \partial_\mu W^i_\nu - \partial_\nu W^i_\mu - g\epsilon^{ijk} W^j_\mu W^k_\nu, \tag{2.71}$$

$$F_{\mu\nu} = \partial_\mu B_\nu - \partial_\nu B_\mu. \tag{2.72}$$

Finally the mass term can't be added for fermions in the Lagrangian so we make a Dirac mass term that has left and right-handed couplings.

$$m\overline{\psi}\psi = m(\overline{\psi_L} + \overline{\psi_R})(\psi_L + \psi_R) = m(\overline{\psi_L}\psi_R + \overline{\psi_R}\psi_L). \tag{2.73}$$

2.4 Higgs boson Physics

In the area of experimental high energy physics, after the discovery of the Higgs boson, a new era has emerged [15]. After measuring the Higgs' boson aspects and decays, everything is according to SM theory. There is however, a theory prediction that goes beyond that model, which is known as BSM.
So we conclude that searching for a Higgs-like particle that is BSM is difficult because of the rare nature of these decays [16]. Such experiments are performed at LHC (CERN).
As said before EW spontaneous symmetry braking of SM, predicts the Higgs boson [16]. It has been measured that Higgs' mass is around $125\ GeV/c^2$. This Higgs like boson is "suffering from quadratically divergent self-energy correction at high energies" [16]. To solve this problem there is urgent need to extend the SM.
Until now there is no analysis that sees that decays and the energy scales that will be able to show such bosons are yet relatively unknown [16]. In this section we will present certain models that have been purposed to extend the SM.

2.4.1 Production Mechanism

Coupling between the Higgs boson and other fermions or bosons, is proportional to their mass. There are different production modes that contain some more massive bosons, such as weak force's W and Z and top quark. We will mention the most important ones that are:

- ggf through a heavy quark loop $gg \to H$.
- VBF $q_1 q_2 \to V^* V^* \to q_1' q_2' + H$.
- associated production of the Higgs boson with a heavy boson (VH) $q\overline{q} \to V^* \to V + H$.
- associated production of the Higgs boson with a pair of top quarks (ttH) $gg \to t\bar{t} + H$.

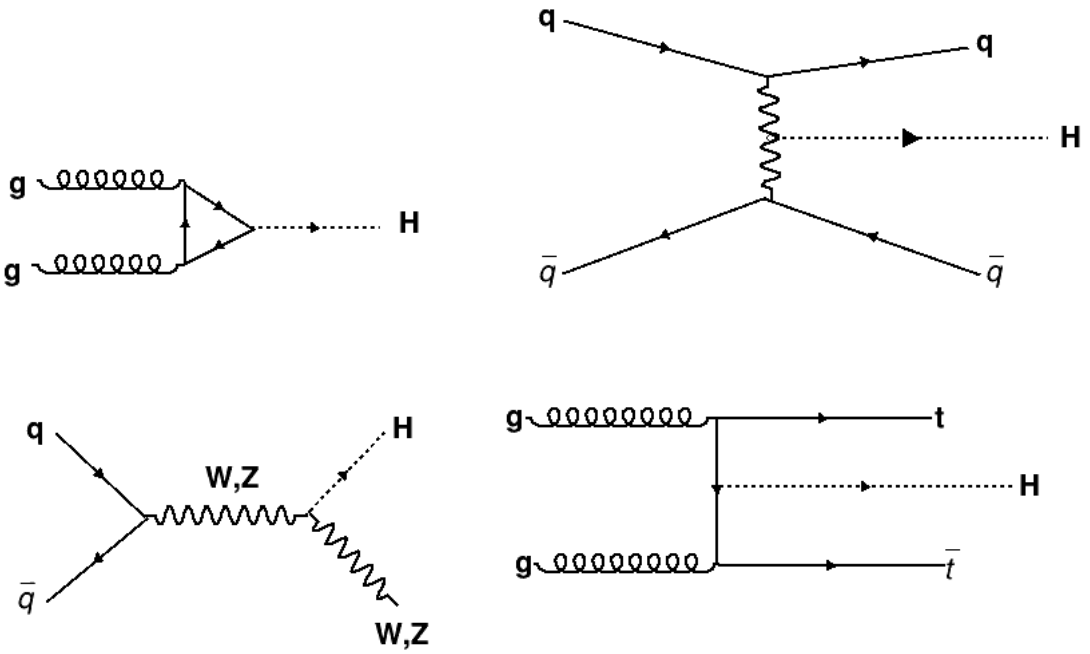

FIGURE 2.1: Feynman diagrams of the Higgs production. On the upper left corner is ggf fusion, on the upper right is VBF, on the bottom left is VH and on the bottom right is ttH.

To elaborate about production decays, the most dominant one in the LHC is ggf, via an intermediate top-quark loop. The Yukawa coupling of the Higgs and heavy quarks enhances ggf's cross-section, because they are abundant in the loop. The theoretical cross section of the lowest order is well-known and frequently used in many LHC studies to evaluate the experimental discovery potential of the Higgs particle. Although theoretically all quarks should be considered in the loop, practically, including only the top quark is sufficient. This is because the Higgs particle couples to the top quark about 35 times more strongly than to the next heaviest fermion, the bottom quark, resulting in a suppression of the bottom quark's contribution by a factor of 35^2. Consequently, measuring the ggF cross section also indirectly probes the Higgs

coupling to the top quark.
The VBF mechanism is notable for being the second most significant cross section in the production channels of the SM Higgs boson during hadronic collisions. Although its cross section is roughly an order of magnitude smaller than that of gluon-fusion, VBF still offers valuable additional insights. Illustrated in figure 2.1 , the VBF process involves heavy vector bosons being radiated from each incoming parton, which then "fuse" to create a Higgs boson. This production method is particularly intriguing due to its unique identifiers for Higgs boson detection, especially the presence of two forward quark jets that can be utilized for event identification. Additionally, VBF can be employed to examine the Higgs boson's coupling to W and Z bosons. This production method involves the annihilation of a quark pair into an off-shell (virtual) vector boson, followed by the emission of a Higgs boson and a real vector boson. Although it has a smaller cross section compared to other production mechanisms, Higgsstrahlung can be effectively utilized in Higgs boson searches due to its distinct signature. This is because the vector boson in the final state can decay into leptons, which can be reconstructed with high efficiency.
Measuring the production cross section of a Higgs boson alongside a pair of heavy quarks (primarily top quarks) serves as an excellent test for the Yukawa couplings. Since on-shell top quarks are too massive to result from Higgs boson decay, this decay process is kinematically impossible. Consequently, the process $pp \rightarrow ttH^{-}$ is the sole method to directly constrain the top Yukawa couplings. At the leading order, this mechanism occurs through the annihilation of a quark and an antiquark into a pair of top-antitop quarks, with the Higgs boson being radiated from a top quark in the final state.

2.4.2 Higgs Decays

In the Standard Model (SM), a Higgs boson with a mass of $125\ GeV$ can decay into four b quarks through an intermediate ZZ^{*} state. However, this branching ratio is quite small, around 10^{-4}. The $b\bar{b}$ pair produced by the on-shell Z boson is not tightly collimated due to the large mass of the Z boson, leading to a significant and challenging QCD background.[8]

2.4.2.1 Motivation for Exotic Higgs

The exploration of exotic Higgs particles is a rich and multifaceted area of research. It encompasses theoretical motivations to extend and complete the Standard Model, experimental searches for new phenomena, and phenomenological implications for cosmology and particle

physics. Future experiments at the LHC and other colliders, will continue to probe these possibilities, potentially uncovering new aspects of the Higgs sector.
In the 2HDM+S model, which includes two Higgs doublets and an additional light singlet, the Higgs boson can decay as $h \to ss$ or $h \to \alpha\alpha$, where $\overline{s}$ (or $\overline{\alpha}$) represents a mostly-singlet (pseudo)scalar. Depending on the value of $\tan\beta$, the decays $s \to b\overline{b}$ or $\alpha \to b\overline{b}$ are also typical, though not guaranteed, in all four types of 2HDM, provided that the masses m_α and m_s are greater than twice the mass of the b quark.[8]

2.4.3 Extended Higgs sectors

Recent research on the observed scalar particle with a mass of $125\ GeV$ and properties matching the Standard Model (SM) Higgs boson has led to stringent constraints on SM extensions that include scalar sectors. Numerous theoretical models predict that the Higgs boson can decay into non-SM particles. Without relying on specific assumptions about the Higgs boson's interactions, the ATLAS and CMS collaborations at CERN have set exclusion limits on the branching fractions of the Higgs boson to beyond the SM (BSM) particles. These experiments combined their results to constrain these branching fractions to less than 50% at a 95% confidence level. It is anticipated that future LHC experiments will be able to limit branching fractions to a few percent with improved measurement precision. An intriguing possibility is that the observed Higgs boson decays to lighter scalars or pseudoscalars.[11]
The SM Higgs boson has a naturally narrow width relative to its mass, attributed to its weak Yukawa couplings with SM fermions. This suggests that any new non-SM state is likely to possess a larger partial width and a notable branching fraction compared to decays into SM particles. Examples of BSM models that account for such decays include those with Higgs sectors that couple to both SM gauge bosons and fermions. Other models feature extended scalar sectors, such as those in 2HDM or the MSSM, where one Higgs field serves as the SM Higgs and another acts as a BSM doublet. The NMSSM, a variation of the MSSM, predicts an additional light scalar singlet that mixes with the observed Higgs boson and could influence baryogenesis.[11]
Both 2HDM and MSSM can yield a light pseudoscalar, with the NMSSM's a1 potentially being very light. In 2HDM, the mass of the light pseudoscalar is a free parameter, but for MSSM and NMSSM, fine-tuning is needed to maintain consistency with LHC data. The phenomenology of observed Higgs boson decays into pairs of lighter Higgs bosons is explored in various studies. Additionally, the alignment limit scenario, where the Higgs boson mass closely matches the observed value, allows for a wide range of parameter space.[11]
In the case of the 2HDM, it includes five physical states with distinct masses and couplings. One of these parameters, $\tan\beta$, represents the ratio between the vacuum expectation values of the two doublets. The scalar sector of the 2HDM can significantly influence the properties

of the discovered Higgs boson, especially in the alignment limit where the observed Higgs has properties closely resembling the SM prediction. The 2HDM, particularly when including a light pseudoscalar, offers a rich phenomenology that remains consistent with LHC observations for a wide range of parameters.

At the lowest order, there are four types of 2HDM that do not involve flavor-changing neutral currents (FCNC). These can be categorized based on how each fermion couples to the doublet structure, as shown in table 2.1. The Yukawa couplings of the pseudoscalar boson in the 2HDM, relative to those of the Higgs boson in the SM, are functions of $\tan\beta$ and the type of 2HDM, as detailed in table 2.2. Type-1 and Type-2 models are the most commonly considered, with the latter being required in supersymmetric models. In these two cases, leptons have the same couplings as down-type quarks. In Type-3 2HDM, all quarks couple to Φ_2, and all leptons couple to Φ_1, resulting in leptonic or quark couplings of the pseudoscalar being proportional to $\tan\beta$ or $\cot\beta$. Thus, for large $\tan\beta$, the leptonic decays of a dominate.[11]

As previously mentioned, a complex $SU(2)_L$ singlet field S can be added to 2HDM; such models are termed 2HDM+S and include the NMSSM as a special case. If S mixes only weakly with the doublets, one of the CP-even scalars can exhibit SM-like properties. The inclusion of the singlet S leads to two additional singlet states: a second CP-odd scalar and a third CP-even scalar. These states inherit a mix of fermion interactions from the Higgs doublets. With mixing among the spin-0 states, the result is two CP-odd scalars. Of these, one can be identified with the observed SM-like state, h. The branching fraction of the h boson into a pair of CP-even or CP-odd bosons can be significant, leading to a wide array of possible exotic Higgs decays.[11]

	Type-1	Type-2	Type-3(lepton-specific)	Type-4(flipped)
Up-type quarks	Φ_2	Φ_2	Φ_2	Φ_2
Down-type quarks	Φ_2	Φ_1	Φ_2	Φ_1
Charged leptons	Φ_2	Φ_1	Φ_1	Φ_2

Table 2.1: The Higgs doublets to which various types of fermions couple in the four types of 2HDM without FCNC at the lowest order.[11]

	Type-1	Type-2	Type-3(lepton-specific)	Type-4(flipped)
Up-type quarks	$\cot\beta$	$\cot\beta$	$\cot\beta$	$\cot\beta$
Down-type quarks	$-\cot\beta$	$\tan\beta$	$-\cot\beta$	$\tan\beta$
Charged leptons	$-\cot\beta$	$\tan\beta$	$\tan\beta$	$-\cot\beta$

Table 2.2: The ratio of the Yukawa couplings of the pseudoscalar boson $\overline{\alpha}$ in the 2HDM, compared to those of the Higgs boson in the SM, for the four types of 2HDM without FCNC at the lowest order.[11]

Chapter 3

The CMS detector

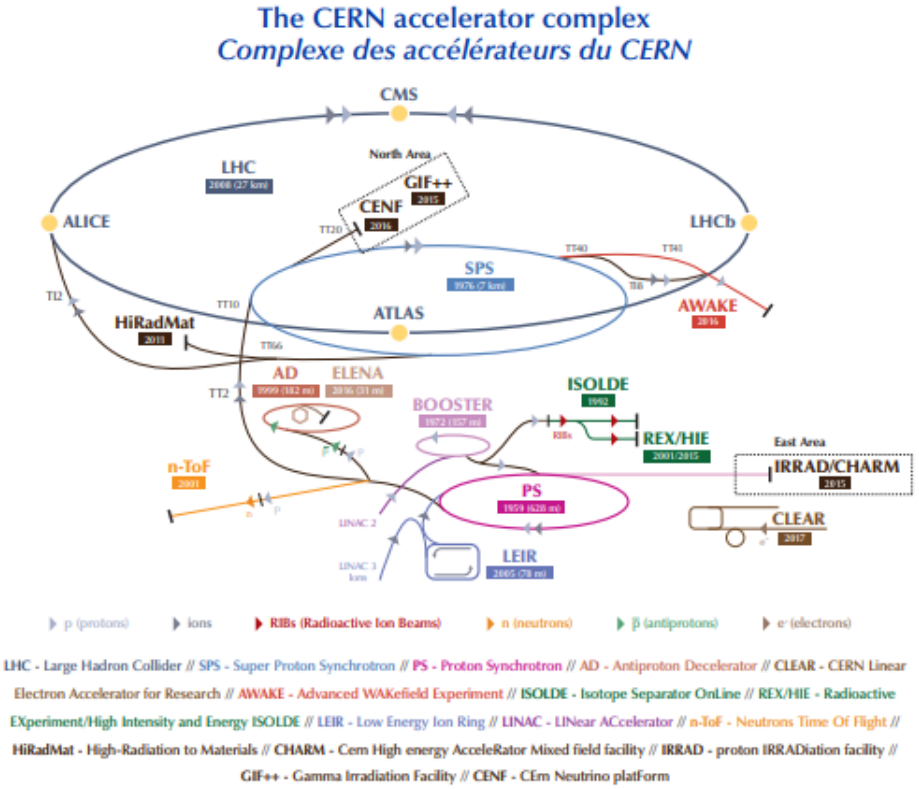

FIGURE 3.1: Render of the LHC detector, with the four large experiments, injecting and detection.

3.1 The Large Hadron Colider (LHC)

The LHC main purpose is to unwind the mysteries behind EW symmetry breaking. That breaking is direct result of the Higgs mechanism. LHC's design main goal is to study phenomena at the TeV scale [17].

Particles used	Protons
Circumference	$26659\ m$
Injected beam energy	450 GeV (protons)
Nominal beam energy in physics	7 TeV (protons)
Magnetic field at 7 TeV	8.33 Tesla
Operating temperature	1.9 K
Number of magnets	9300
Number of main dipoles	1232
Number of quadrupoles	858
Number of correcting magnets	6208
Number of RF cavities	8 per beam. Field strength at top energy 5 MV/m
RF frequency	400 MHz
Revolution frequency	11.245 kHz.
Power consumption	180 MW
Gradient of the tunnel	1.4%
Difference between highest and lowest points	122 m.

TABLE 3.1: The LHC parameters.[1]

LHC is the biggest collider in the world, not only by size but by energy too. It is located between Geneva, Switzerland and France. It was firstly used at 2008. Its shape is a huge cycle, with a perimeter of about 27 km. It is buried $100\ m$ deep into the ground. LHC's huge energies make measures of cross sections, that have never seen before possible.

LHC is accelerating hadrons, that are mostly protons, but can accelerate ions too. Two opposite moving beans are accelerated to different directions, in to different solenoids. The two main parameters of LHC are the colliding energy and the luminosity. Energy is used in order to determine if and what particles will be produced. Luminosity measures the rate of all possible combinations of collisions over the area of the beam.

In order to reach the luminosity needed to create big data[1], we need as many collisions as possible. That can be achieved by increasing the frequency of these collisions and the hadron number in each beam. For luminosity $L = 10^{34} cm^{-2} s^{-1}$ there are about 2800 bunches. Each one of these has about 1.15×10^{11} protons. The collision frequency is $f = 40\ MHz$. LHC's energy has reached a point where its energies are $\sqrt{s} = 14\, TeV$. In order to curve each bunch we use about 1200 superconducting magnets and for focusing the bunch there are used about 400. All these magnets are producing a magnetic field of about 8 Tesla. To achieve a magnetic field that high, these magnets have a temperature of $-273.3\ ^oC$ that use liquid Helium to achieve such temperatures. Lastly inside each magnet there are two vacuum chambers that are the tracks for the bunches. As seen in figure 3.2 the LHC is not a perfect cycle. It is consisted of eight arcs and insertions, to be more specific, there are eight 2.45km arcs and eight 545 m straight sections.[1]

[1] the bigger the data the better analyses

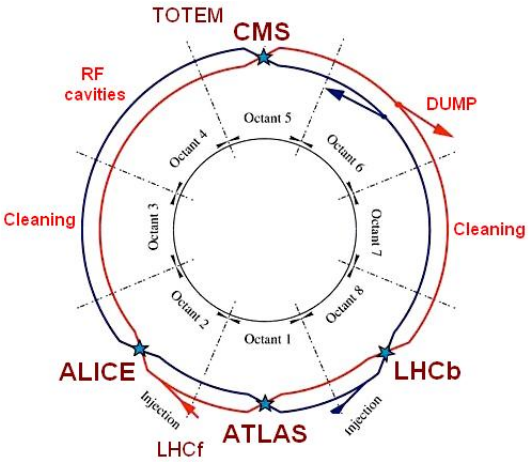

FIGURE 3.2: LHC layout.[1]

Inside LHC there are four particle detectors. Each one is a different experiment, the detectors are

1. ATLAS, that is a toroidal LHC apparatus[1],
2. CMS, that is the compact muon solenoid[1],
3. ALICE, that is a large ion collider[1],
4. LHCB, that is the study of physics in B-meson decays at LHC[1],

finally there are smaller projects such as antimatter factory, TOTEM, etc.

3.2 CMS: Compact Muon Solenoid

CMS is a detector that is placed inside the LHC, it's purpose is to search the Higgs boson and see if the SM is correct. It is also looking for dark matter, exactly as ATLAS[1], with differences in hardware and in design.
This detector is inside a huge superconducting coil. It was build in pieces and assembled underground, its dimensions as seem in figure 3.1 are absolutely huge.
Inside the CMS, there is a layer of silicon-based that is working as a particle tracker,[1] this tracker is inside a calorimeter that measures electromagnetism and after that there is an even bigger hadron calorimeter. All of these measuring tools rest inside a superconducting solenoid magnet, which can count the momentum and lastly all of the above are inside the huge muon detector.

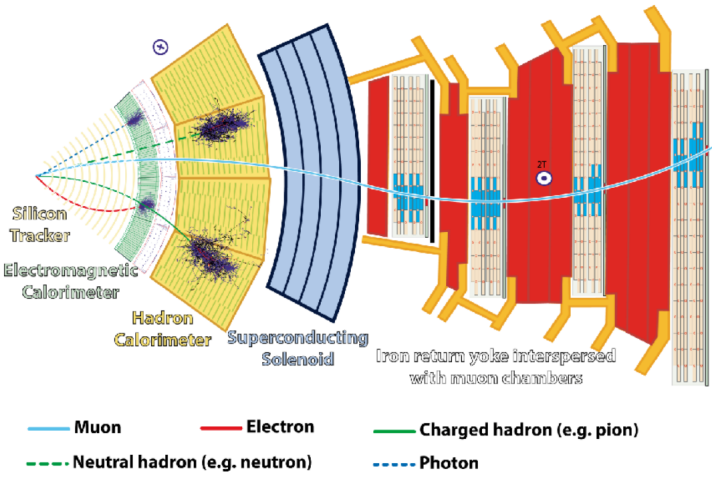

FIGURE 3.3: A transverse slice of the CMS detector and the particles detected by each subdetector.

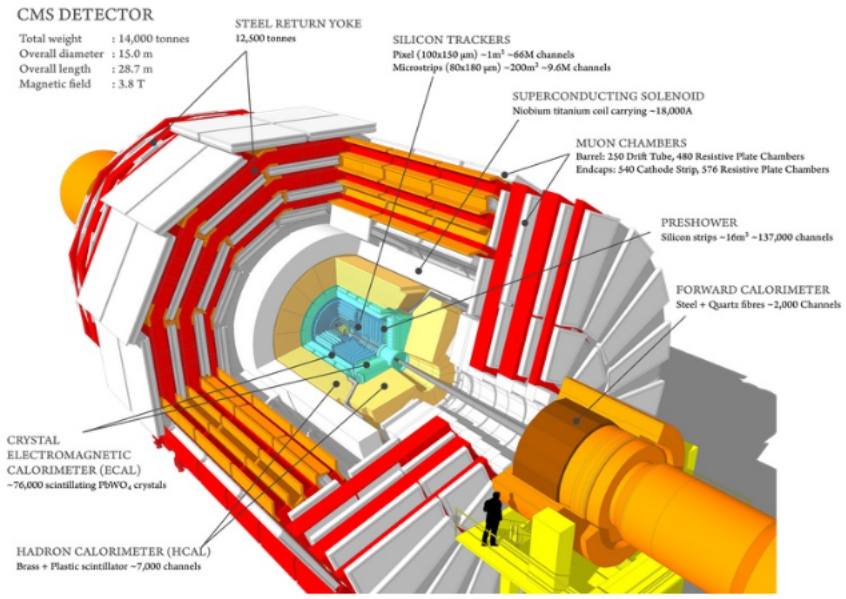

FIGURE 3.4: 3-D render of the CMS detector that shows its parts [1]

3.2.1 Tracker Detector

The tracker detector is a momentum measuring tool. They don't directly measure it but instead they see it's path in the magnetic field. Path's curvature is in a way inversely proportional to the momentum.[2] At CMS, the tracker is keeping up with the paths that photons are taking, by seeing their position in comparison to a number of fixed points. These trackers are able to see the paths of all kinds of particles, so they see the hadrons before and during the collision and their products and even the relatively short lived ones such as b-quarks.

There are some building challenges for those trackers. One of them is that although the tracker must be as accurate as possible to keep up with all kids of particles, it needs to be as much light

[2] the bigger the curvature the smaller the momentum

	coverage in $\mid \eta \mid$	radius in m	measures
Tracker	pixel: < 2.4 strip: < 2.4	0.05→0.11 0.02→1.16	momentum change
ECAL	barrel: < 1.479 endcap: $1.479 \rightarrow 3.0$	1.24→1.86 3.2	γ & e^- energy
HCAL	barrel: < 1.4 endcap: $1.3 \rightarrow 3.0$ forward: $3.0 \rightarrow 5.2$	$1.77 \rightarrow 2.95$ 3.9 11.2	hadron energy
Solenoid Magnet	-	$2.95 \rightarrow 3.25$	particle tracks bent
Muon Detectors	barrel: < 1.2 endcap: $0.9 \rightarrow 2.4$	$3.8 \rightarrow 7.38$ 5.0	muons (identification)

TABLE 3.2: CMS characteristics

as possible, because if it isn't, it will mess up the courses of everything during the collisions. This riddle was solved by recreating the tracks by measuring as little points as possible, with an accuracy of $10\mu m$. Because tracker is located in the heart of the detector, its materials should endure big chunks of radiation. That material is silicon, which makes up the pixels at detectors heart and the microchips that are aright outside the core.[2]

Detection of the actual particles is talking place in the pixels, that produce signal each time a particle interacts each them and the chips are processing it. That signal is almost infinitesimally small, it is then stored in the chip and after a short amount of milliseconds it is processed and sent to a laser, so it can be translated to infrared pulses. Those pulses need to be send in a tiny radiation place and that job is done by a long fiber optic. The last step is the analysis of the signal.[2]

3.2.1.1 Silicon Pixels

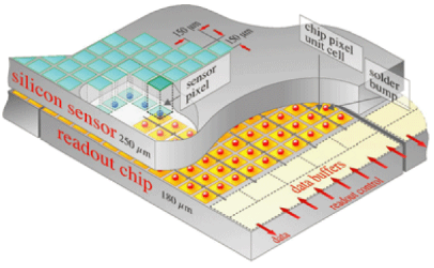

FIGURE 3.5: CMS silicon pixel inside the detector [2]

The CMS is consisted of millions of pixels, that are making up its laser focused accuracy. In addition CMS is built extremely close[3] to the hadron tracks. In figure 3.5 we see a silicon sensor and a readout chip.

Each layer is consisted of modules, that are spit into sensors, which are the pixels.[2] Every

[3] the closest of all the other detectors [2]

time a particle passes through a pixel, its energy is enough to ionise the electrons of these silicon atoms.[2] After that, the voltage that is applied to the senors is collecting the electrons and creates a signal, that is later read by the chip.[2]

3.2.1.2 Silicon Strips

The next thing that rests after pixels are silicon strips and particles interact with ten layers of them.[2] It has four inner barrel layers that are placed inside shells, that posses two inner endcaps, that each one contains three discs. And the outer barrel is composed of six cycles with the same center. The tracker closes with two endcaps[2]. Pixels and silicon strips are the first layer of the CMS and they called all together the tracker

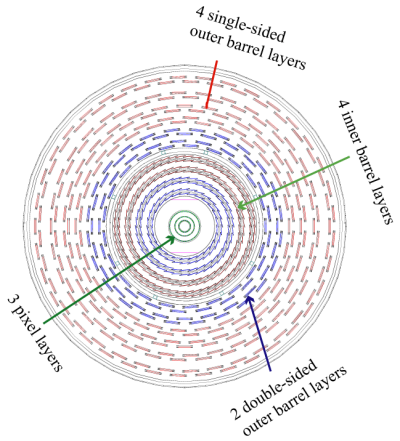

FIGURE 3.6: CMS silicon strips, perpendicular render[2]

3.2.2 Electromagnetic and Hadron Caloriemeters

Each particle that is the outcome of the collision has energy information. It is really important to understand the series and the results of each collision. To take these measures CMS is using two different tools.

The first tool is called electromagnetic caloriemeter (ECAL) and is placed in the inner layer (layer 2) in order to measure electron's and photon's energy and does so by stopping them completely.[2] We know that hadrons are not elementary, but rather made up from quarks and gluons can pass through the ECAL, that's where we need the hadron caloriemeter (HCAL) to stop them completely in order to measure them and that is the next layer (layer 3).

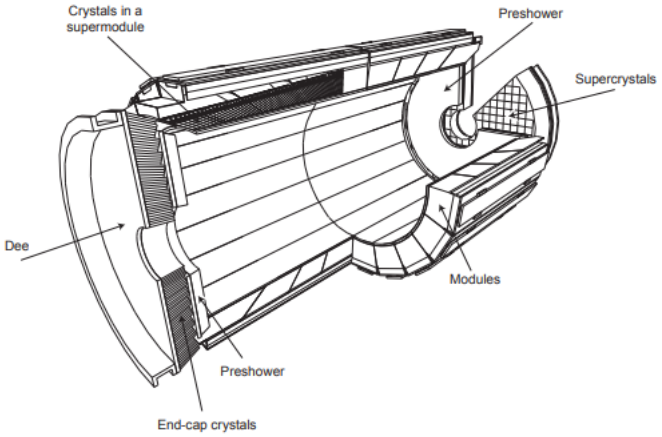

FIGURE 3.7: CMS electromagnetic calorie-meter.[3]

3.2.3 Solenoid Magnet

CMS is built around a solenoid magnet, that its magnetic intensity is 4 Tesla. This magnet is helping the measures of change and the mass, so that we can get their ratio. The curve that the magnet causes is the key component for that measurement. While operating the intensity is lowered to 3.8 Tesla to maintain longevity.
So the usage of this magnet is to oversea the paths of the particles, the curvatures are inversely analogous to the magnetic field and that path gives information about the momentum. This magnet is layer 4.

3.2.4 Muon Detectors

Letter M in CMS,stands for muons. So one can realise that detecting them has a great significance. A muon is a particle that has charge as electrons, with the difference that is is about 200 times heavier.[2] Muons are emitted via a number of decays, with the most important one being Higgs decaying to four muons.
When muons are emitted, they penetrate without the loss of information, so they are not stopped at the ECAL and HCAL.
Hence to measure them we need an extra layer, that would be layer 5. This is the most external layer and contains chambers[2] that would only detect muons[4]. There are four muon stations, located right outside the magnet coil. These station inform us about the path, that is bended by the high magnetic field, by tracking the muon. To make the precision higher, we combine there measures with the silicon trackers.[2] This system has the potential to generate massive amounts of data, so the system must (and is) able to erase background noise and is naturally robust.[2]

[4]as they will be the only ones to survive

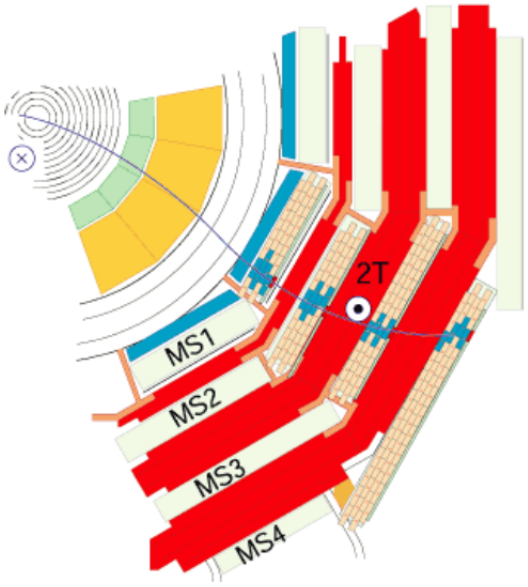

FIGURE 3.8: Muon detector render[2]

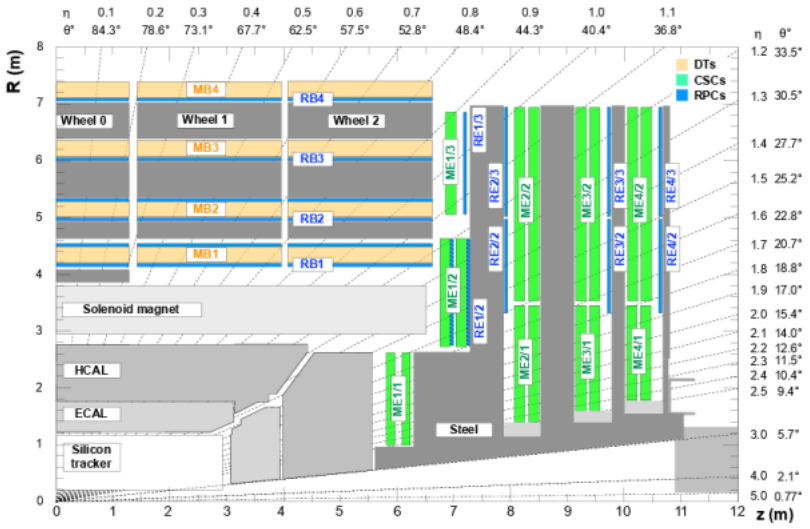

FIGURE 3.9: Cross-sectional view of the CMS detector in the (r,z) plane. We can see the muon detector layout.

The muon system as we see at figure 3.8 is consisted of 2 million cathode strip chambers, that are thinner than human hair. [2]

3.2.5 Trigger

CMS gets a big load of data every second, form these data only a very small fraction has significant information.[2] Hence the need of a trigger system, that will separate those events that are somewhat interesting and are producing the Higgs like boson.[2]

These procedures cut some of the ”junk”, but still the volume of data is tremendous. The solution to this problem is to store these data and process it in the same time, that storage must be able to separate the events chronically.
The first level is a fully automated process that is looking for some spectacular or unusual events.[2] This level acquires a huge computing power. Despite the first level triggering, the data acquisition is still immensely big, so we need more triggering technology to extract information.
So the need for a two level trigger is born. Before CMS, triggers were simple counters of particles, but after CMS we needed to characterise the objects before selecting them. That sorting technique is very time thirsty, so to meet these needs, customs chips where built. Now triggering answers to the question: ”Is there an electron above an ET threshold back-to-back with a jet above that threshold?”[2] instead of searching just for the number of them.

Chapter 4

Physics of pp collisions at the LHC

Inside LHC, protons are accelerated at speeds near the speed of light. These particles are then collided in the detectors, which are then analysed. These collisions produce new smaller particles, so one can say that big accelerators are ”super microscopes”.[1]

4.1 Proton's Structure

Protons are stable particles that live in the nucleus of an atom. It electric charge is the same as electrons but positive. It's mass is about 1836 times bigger than an electron and a bit less massive than neutron. Proton is following Fermi's statistics, so its spin is $\frac{1}{2}$ and are consisted of three quarks that are connected with three gluons, two up and one down, which makes them hadrons.[4]

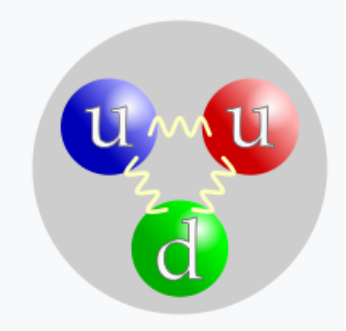

FIGURE 4.1: Render of a proton and its structure, forces are shown with gluons and colors are arbitrarily assigned [4]

Proton's mass as ,explained by QCD, needs special relativity to make sense. And that's because, proton's mass is about 90 times bigger than the sum of all three quarks, that consist it. While gluons are massles at their rest state. The mass that we miss is the energy ($E = mc^2$) accounts

for more than 99% and is the internal kinetic energy of quarks and gluons.[4]
The mass of the quarks that are making up protons is spit in two categories.

1. Current quark mass, that is quarks rest mass.[4]
2. Constituent quark mass, is the current mass plus the gluon field around the quark.[4]

QCD tells us that protons mass is consisted $\sim 9\%$ of up and down comprehensions plus a near to infinity number of virtual particles, $\sim 32\%$ of quark kinetic energy, $\sim 37\%$ of gluon kinetic energy and $\sim 23\%$ of anomalous gluonic contribution.[4] Protons wavefunction would then be

$$\begin{aligned} |p_\uparrow\rangle = \frac{1}{18}(2\,|u_\uparrow d_\downarrow u_\uparrow\rangle + 2\,|u_\uparrow u_\uparrow d_\downarrow\rangle + 2\,|d_\downarrow u_\uparrow u_\uparrow\rangle - |u_\uparrow u_\downarrow d_\uparrow\rangle - \\ |u_\uparrow d_\uparrow u_\downarrow\rangle - |u_\downarrow d_\uparrow u_\uparrow\rangle - |d_\uparrow u_\downarrow u_\uparrow\rangle - |d_\uparrow u_\uparrow u_\downarrow\rangle - |u_\downarrow u_\uparrow d_\uparrow\rangle).[4] \end{aligned} \tag{4.1}$$

So it is clear that protons structure and mass is really complicated, making it the perfect candidate to be studied in the huge microscope that is the LHC.

4.2 Hard Parton Scattering

At particle collision experiments, one of the most important variables is the center of mass energy. We write it as $\sqrt{s}$ and is the energy that creates particles and their kinetic energy. This energy is based on the four-vectors, of the protons

$$\begin{aligned} s = (P_1 + P_2)^2 = P_1^2 + P_2^2 + 2P_1P_2 = \\ (E_1^2 - \vec{p}_1^2) + (E_2^2 - \vec{p}_2^2) + 2(E_1E_2 - \vec{p}_1\vec{p}_2), \end{aligned} \tag{4.2}$$

where $E_1,\ E_2,\ \vec{p}_1,\ \vec{p}_2$ are energies and three dimensional momentums. We know that $E_1 = E_2$, because each bunch has the same energy. If we take these to 4.2 we got

$$\sqrt{s} = 2E_p \tag{4.3}$$

Perturbation theory is describing the hard scattering. For partons that have a small percentage of the initial momentum of protons, the center of mass energy is not the same as the one that protons had. Their masses are small in relation to their momentum, the center of mass energy is

$$\hat{s} = (p_i + p_j)^2 = 2x_ix_jP_1P_2, \tag{4.4}$$

where $x_i,\ x_j$ are the percentages.

4.2.1 Cross Section

Cross section for a pp collision is about $100mb$[5], but only a small fraction of it is related to LHC, as protons are elastically scattered and then react with their partons. So after subtracting those difractive interactions, cross section is about $70mb$.[5]

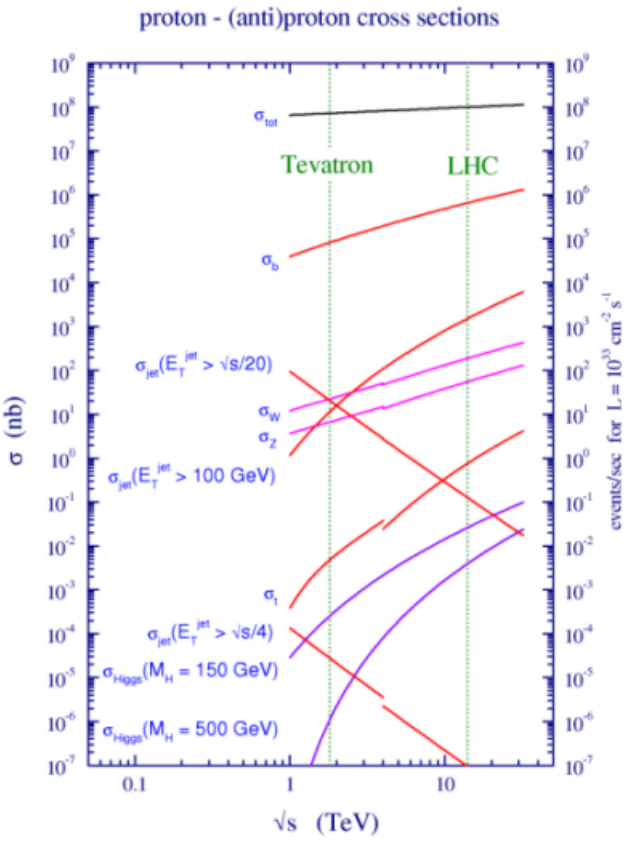

FIGURE 4.2: Cross sections per center mass energy, for typical pp collisions[5]

This number is seem quite big, while looking at figure 4.2 one can realise that these cross sections, for absolutely typical procedures, are small. That's the reason that proton bounces should be big enough[1] to produce interesting collisions.

4.2.2 Luminosity

As we analyse proton-proton collisions, one of the most important quantities[2] is luminosity. Which is the number of events that are detected over a finite amount of time and the cross-section[18]

$$L = \frac{dN}{\sigma dt}. \tag{4.5}$$

[1] with a lot of protons per bunch
[2] in scattering theory and accelerator physics[18]

As we can imagine, luminosity should depend on the parameters of the beam. These parameters are its width and flow rate, additionally target properties like size and density.[18] One quantity that springs from luminosity is the integrated luminosity that is

$$L_{int} = \int L dt. \tag{4.6}$$

These quantities can give information about the quality and strength of particle accelerator, that needs big values of integrated luminosity to extract a bigger amount of data.[18]

4.2.3 Underlying Event

The interaction between two beams, at a collision point that is not the collision that we investigate is an underlying event. In the LHC, there are events that their origin doesn't come from hard scattering, those are UE.[19]
After a scattering reaction, there are remained products of the event. These should be filtered out to see the signal.[19]
In the collisions between two protons, there are particles that are coming from parton scattering. If these particles have high Q^3 relative to the QCD one, then hard process will have a low p_T and remnants from the collisions. All these parton interactions are not easy to be separated. So to clean the signal, one should make a separation between the kinematic region, which has pieces of partons that hard scattering creates and the rest that are called as said UEs.

4.2.4 Pile Up

Pile up is the phenomenon of multiple collisions, additionally to the one of interest.[20] Pile up is a very hard to solve problem at the analyses that are done at LHC, as the collision number is huge and the window of detection not small enough. Luminosity is rising per run, so the majority of objects are affected by pile up. So there is immense need for deep understanding and eradicating as possible of this phenomenon. To eradicate pile up background, we need to understand it. There are five categories of pile up:

1. In time pile up, contemporary collisions between protons that are in the same bunch with the ones that we are interested.[20]

2. Out of time pile up, collisions between protons that took place right before or right after the collision of interest. These collision affect measurements, because the window of detection is bigger than the time that occurred between them.[20]

[3] here Q is the transfer of four-momentum

3. Cavern background, random collisions that origin from a cloud of neutrons and photons that are almost everywhere at the time of the collision.[20]
4. Beam halo events, as the bunch of protons is scraping against an up-stream collimator, sprays of muons will run paraller to the beam line.[20]
5. Beam gas events, these occur away from center of the detector and in that place there are collisions between proton bunch an residual gas inside beam-pipe.[20]

So now the bunch Luminosity will be

$$L_b = \frac{\mu f_r}{\sigma}, \tag{4.7}$$

where μ is the pile up parameter that is the average number of inelastic interactions per bunch, f_r is the frequency of the bunch revolution. And the total instantaneous luminosity will be

$$L = \sum_{b=1}^{n_b} L_b = n_b < L_b >= n_b \frac{< \mu > f_r}{\sigma}, \tag{4.8}$$

where n_b are the bunch pairs.[21]

4.3 Detector Simulation

When a charged particle traverses the detector, it generates electron-hole pairs in semiconductors or electron-ion pairs in gaseous mediums, which drift toward the electrode, producing an induced signal. Consequently, the presence of an incoming charged particle is detectable via the signal on the electrode. A specific energy loss alone is insufficient to identify the type of incident particle (e.g., electron, muon, pion). Hence, to ascertain the particle type, momentum measurement is also necessary. Determining momentum involves reconstructing the charged particle's trajectory in a magnetic field.[6]
The performance of the HEP experimental apparatus (detector) is assessed using numerical Monte Carlo (MC) simulations. To determine the track's radius of curvature, at least three points (i.e., three detector layers) are necessary. This ultimately determines the minimum transverse momentum that can be reconstructed. Key questions arise, such as: how many layers are required? What is the optimal spacing between layers? What are the uncertainties on the measured points and momentum? Precise determination is achievable only through detector simulation.[6]
We begin by simulating a charged particle with a specified momentum in our experimental setup. The track's intersection with the detector planes marks the true points. Next, we attempt to reconstruct these points using the signals from the detectors to determine the reconstructed momentum. There is a distinction between the true and reconstructed positions and

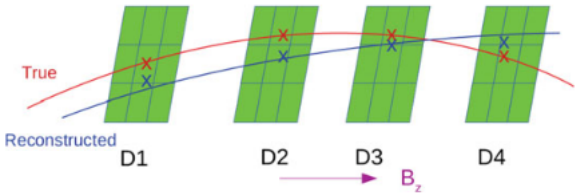

FIGURE 4.3: Detector layers (D1, D2, D3, D4) are shown alongside the true track (red line) with true points (red markers), as well as the reconstructed track (blue line) with reconstructed hits (blue markers).[6]

momentum due to finite uncertainties related to the pixel size (measuring points), effects of multiple scattering within the material, residual biases in the track fitting algorithm, and other factors. Consequently, the RMS of the differences between the reconstructed and true positions or momentum, known as spatial and momentum resolutions respectively, is evaluated. These parameters are crucial for driving physics performance and must be optimized in the apparatus design. To achieve this, simulations employing a particle generator and transport code for Geometry and Tracking are utilized.[6]

4.4 Hadron Jets

With the word jet, we define a narrow cone that is consisted mostly of hadrons and in a smaller rate of other particles. These jets are produced after the collisions by the hadronization of quarks and gluons.[22] QCD dictates that quarks and gluons are not found alone in nature and it is known that these particles have color and all their final stages are colorless. After a high energy pp collision, quarks and gluons carry some of their color away, which due to QCD create other colored particles so the final product is colorless. The summation of all these objects is called a jet and is moving as a hole almost always at one direction.[22] We need jets to find out what properties did the initial quarks had.

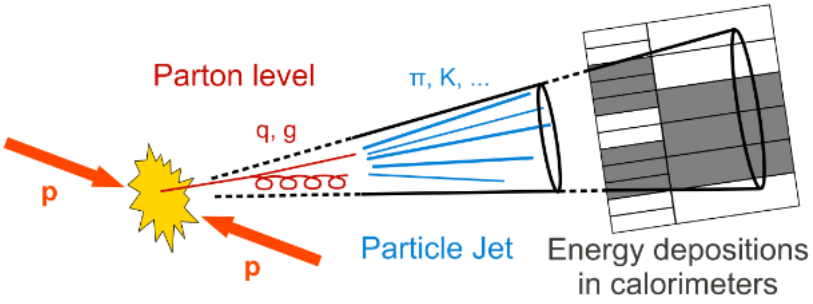

FIGURE 4.4: Jets at the CMS[2]

These jets are traveling in the detector and in the meantime they react with the tracker, ECAL

and HCAL. So to analyse these signals one have to built certain algorithms, with the goal to reconstruct the jet.

4.4.1 Reconstructing Hadron Jets

When reconstructing a jet, its energy is not the true particle-level energy, regardless the detector. There are two parameters that correct jet's energy to a certain number. The first is the detailed understanding of its energy scale the second is their systematic uncertainty.[2] This master thesis, is studying a decay that is detected in the CMS, so our method analyses will be within CMS. There are three reconstruction methods. These are

1. Calorimeter-based approach.[2]
2. Jet Plus-Track, that improves measures of the jets that are measured in calorimeter by exploited the associated tracks.[2]
3. Particle Flow, that reconstructs every single particle inside an event, by taking information from all the parts of the detector.[2]

Most analyses in the CMS use the third method and additionally they follow a specific sequence in correcting the jet energy. Initially, we take out pile up, then we find the non-linear response of ECAL and HCAL as a function of p_T and different scenarios of the response in pseudo-rapidity η, with their corrections found via the actual simulation.[2]

4.4.2 B-tagging

In the LHC, there is a big number of final states, that can be $t\bar{t}$ and $H \rightarrow b\bar{b}$, which include b quarks. Some of the most significant backgrounds in SM, BSM and SUSY analyses are $W/Z + b$ and $\gamma + b$, which also are b flavored. So a new challenge emerges while analysing data with b quarks, the actual identification of the b-jet along with its energy which is called b-tagging.[23] Three are the main characteristics of b-jets, that distinct them from other flavored ones.

1. they are long-lived
2. they are more massive
3. their energetic semileptonic decay

B-tagging is implemented by certain algorithms and in CMS they primarily rely on the three characteristics above. Their observables are, the impact parameter significance of the tracks,

secondary vertexes position and muons p_T relative to the direction of the jet.[24]
The actual algorithm's main goal is to create a discriminator value[24] that will give user the choice to select from a variety of regions. Each region has a trade-off that is efficiency vs purity.[24]
The algorithms are

1. Track counting algorithm, that is b-tagging if there is a number of tracks significant enough.[24]
2. Jet probability algorithm.
3. Soft-Lepton tagging algorithms, which work with electrons and muons from the semileptonic b-decay.[24]
4. Secondary vertex tagging algorithms, that reconstruct at least one secondary vertex.[24]

Each b-tagging algorithm can only perform so much. Each algorithm has a tagger with a varying efficiency. Selection tracking selection prevents the compromisation by pileup events.[24]

4.5 Kinematic Variables

Collider experiments, sometimes, use the Cartesian systems, where z-axis, is beams direction. So in that case the momentum $\vec{p} \equiv (p_x, p_y, p_z)$ will be decomposed into a longitudinal component p_z and a transverse momentum $\vec{p_T} \equiv (p_x, p_y)$.[7] In CMS some Cartesian components are traded for the magnitude of p_T

$$p_T \equiv \sqrt{p_x^2 + p_y^2}, \tag{4.9}$$

azimuthal angle

$$\phi \equiv \tan^{-1}(\frac{p_y}{p_x}) \in [0, 2\pi) \tag{4.10}$$

and polar angle

$$\theta \equiv \tan^{-1}(\frac{p_T}{p_z}) \in [0, pi) \tag{4.11}$$

The momentum is a vector with three dimensions, if we add energy we got a four-dimensional (3+1) four-vector $p^\mu = (E, \vec{p})$ and the invariant mass emerges that is

$$m \equiv \sqrt{p^\mu p_\mu} = \sqrt{E^2 - \vec{p}^2}. \tag{4.12}$$

Hence transverse energy is

$$E_T \equiv \sqrt{m^2 + p_T^2}, \tag{4.13}$$

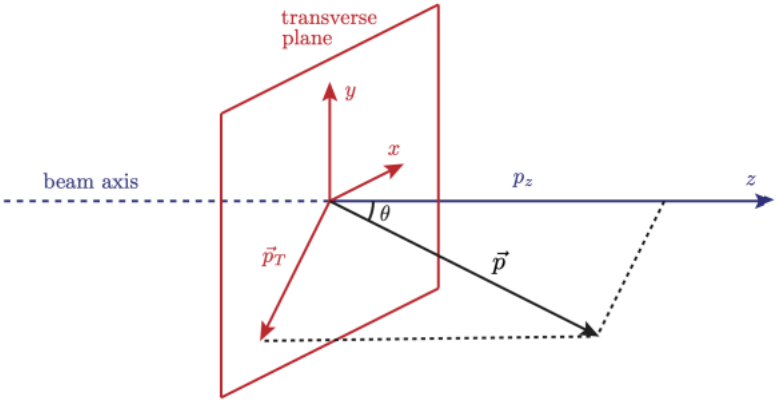

FIGURE 4.5: Any three-dimensional vector can be a longitudinal component p_z and a transverse one $\vec{p_T}$.[7]

where $\vec{p_T}$ is a (2+1) dimensions vector $p^\alpha = E_T, \vec{p_T}$.[7]
The next kinematic variable that we want to create is rapidity, which is

$$y \equiv \frac{1}{2} \ln \left(\frac{E + p_z}{E - p_z} \right), \tag{4.14}$$

if the particles are massless this variable reduces to pseudo-rapidity

$$\eta \equiv - \ln \left[\tan \left(\frac{\theta}{2} \right) \right]. \tag{4.15}$$

The initial state's transverse momentum is zero

$$\sum_a \vec{p}_{aT} + \sum_b \vec{q}_{bT} = 0, \tag{4.16}$$

where $\vec{p}_{aT}$ is the visible particles momentum and $\vec{q}_{bT}$ is the invisible particles momentum. And the missing transverse momentum $\not{\vec{p}}_T$ that is[7]

$$\not{\vec{p}}_T \equiv \sum_b \vec{q}_{bT} = - \sum_a \vec{p}_{aT}. \tag{4.17}$$

In addition there is MET, that is the energy lost due to invisible particles and is equal to

$$\not{E}_T \equiv | \not{\vec{p}}_T | = | - \sum_a \vec{p}_{aT} | \text{ , } \alpha\text{=jets or leptons.} \tag{4.18}$$

For our analysis there are additional variables, such as the scalar sum of the transverse momentum of hadron jets.

$$H_T = | \sum_a \vec{p}_{aT} | \text{ , } \alpha\text{=jets} \tag{4.19}$$

and the scalar sum of all transverse momentum that are visible and are either hadronic and leptonic.

$$S_T = \left| \sum_a \vec{p}_{aT} \right| , \alpha\text{=jets or leptons.} \tag{4.20}$$

4.5.1 Cylindrical Coordinates

To understand the above, we need to analyse cylindrical coordinates. The momentum of a particle is defined as the product of its mass and velocity:

$$\mathbf{p} = m \cdot \mathbf{v} = (p_x, p_y, p_z)$$

In spherical coordinates with the origin at the collision point, the momentum ($\mathbf{p} = (|\mathbf{p}|, \theta, \phi)$), where ($\theta$) is the polar angle and (ϕ) is the azimuthal angle. Due to the cylindrical shape of most detectors, a new parameter called *pseudorapidity* is used:

$$\eta = -\ln[\tan(\theta/2)] \tag{4.21}$$

with values ranging from ($(-\infty, \infty)$).
In the context of hadron collider physics, pseudorapidity is favored over the polar angle (θ) because particle production is approximately uniform as a function of pseudorapidity.[1]
Additionally, transverse momentum, (p_T), is preferred and is calculated from the transverse energy measured by calorimeters. Thus, in particle physics, the linear momentum is expressed as:

$$\mathbf{p} = (p_T, \eta, \phi) \tag{4.22}$$

To convert to Cartesian coordinates (p_x, p_y, p_z) with the z-axis as the beam axis, the following transformations are used:

$$p_x = p_T \cos\phi \tag{4.23}$$

$$p_y = p_T \sin\phi \tag{4.24}$$

$$p_z = p_T \sinh\eta \tag{4.25}$$

and

$$|\mathbf{p}| = p_T \cosh\eta \tag{4.26}$$

Since protons that collide head-on possess identical momentum values of (7 TeV$/c$) but travel in nearly opposite directions (the beams intersect at an angle of about 200 mrad), the resultant particles from the collision must collectively exhibit zero net momentum:

$$\vec{P} \approx 0 \tag{4.27}$$

Chapter 5

Analysis

This chapter is dedicated in the analysis of MC data from the CMS and its purpose is to determine the upper limit of the branching ratio of the exotic Higgs decay $hW \to a(bb)a(bb)ll$. This Higgs decays into two α bosons that have zero spin and each of them decays into a $b\bar{b}$ pair. These data are generated from collisions with center mass energy $\sqrt{s} = 13TeV$, detected by CMS at Run 2 in the year 2017 and have an integrated luminosity of $L = 41.5fb^{-1}$.

5.1 Physical Processes

Here we will analyse the main characteristics of each process that is theoretically taking place inside the CMS.
A more practical experimental scenario is found in models where the Higgs decays into new particles labeled as "X," which subsequently decay into pairs of b quarks. This decay pattern can occur in various new physics scenarios, such as the general 2HDM+S model, extensions of the SM with hidden light gauge bosons, the (R-symmetry limit of the) NMSSM, the Little Higgs model, and the Hidden Valley scenario. In these models, the decay of X into $b\bar{b}$ can be the primary decay mode within specific parameter spaces, making the $h \to 4b$ decay channel particularly important to study.[8]

5.1.1 Theoretical Model $h \to 4b$

In this subsection there will be a brief discussion about some models that are giving birth to BSM models. The model that this paper is going to study is called 2HDM(+scalar).
We know that SM Higgs sector is made up of a $SU(2)_L$ doublet H with hypercharge $Y = \frac{1}{2}$. This model adds a doublet to this minimal picture.

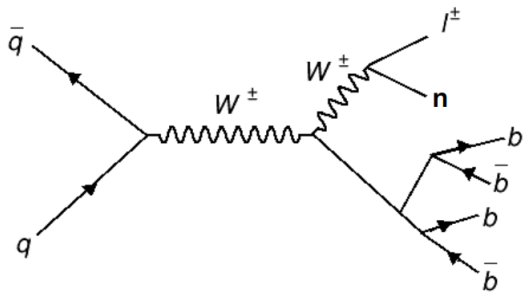

FIGURE 5.1: Feynman diagram of the signal process that corresponds to $hW \to a(bb)a(bb)ll$, where the leptons are muons and one can see the final state of four b-quarks.

A Higgs boson is able to decay into hour b-quarks via the reaction $h \to XX \to b\bar{b}b\bar{b}$. In the model that we analyse, the decay $h \to \alpha\alpha$ is mostly single pseudo-scalar and generic. If $\tan\beta$ allows it, the decay $\alpha \to b\bar{b}$ is also generic in all four 2HDM Types as long as $m_\alpha > 2m_b$.[8]

5.1.2 Signal Process

That process is signal and will be analysed. It is an exotic Higgs decay, with a mass of $125\ GeV$, that splits to two α pseudoscalar bosons, that each one breaks to two b-quarks, more specific a $b\bar{b}$ pair. Higgs production comes from the leptonic decay channel of boson $W^\pm \to l\nu$, so its event choice would be more effective. Leptons should be muons because as we said, they can be used as a powerful selection cut, of the backgrounds in SM and because their tracking is clearer than electrons.
This procedure needs the Higgs mass to be more massive than the sum of α masses $2m_\alpha < m_h = 125\ GeV$ to be energetically possible. So by that standards we search for masses that are $< 60\ GeV$. In this analysis mass samples were $12\ GeV$, $15\ GeV$, $20\ GeV$, $25\ GeV$, $30\ GeV$,$40\ GeV$,$50\ GeV$ and $60\ GeV$. But the two smaller values were later rejected due to the fact that the angle of the bosons is so small that reconstructing the jets wasn't possible in this specific analysis.
We pick the final state to be consisted of four b-tagged jets. We do that because that is the main decay channel, when virtual boson's α mass is bigger than the sum of the two b-quarks $m_\alpha > 2m_b \sim 10GeV$.[8] To be more precise about the decay we must see previous researches like [8] on $h \to \alpha\alpha \to X\overline{X}Y\overline{Y}$, where X and Y are particles predicted by the SM.
As we can see from figure 5.2 for $m_\alpha > 10\ GeV$ the branching ratio is $BR(a \to bb) \sim 1$. In our analysis the branching ratio on the masses that are studied will be equal to one. So the signal processing is $hW \to \alpha(b\bar{b})a(b\bar{b})ll$ and the cross section must be

$$\sigma_{production} = \sigma_{WH}^{SM} \times BR(W \to l\nu) \times BR(H \to 4b). \tag{5.1}$$

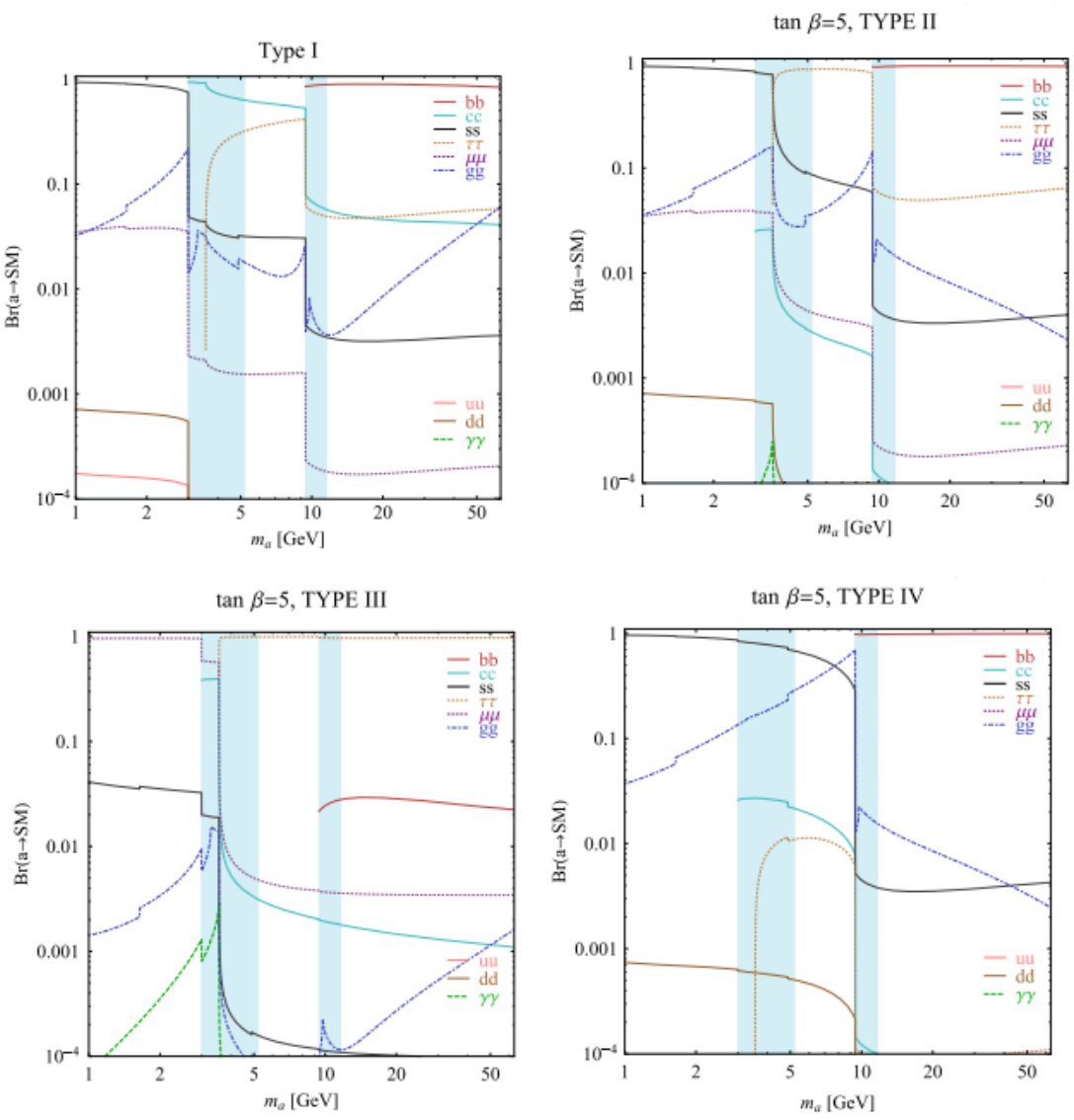

FIGURE 5.2: Branching Ratio for type-I, type-II, type-III and type-IV Yukawa couplings and are based on model 2HDM+S, in the blue area hadronization might differentiate from calculations. In that figure we see the branching ratios for $\tan\beta = 5$ and in the last two subfigures we see them for $\tan\beta = 0.5$ [8]

In our case we know that Higgs is decaying in correlation with $W^{\pm}$, we know that the cross section is $\sigma_{SM} = 1.37\ pb$ and the branching ratio for the leptonic decay is $BR(W \to ll) = 0.1046 + 0.105 + 0.1075 = 0.3171$. The Brancing ratio for the calculations of the event yields we took was $BR(H \to aa \to 4b) = 1$.

5.1.3 Background Processes

Background processes are in the spectrum of SM and their final state is the same as signal's. In this analysis, backgrounds will be the leptonic, semileptonic and hadronic $t\bar{t}$ decays. W to

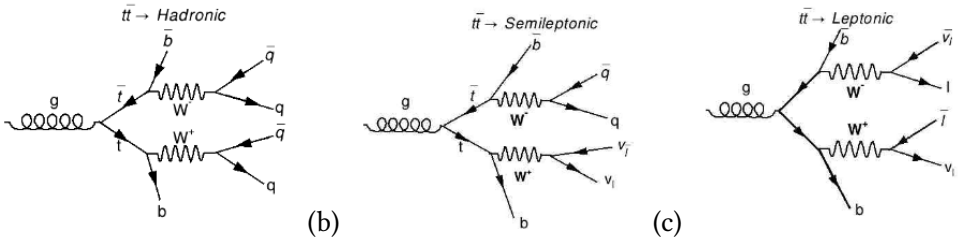

FIGURE 5.3: Feynman diagrams of $t\bar{t}$ background

lepton and neutrino and QCD.
In the $t\bar{t}$ decay as said there are three decaying channels. The name of each one is referring to the final state, of W bosons decay.

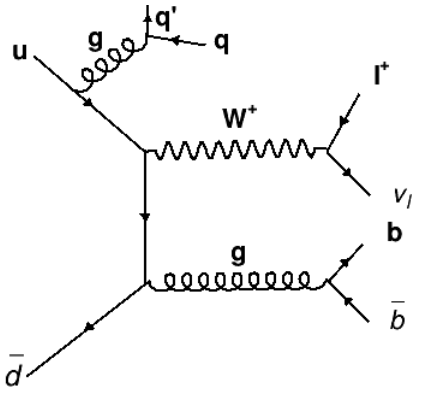

FIGURE 5.4: The qcd background

$t\bar{t}$ Decay Channels

Top pair quarks are produced from strong interactions and almost always decay to a W boson and b-quarks. W boson's decay, determines the final state of the event. There are three primary decay channels for $t\bar{t}$ events, that we categorize based on W boson's decay products, these are:

- Leptonic Decay (Dileptonic Channel)
- Semileptonic Decay (Lepton plus Jets Channel)

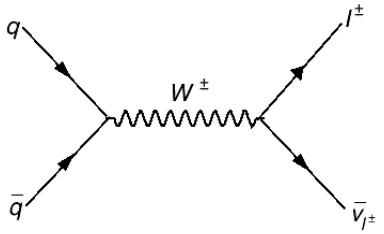

FIGURE 5.5: W to lepton neutrino background

- Hadronic Decay (All-Hadronic Channel)

In the leptonic decay channel both W bosons decay into leptons that are electrons or muons and neutrinos. The final state consists of two charged leptons that is either an electron or a muon, two neutrinos and two b-quarks.
In the semileptonic channel decay we have one leptonic channel and one jets channel. On that channel only one W decays leptonically and the other one decays hadronically. The final state consists of one charged lepton that is either an electron or a muon, one neutrino, two jets from the hadronic decay of the W boson and two b-quarks.
In the hadronic decay, all channels are purely hadronic. The final state consists of four jets from the W bosons decay and two b-quarks.

W to lepton neutrino Decay Channels

The W boson decays into leptons and neutrinos, this decay leads to events with missing transverse energy while the hadronic decay in additional jets in the final state.

QCD Background

Quantum Chromodynamics (QCD) processes are strong interaction processes that predominantly produce jets. These can mimic the signal in all-hadronic and semileptonic $t\bar{t}$ channels, where multiple jets are present. QCD multijet events are particularly challenging to discriminate from $t\bar{t}$ events due to the sheer number of jets produced and their high cross-section.
To summarize $t\bar{t}$ decay events can be classified into leptonic, semileptonic, and hadronic channels based on the decay products of the W bosons. Each channel has distinct signatures and challenges. The dileptonic channel has clear leptonic signals with missing energy from neutrinos. The semileptonic is a mix of leptonic and hadronic signatures, useful for reconstruction, The hadronic channel has, as the name states, purely hadronic final state with multiple jets, difficult to distinguish from QCD backgrounds.

5.2 Preselection Cuts

In this section, we will explain the strategy behind the preselection cuts in two categories. The first is the detector acceptance cuts and the second is background determination cuts. These cuts are algorithms that help in the separation of signal and background.

5.2.1 Geometrical Acceptance Cuts

In the case of reconstructing leptons that in our case are electrons and muons. The cuts to do so are $\mid \eta \mid < 2.4$ and $p_T > 20$. Leptons require quality and isolation. Muons are are separated into tracker and standalone ones. To detect them and analyse them correctly, they should pass some filters, as the quality of the track fit, the large number of hits at the pixel, the tracker and the events where the muons detected are the actual lepton candidates.
Reconstruction of jets is done by using all the remaining candidates after removing leptons. Their cuts are $\mid \eta \mid < 3$ and $p_T > 20\ GeV$. High level analysis objects, that in our case are muons and electrons are reconstructed too. They do so by dedicated reconstruction groups, that are known as physics object groups were every object of the analysis belongs to a separate one.Finally we cross-cleaned jets, meaning that the code is rejecting jets close to a tight ID and isolated leptons that are inside a cone radius of $\Delta R = 0.4$[25], where ΔR is

$$\Delta R = \sqrt{(\Delta\eta)^2 + (\Delta\phi)^2}. \tag{5.2}$$

Lets take a deeper look at cross-cleaning and why we used it. We see that electrons and muons are combined in order to form a single candidate. These leptons are gathered information from several sub-detectors. These leptons are objects that belong to the same category, so there would overlap and because they are the same we could refer to that phenomenon as duplication.
In our case we are interested to configure jet overlaps in order to reconstruct them. Jets overlap with muons, electrons, photons and taus. So to summarize our algorithm is a default overlap algorithm that does the following:

1. Preselecting the list of items to check for overlaping.
2. ΔR matching with cone size that is equal to the parameter (0.4 in our case).

Sometimes the reconstructed jets are not jets actually but leptons, so to avoid that we are coss-cleaning our jets.
After the jet reconstruction, we need to see which of these are actually b-jets. This procedures is a direct result of the contamination of $t\bar{t}$ events, so we apply the tag veto tag[25], which is firstly to make sure that there is no overlapping in the muon or electron jets by demanding that their cone radius is $\Delta R < 0.4$ and then to satisfy the medium discrimination working point.[25] Hence that cut is an algorithm called Combined Secondary Vertex[26], which takes the produced B hadron's distance before decaying. That hadron is produced by the hadronization of a b-quark and this behavior leads to the conclusion that there is a secondary displaced inner vertex with a flying distance higher than its resolution.[26] Actual cut is the CSV Jet tag to be > 04941.

Lastly, there is a pair of constructed variables which are MET and transverse mass. As we said in 4.18 $\not{E}_T = \mid -\sum_a \vec{p}_{aT} \mid$.

5.2.2 Background Discrimination Cuts

One goal of this analysis is to separate signal from background events. To achieve that, we impose some cuts that will reduce background events. These cuts are the demand to have at least one lepton, at least three jets and at least three b-tagged jet. Finally transverse mass should be greater than $50GeV$ and MET should be bigger than $30GeV$.
In each cut we measure efficiency by taking the Number of events that survive each cut, over the total number of events

$$eff = \frac{\#events\_survived}{\#total\_events}. \tag{5.3}$$

Then we calculate the number of expected events that is

$$N_{exp} = \sigma_{background} \times L_{integrated}, \tag{5.4}$$

so combining 5.3 and 5.4, the expected number of events is calculated by multiplying N_{exp} with efficiency

$$N_{exp}^{after\_cut} = N_{exp} \times eff. \tag{5.5}$$

The backgrounds that we used in this analysis are, $t\bar{t}$ hadronic, $t\bar{t}$ semileptonic, $t\bar{t}$ dileptonic, W to lepton and neutrino, is separated into H_T, that is the scalar sum of jets momentum which have $p_T > 30GeV$ and $\eta > 2.5$. QCD is also separated by H_T.

5.2.3 Kinematic Analysis

In this subsection there will be a brief introduction on the variables that used in my analysis.[1] These variables are all plotted after all cuts, so they can give us a good picture about how good the background cuts work and how much actual background survives. The following diagrams have every bit of background information that was given and the $m_\alpha = 60\ GeV$ α boson hypothesis.

In figure 5.7 we see a detection void. This void is explained in figure 3.9. As we can see there is nothing at 25.2^o $(1.5\ rad)$ to 27.7^o $(1.4\ rad)$ to actually measure electrons. In the figures of this subsection (except the ones of figure 5.15), signal has been multiplied by a factor of 100 and in 5.15 by a factor of 50, in order to be distinguished.
As we can see the cuts are very effective at killing QCD an W to lepton-neutrino backgrounds. The most dominant background is $t\bar{t}$ semileptonic.

[1] some of them where used in the MVA

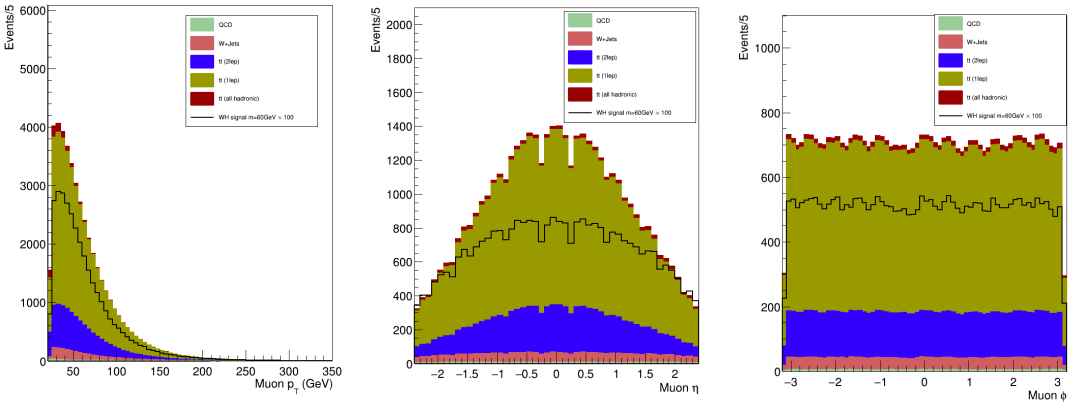

FIGURE 5.6: Kinematics of muons. In the left we can see muon's momentum that has a cut at 20 GeV, in the middle there is muon's pseudorapidity (η) that and on the right muon's azimuthal angle (ϕ).

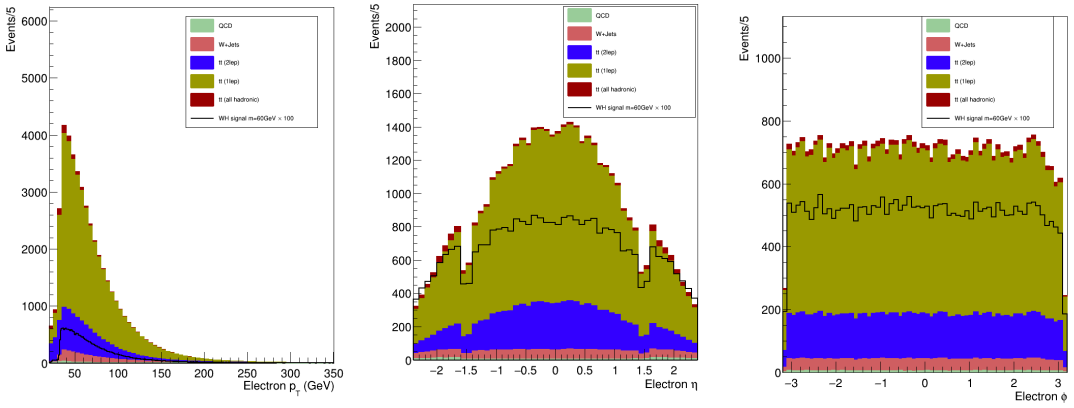

FIGURE 5.7: Kinematics of electrons. In the left we can see electron's momentum that has a cut at 20 GeV, in the middle there is electron's pseudorapidity (η) that and on the right electron's azimuthal angle (ϕ).

5.3 Selection of Events

At Tables 5.3 and A.1 we saw the results of the cuts that help separate signal from backgrounds. These cuts can be summed up in the following Table As showed after imposing these cuts, a small fraction of the initial events survives and it will be shown at an Event Flow table. In that analysis we have eight different sets of data for signal. Each set represents the mass of α boson, $m_\alpha = [12, 15, 20, 25, 30, 40, 50, 60]GeV$ and the cuts leave them as shown bellow at table A.2.

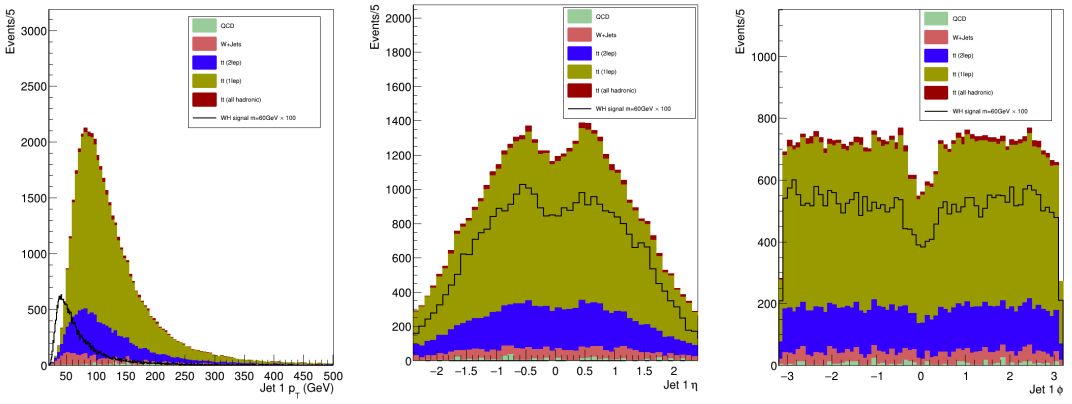

FIGURE 5.8: Kinematics of the leading Jet. In the left we can see jet's momentum that has a cut at 20 GeV, in the middle there is jet's pseudorapidity (η) that and on the right jet's azimuthal angle (ϕ).

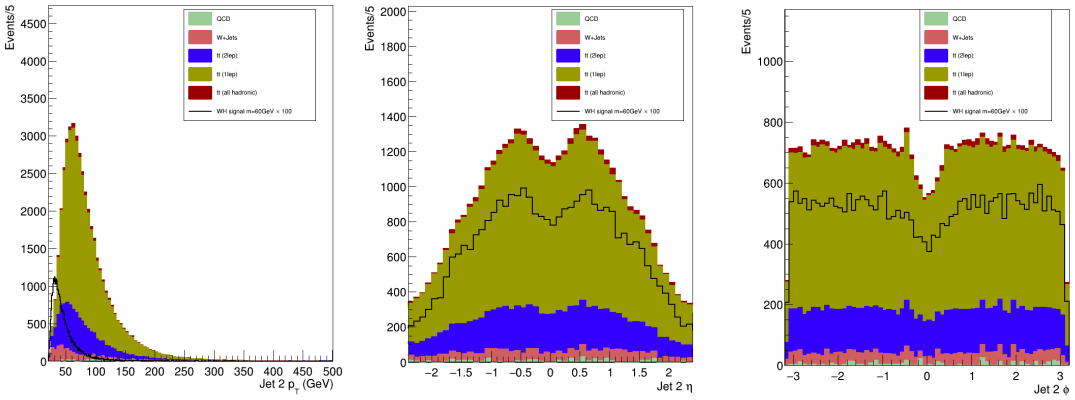

FIGURE 5.9: Kinematics of the second reconstructed Jet.

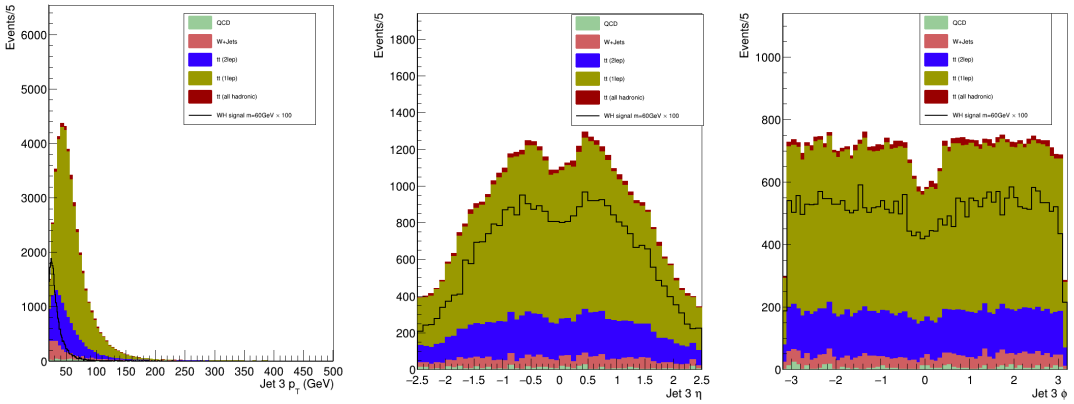

FIGURE 5.10: Kinematics of the third reconstructed Jet.

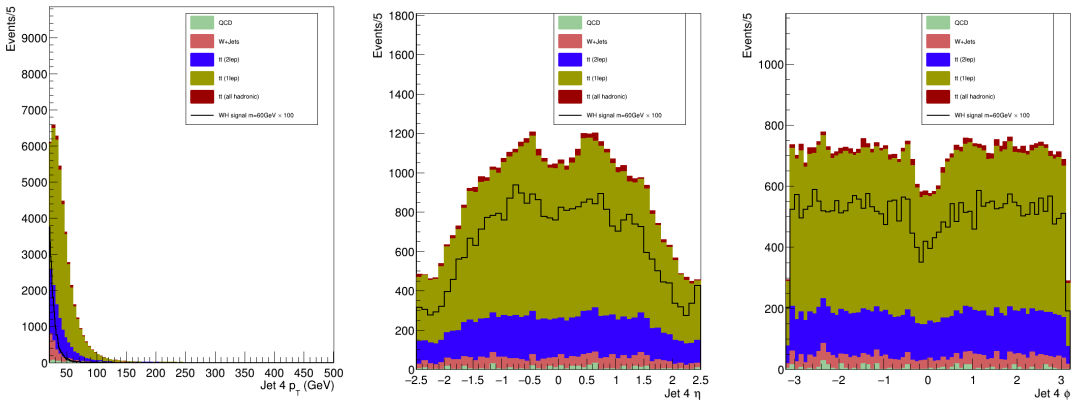

FIGURE 5.11: Kinematics of the fourth Jet if it exists which is why the number of entries is smaller that the previous three reconstructed.

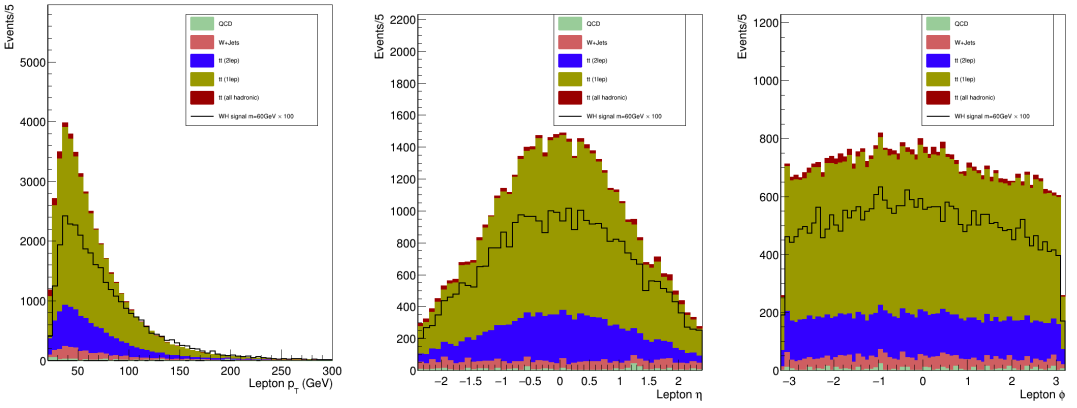

FIGURE 5.12: Kinematics of leptons. In the left we can see lepton's momentum that has a cut at 20 GeV, in the middle there is lepton's pseudorapidity (η) that and on the right lepton's azimuthal angle (ϕ).

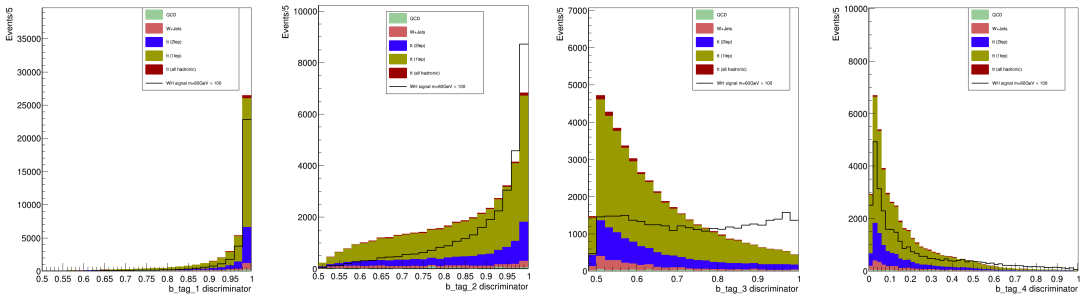

FIGURE 5.13: b-tag discriminators

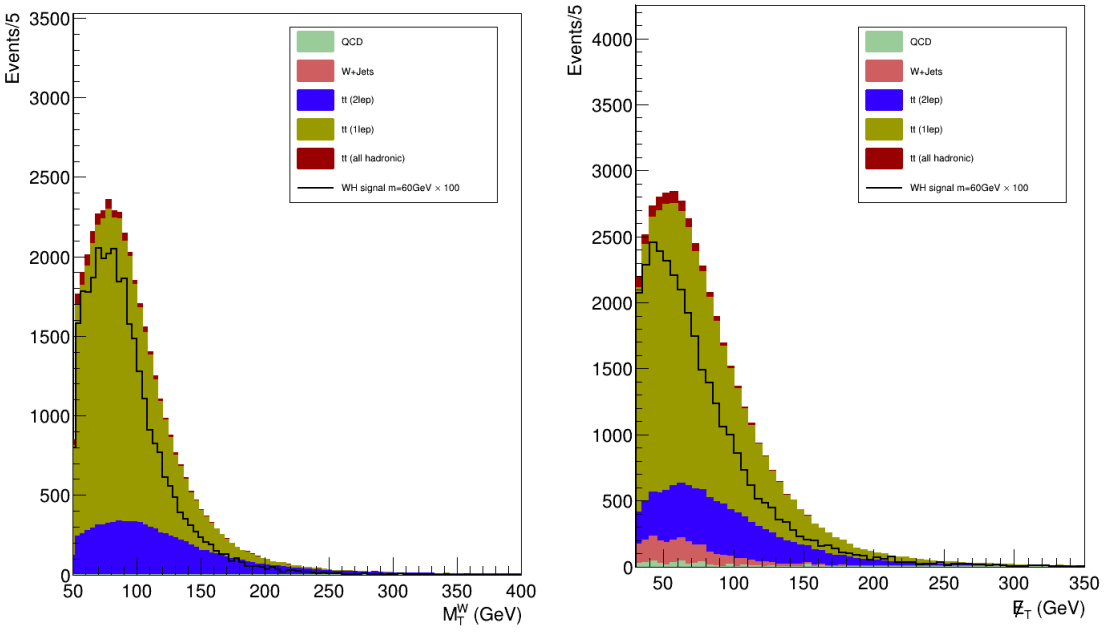

FIGURE 5.14: MET_{pt} and transverse mass.

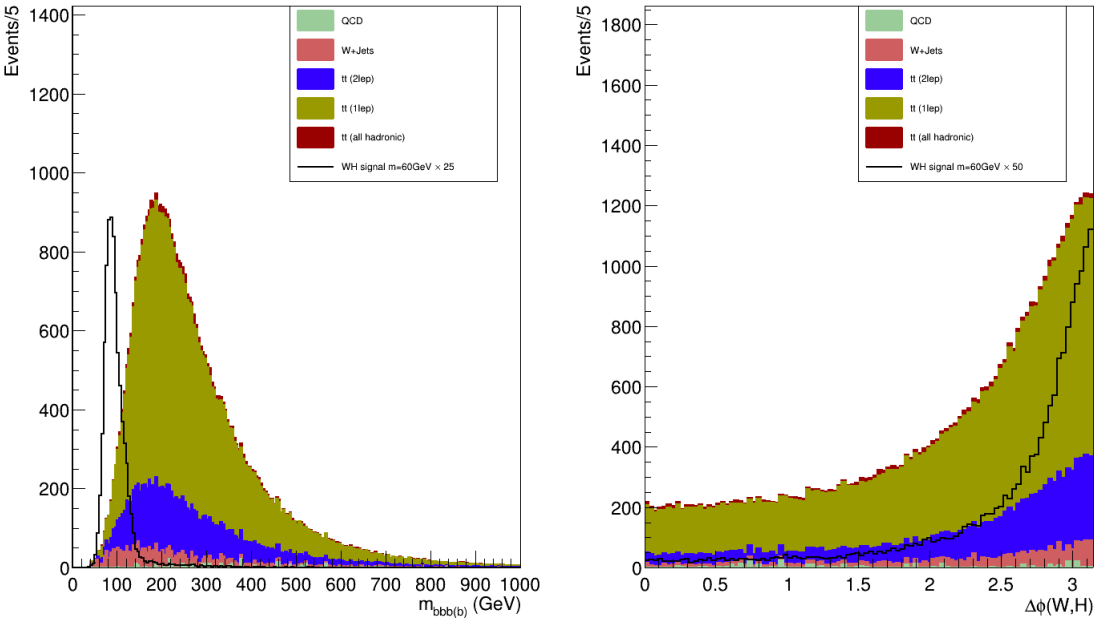

FIGURE 5.15: Reconstructed Higgs mass on the left and the azimuthal angle between W boson and Higgs.

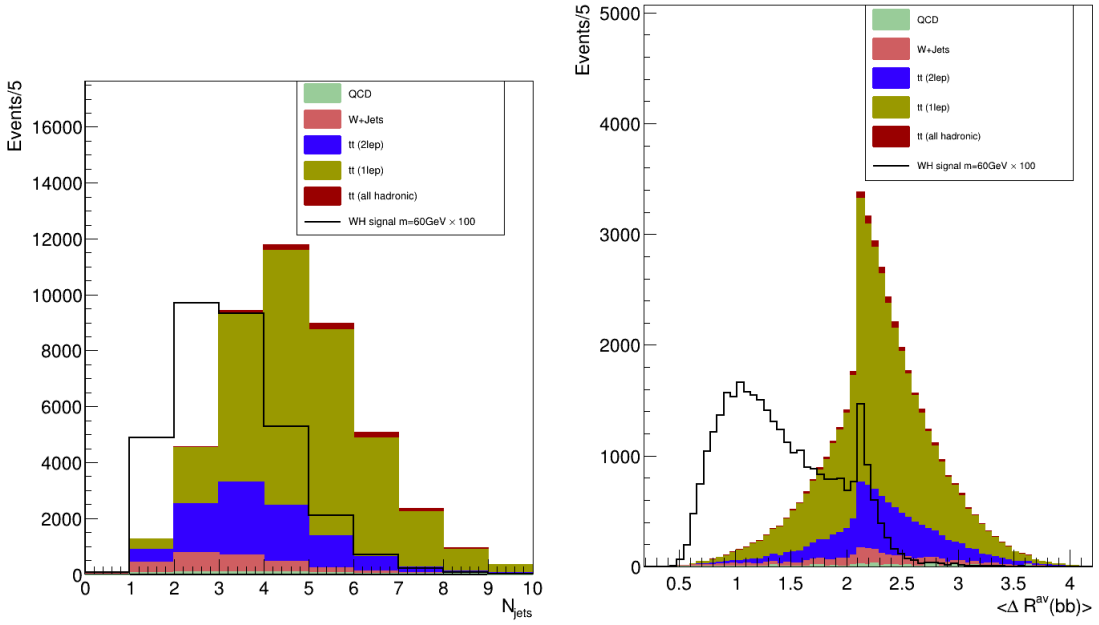

FIGURE 5.16: Multiplicity of the jets on the left and distance in the eta-phi plane between any b-tag pair, averaged over all possible combinations per event

	Cuts
Leptonic system	at least one lepton (e or μ) $p_T^e > 20GeV$ and $\eta^e < 2.4$ $p_T^\mu > 20GeV$ and $\eta^\mu < 2.4$
Hadronic system	at least three jets at least three b-tagged jets
	$\not{E}_T > 30\ GeV$ $M_T^W > 50\ GeV$

TABLE 5.1: Cuts on the leptons and jets

Steps	$W \to l^\pm + \nu$	$t\bar{t}$	QCD	WH $m_\alpha = 60\ GeV$
At least one lepton	49779432	10.9×10^6	1.74×10^9	10997.5
At least three jets	4198289	2021796	477768	3098.4
Configuration of b-jets	1215.7	69224.5	4063.4	592
$\not{E}_T > 30\ GeV$ and $M_T^W > 50\ GeV$	749.2	41936.7	1306.5	323.9

TABLE 5.2: Event flow table, after each cut

5.3.1 Event Flow Table

As we mentioned at equations 5.4 and 5.5 the number of events expected is $N_{exp}^{after\_cut} = N_{exp} \times eff$. so we can rewrite that as

$$N_{exp} = \sigma \times L_{integrated} \times \frac{N_{survived}}{N_{total}}, \tag{5.6}$$

Background	Number of entries	At least one lepton	At least three jets	At least three b-jets	$MT > 50 \& MET > 30$
$t\bar{t}$ Semileptonic	3.4136×10^7	11618601 $eff = 34\%$	10771139 $eff = 31.5\%$	383349 $eff = 1.1\%$	228490 $eff = 0.7\%$
$t\bar{t}$ Dileptonic	2.1188×10^7	12590926 $eff = 59.4\%$	9417664 $eff = 44.4\%$	227191 $eff = 1\%$	161054 $eff = 0.8\%$
$t\bar{t}$ Hadronic	1.3026×10^8	148136 $eff = 0.01\%$	140891 $eff = 0.01\%$	2818 $eff = 2.16 \times 10^{-6}\%$	950 $eff = 7.29 \times 10^{-6}\%$
$t\bar{t}$ W to lepton neutrino $H_T \rightarrow 70to100$	2.2255×10^7	5565165 $eff = 25\%$	942113 $eff = 4\%$	80 $eff = 3.59 \times 10^{-6}\%$	58 $eff = 2.6 \times 10^{-6}\%$
$t\bar{t}$ W to lepton neutrino $H_T \rightarrow 100to200$	3.5862×10^7	9891303 $eff = 27\%$	3304110 $eff = 9\%$	584 $eff = 1.62 \times 10^{-5}\%$	372 $eff = 1 \times 10^{-5}\%$
$t\bar{t}$ W to lepton neutrino $H_T \rightarrow 200to400$	2.1251×10^7	6520377 $eff = 30\%$	3923044 $eff = 18\%$	1785 $eff = 8.4 \times 10^{-5}\%$	1049 $eff = 4.94 \times 10^{-5}\%$
$t\bar{t}$ W to lepton neutrino $H_T \rightarrow 400to600$	1.4313×10^7	4711973 $eff = 32\%$	3672527 $eff = 25\%$	3492 $eff = 0.02\%$	2123 $eff = 0.01\%$
$t\bar{t}$ W to lepton neutrino $H_T \rightarrow 600to800$	2.1709×10^7	7245949 $eff = 33\%$	6108963 $eff = 28\%$	7649 $eff = 0.03\%$	4643 $eff = 0.02\%$
$t\bar{t}$ W to lepton neutrino $H_T \rightarrow 800to1200$	2.0432×10^7	6867092 $eff = 33\%$	6057839 $eff = 29\%$	9281 $eff = 0.04\%$	5706 $eff = 0.02\%$
$t\bar{t}$ W to lepton neutrino $H_T \rightarrow 1200to2500$	2.0258×10^7	6842434 $eff = 33\%$	6210469 $eff = 30\%$	10303 $eff = 0.05\%$	6719 $eff = 0.03\%$
QCD $H_T \rightarrow 80to170$	1.5999×10^7	10920 $eff = 0.06\%$	4309 $eff = 0.02\%$	34 $eff = 2.1 \times 10^{-6}\%$	10 $eff = 6.3 \times 10^{-7}\%$
QCD $H_T \rightarrow 170to250$	9.8476×10^6	5793 $eff = 0.05\%$	3587 $eff = 0.03\%$	42 $eff = 4.2 \times 10^{-6}\%$	18 $eff = 1.8 \times 10^{-6}\%$
QCD $H_T \rightarrow 250to\infty$	9.9968×10^6	5625 $eff = 0.05\%$	4073 $eff = 0.04\%$	80 $eff = 8 \times 10^{-6}\%$	40 $eff = 4 \times 10^{-6}\%$
WH $m_\alpha = 60\ GeV$	953909	490608 $eff = 51.4\%$	268746 $eff = 28.1\%$	51351 $eff = 5.3\%$	28097 $eff = 2.9\%$

TABLE 5.3: Background efficiency cuts

where $\frac{\sigma \times L_{int}}{N_{total}}$ is normalising the final number of events[2] and is the weight of each procedure. The event flow table of signal and background events will be Table 5.4

Process	$\sigma(pb)$	Weight	N_{exp}
$WH(m_\alpha = 12\,GeV)$	1.37	0.012	27.2
$WH(m_\alpha = 15\,GeV)$	1.37	0.012	37.0
$WH(m_\alpha = 20\,GeV)$	1.37	0.012	136.0
$WH(m_\alpha = 25\,GeV)$	1.37	0.012	247.0
$WH(m_\alpha = 30\,GeV)$	1.37	0.012	297.9
$WH(m_\alpha = 40\,GeV)$	1.37	0.012	319.0
$WH(m_\alpha = 50\,GeV)$	1.37	0.012	313.9
$WH(m_\alpha = 60\,GeV)$	1.37	0.012	323.9
$W \to l\nu\,(H_T:\ 70\,to\,100)$	1637.13	3.053	177.1
$W \to l\nu\,(H_T:\ 100\,to\,200)$	1628.66	1.885	701.1
$W \to l\nu\,(H_T:\ 200\,to\,400)$	435.237	0.85	891.6
$W \to l\nu\,(H_T:\ 400\,to\,600)$	59.1811	0.172	364.3
$W \to l\nu\,(H_T:\ 600\,to\,800)$	14.5805	0.028	129.4
$W \to l\nu\,(H_T:\ 800\,to\,1200)$	6.65621	0.014	77.1
$W \to l\nu\,(H_T:\ 1200\,to\,2500)$	1.685409	0.003	22.1
$QCD\,(H_T:\ 80\,to\,170)$	322100	98.84	988.4
$QCD\,(H_T:\ 170\,to\,250)$	105771	11.11	199.9
$QCD\,(H_T:\ 250\,to\,\infty)$	21094.1	2.96	118.2
$t\vec{t}$ Semileptonic	365.3	0.181	32155.3
$t\vec{t}$ Dileptonic	88.3	0.054	8831.4
$t\vec{t}$ Hadronic	377.7	0.0381	950

TABLE 5.4: The expected numbers of each procedure after all cuts, along with their cross sections and weights. Due to its big weight, we expel QCD (H_T: 80 to 170) background from our analysis. By doing so we expect less spikes in our plots.

5.3.2 Variable Distribution

Before multi-variant analysis, there will be a brief presentation of the variables and their distribution. These variables were used after all cuts. The histograms that will follow, will have the mass of $m_\alpha = 60GeV$ and only one W to lepton neutrino and QCD backgrounds[3]. The rest of the signals and backgrounds have similar distributions. These variables are presented bellow and will be used at BDT.[27] These variables are crucial in distinguishing signal from background in the context of the search for the Higgs boson and its decay products.

1. p_T^H, that is the vector sum, of the (three or four) b-tagged jets that are forming the Higgs boson.[27] This variable represents the transverse momentum of the Higgs boson candidate, calculated as the vector sum of the transverse momenta of the three or four b-tagged jets that form the Higgs boson. It is a vital variable as it provides information about the

[2] which is called yield

[3] those that have greater weight

momentum distribution of the Higgs boson in the transverse plane, which is crucial for distinguishing signal events from background noise.

2. m_H, that is the invariant mass of the b-jets that Higgs boson is consisted of.[27] The invariant mass of the Higgs boson candidate is calculated from the b-jets that constitute the Higgs boson. This variable is critical as it directly relates to the mass of the Higgs boson, allowing us to identify events that are consistent with the expected Higgs boson mass of around $125\ GeV$.

3. p_T^V, that in our case[4], is the magnitude of vector sum of the lepton's p_T.[27] In the context of this analysis, p_T^V represents the transverse momentum of the W boson, which is derived from the magnitude of the vector sum of the lepton's transverse momentum. This variable helps in identifying the presence of the W boson and its kinematic properties, which are important for separating signal events from background processes involving W bosons.

4. H_T, which is the scalar sum of the b-lets (three or four) that are consisting the Higgs boson.[27] This variable is the scalar sum of the transverse momenta of the b-jets that form the Higgs boson. H_T provides a measure of the overall energy scale of the event in the transverse plane, helping to differentiate high-energy signal events from lower-energy background events.

5. $\mid \Delta R(b, b') \mid$, that is the separation radius of the $\eta - \phi$ plane between any two b-jets, of an event and are averaged over all such combinations.[27] The separation radius in the $\eta - \phi$ plane between any two b-jets, averaged over all such combinations in an event, provides insight into the spatial distribution of the b-jets. This variable helps in identifying the characteristic jet structure of Higgs boson decays compared to background processes.

6. $\mid \Delta\phi(V, H) \mid$, that is the azimuthal angle of the W boson's direction and the Higgs' boson one.[27] This variable is useful for understanding the angular correlation between the Higgs and W bosons, which can be different for signal and background events.

7. $\mid \Delta\phi(j, \not{p}_T) \mid^{min}$, the minimum azimuthal angle between the directions of $\vec{\not{p}_T}$ and a jet.[27] This variable is important for identifying events with significant missing energy, indicative of neutrinos or other undetected particles, which are common in signal events but less so in many background processes.

8. p_T^l, the leptonic momentum. The transverse momentum of the lepton, providing information about the energy and momentum of leptons in the event. High p_T^l values are often associated with signal events involving W boson decays to leptons.

[4] which is the W boson

9. $\not{p}_T$, that is the missing transverse momentum's magnitude.[27] he magnitude of the missing transverse momentum, $\not{p}_T$, represents the momentum carried away by undetected particles such as neutrinos. This variable is essential for identifying events with missing energy. High $\not{p}_T$ values are indicative of significant missing energy consistent with neutrino production in signal events.

10. m_T, transverse mass.[27] The transverse mass (m_T) is calculated by combining the transverse momenta of the lepton and the missing transverse momentum. This variable helps in reconstructing the mass of particles that decay into leptons and neutrinos, providing a way to separate signal events from background processes that have different transverse mass distributions.

11. $\Delta m_{b\bar{b}}^{min}$, that is the minimum difference in $m(b_1b_2) - m(b_3b_4)$ between pairing possibilities.[27] This variable represents the minimum difference in the invariant mass between two pairs of b-jets in all possible pairings. It is used to find the pair of b-jets that best matches the Higgs boson mass, helping to identify the correct b-jet combinations and distinguish signal events from background where such a pairing is less likely.

12. b-tag Discriminators These are variables used to identify jets originating from b-quarks (b-jets). The b-tagging algorithms assign a discriminator value to each jet, indicating the likelihood that the jet originates from a b-quark. High b-tag discriminator values help in identifying b-jets more accurately, which is essential for reconstructing the Higgs boson from its decay products.

These variables were used in the BDT's training process along with the number of b-jets. The shapes of BDT distribution are independent of the mass of α bosons, which allows us to use the same training process for all masses.[27]

5.4 Multivariate Data Analysis

MVA is a technique that deals with problems of regression and classification. This paper will use only classification. In high energy physics we need to define between two classes that are signal and background. That makes it a multiclass problem.
After making the variables that were analysed at the previous subsection, we now are producing a multivariate discriminator. That method is taking information from these variables and then we will separate signal and background procedures. This separation will be done using machine learning algorithms. Machine learning is the key aspect of a data analysis that is done in high energy physics. The multivariate analysis (MVA) used in this study uses the Toolkit

for Multivariate Data Analysis (TMVA). This toolkit is basic for statistical analysis and classification in high-energy physics. The primary goal is to separate signal from background using machine learning algorithms, specifically BDT's.
The ROOT data analysis toolkit, via TMVA, offers numerous machine-learning methods for data analysis in high-energy particle physics (HEP) and related fields, included since 2005. Boosted decision trees (BDTs) have been a preferred method, notably contributing to the 2012 Higgs discovery. However, since the early 2010s, advancements in modern neural network architectures have rapidly transformed the field, as seen in ILSVRC challenge improvements. The academic and industrial landscapes evolved quickly, with major technology companies driving this change. The HEP community has adopted these modern machine-learning methods and software tools early on, and they are now effectively used in production, such as in the CMS DeepJet tagger or the ATLAS quark-gluon tagger.[28]

5.4.1 Multivariate Analysis - TMVA

In order to separate events, we use variables that we defined in the phase space of the data. These are our inputs and called features x. In multivariate analysis, for every vector x, it assigns a scalar value y that is classifying the method output and is thus called classifier. This results in two different probability distributions, the first is for signal events and the second for background

$$\begin{aligned} p(y \mid x \in Sig) \\ p(y \mid x \in Bkg), \end{aligned} \tag{5.7}$$

if the distributions above are separated to a certain point, then y is used as a discriminating variable, that separates signal and background.
For this machine learning procedure we will use TMVA, that is a toolkit of ROOT framework. It consists techniques of statistical analysis, in order to process, evaluate and categorize multivariance variables. These methods are responding to supervised learning only. This means that it uses data samples, that their input information is mapped in feature space to the desired outputs. After training is tested in a sample and is evaluated, multivariate discriminator is used in new files, and act in accordance to its training. TMVA is designed for high energy physics and in our analysis will be used to separate signal and background procedures.[9]

5.4.2 Receiver Operator Curver

The Receiver Operator Curver or ROC, is a mathematical tool that helps us measure quality of the separability. It is a curve that measures signal efficiency and background rejection. If the algorithm achieves two perfectly separated and uniformed distributions[5] this curve will be

[5] and the guess is 100% random

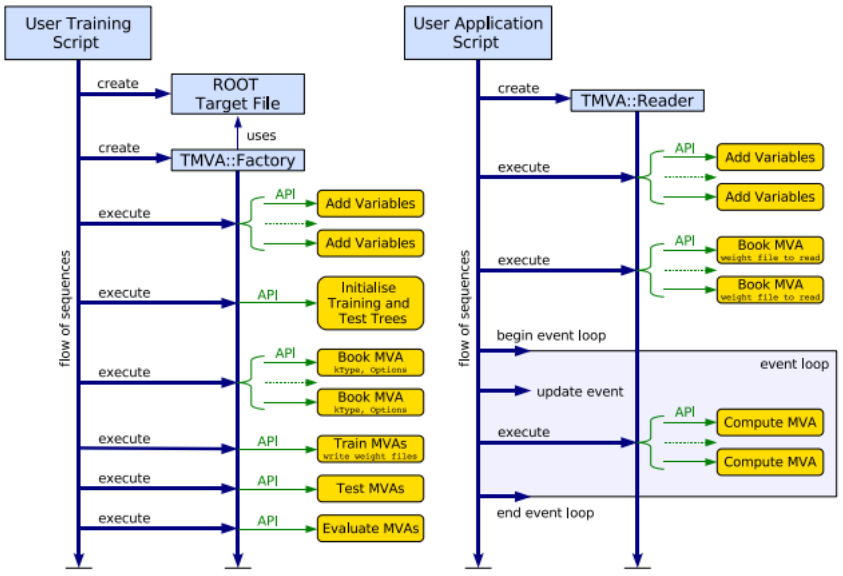

FIGURE 5.17: In the left we see a typical TMVA training application. In the right we see a typical TMVA analysis application.[9]

formulated as $y = -x$. In a perfect world, we would be able to reject background completely and in the same time keep signal untouched, in reality this is not the case. We are able to seperate signal from background to a certain point and reject some background.
Hence the main objective is to classify the distributions from 5.7 in the most optimal way possible. Each classifier has a unique procedure, but there is a general way, the fact that a sample of data are given labels. In essence the classifier knows which of the given data are signal and which are background.

5.4.3 BDT Discriminator

A decision tree is a classifier, that can be drawn by a simple tree structure. Each decision tree must be able to split the phase space into a number of hypercubes, that each one could be signal/background like. Each event is driven left or right, in accordance to the satisfaction of the criterion of the variable. After passing a sequence of these criteria, events end up in the leafs of the tree. In the end these leafs are recognised as signal or background, see Figure 5.18.[9]
Now lets see what the term "Boosted" is about. Boosting is used because of the successive decision trees that are created. These trees are originated from the same training sample, though they have redefined the weight of each event and the final response is coming from the weighted mean value of the trees. Boosting stabilises the response of the decision tree, taking into account the statistical fluctuations of the training sample. The way this works, is by taking all the false[6] events of the current tree and increasing their weight on the next one, through a function.

[6]events that were poorly distributed

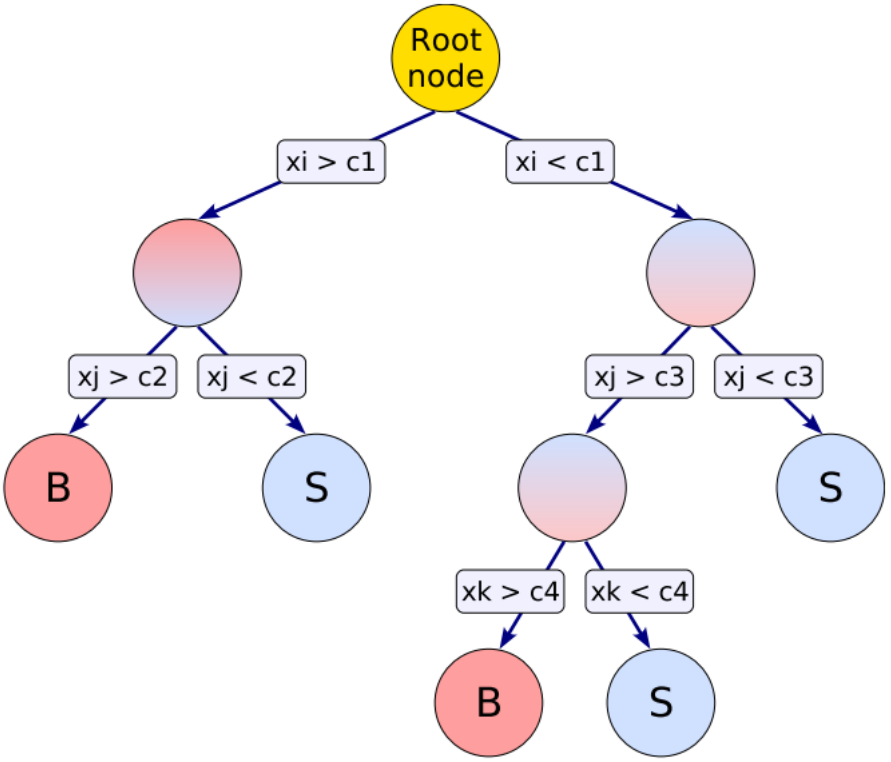

FIGURE 5.18: Decision tree, that starts from the root node. Each binary split is using a discriminating variable x_i, that we are applying to data. Each split takes this variable that should give the best separation between signal and background. The same variable may or may not used on several nodes, while others may be used less or never. Each leaf node has is labeled with letter "S" for signal or "B" for background, that depends on the majority of events that end up in each node.[9]

There are different boosting algorithms available, the one we used was adaptive boost[7].[9] The BDT discriminator that we built used 1000 decision trees. For the leaf separation of signal and background events we used Gini index. The nCuts parameter, that sets the control step of the variable values, so the separation criteria can be applied, was set to 20.

5.4.4 Training Variables

The variables above where chosen on the grounds of [27], in order to maximise the discriminating ability, between signal and background.
Training was done with masses m_α=[20,25,30,40,50,60], masses $m_\alpha = [12, 15]$ where abandoned for reasons that will be later mentioned.
In Figure 5.20 we see the distributions of all the variables used on the BDT. Afterwards in Figure 5.19 we see the correlation matrices and we can conclude that variables are independent with each-other, which increases efficiency. Lastly we need to see the ranking of variable importance at BDT, that is shown at table 5.5.

[7] AdaBoost

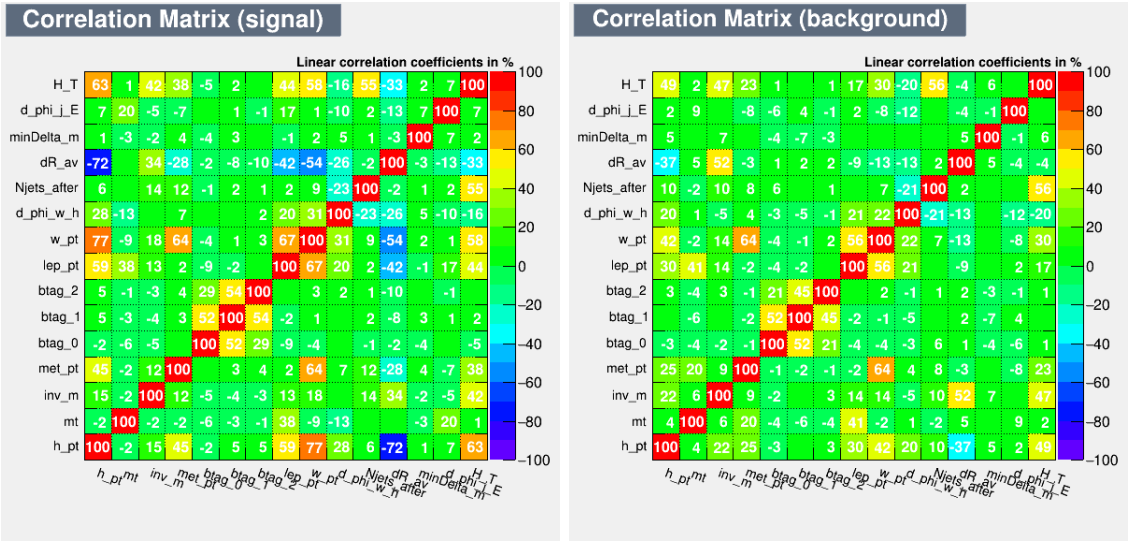

FIGURE 5.19: Correlation matrices of the training variables, on the left is the signal andvs on the right is the background.

Rank	Variable	Variable Importance
1	m_H	9.5%
2	$\mid \Delta R(b,b') \mid$	8.2%
3	H_T	7.8%
4	$b-tag-3$	7.5%
5	$\mid \Delta\phi(j,\not{p}_T) \mid^{min}$	7.2%
6	m_T	7.1%
7	$\mid \Delta\Phi(V,H) \mid$	6.8%
8	$b-tag-2$	6.7%
9	p_T^H	6.1%
10	p_T^W	6.1%
11	p_T^l	6.0%
12	$\not{p}_T$	5.5%
13	N^{b-jets}	5.5%
14	$\mid \Delta R(b,b') \mid$	5.2%
15	$b-tag-1$	4.9%

TABLE 5.5: BDT variable importance

5.4.5 BDT response

On Figure 5.21 we see cut efficiencies and optimal cut values of the BDT response, using signal masses as a hole and background also.

BDT-score is used as the main[8] fitting variable. We do this in order to use a single information variable instead of fifteen. We take advantage of the variable's separating ability.

Actual BDT response is shown in figure 5.22. To be more precise this is the BDT score that trained over the root files of signal and background. Background files are stacked as shown on

[8] and only

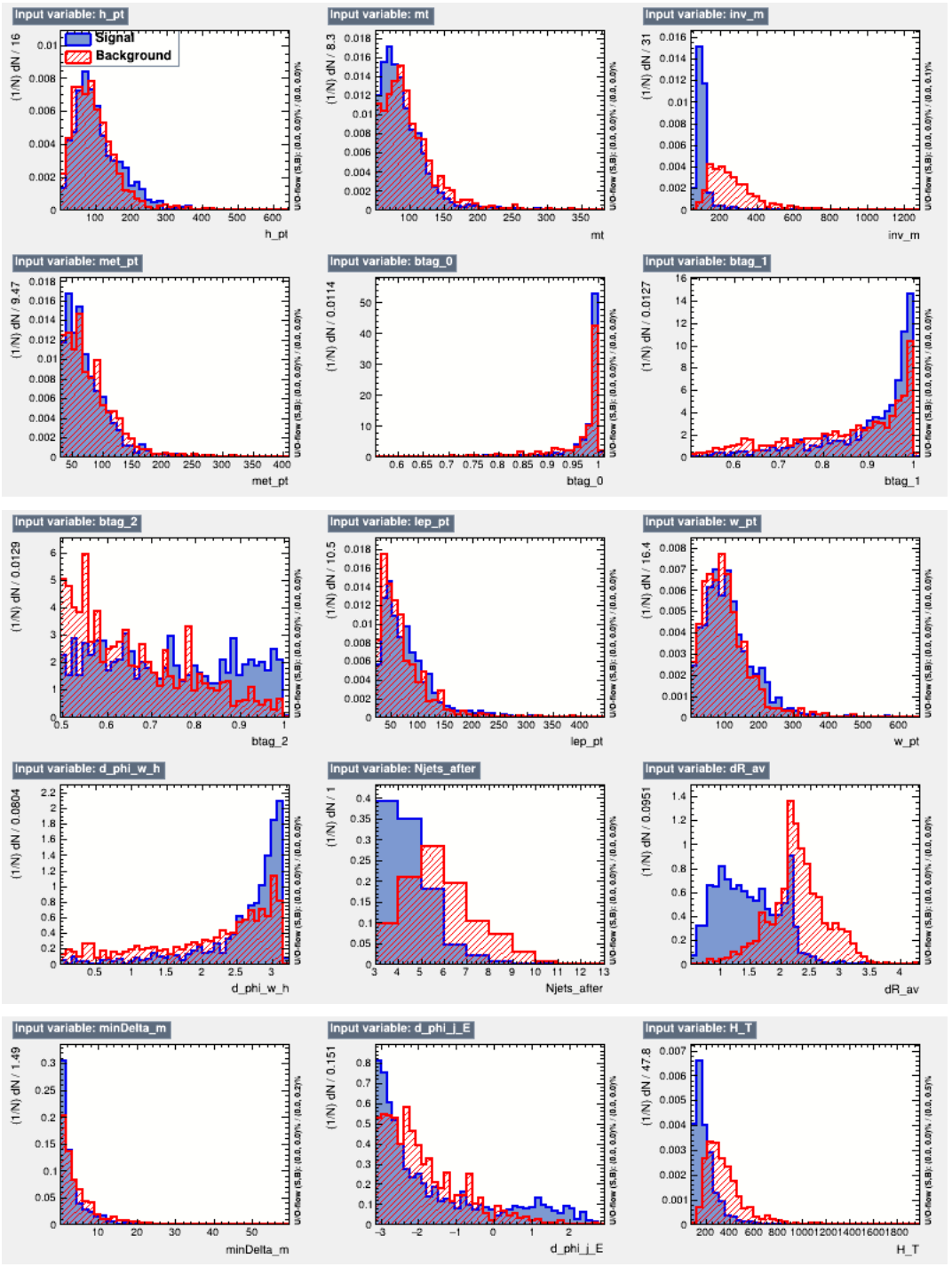

FIGURE 5.20: Distributions of the variables used for training the BDT. Red color is the sum of all backgrounds and blue is the sum of signal α bosons, with masses $m_\alpha = [20,\ 25,\ 30,\ 40,\ 50,\ 60]$.

figure 5.22 and signal is multiplied by a factor of 100 to in order to be distinguished.

At figure 5.23. With blue color we represent signal and with red background, as shown in the same diagram, the distributions of the control samples. Control samples are completely independent from the ones that used at the training phase. The fact that there is some deviation

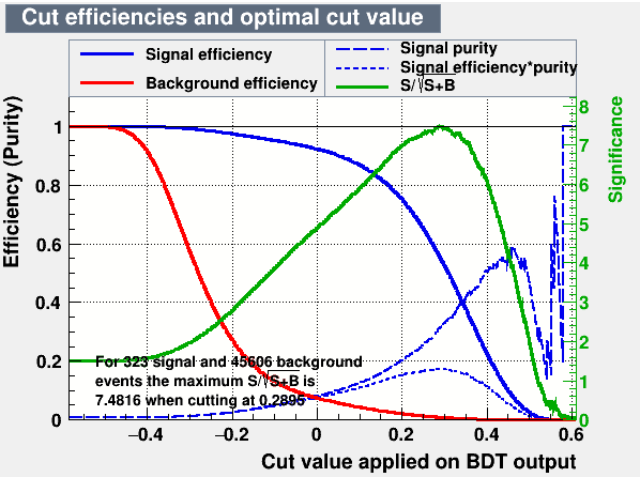

FIGURE 5.21: Cut efficiencies and optimal cut value for the BDT response. There used all 324 signal events, that are the expected events after all cuts for α boson mass $m_{alpha} = 60\ GeV$ and all 43992 background events as you can see at table 5.4.

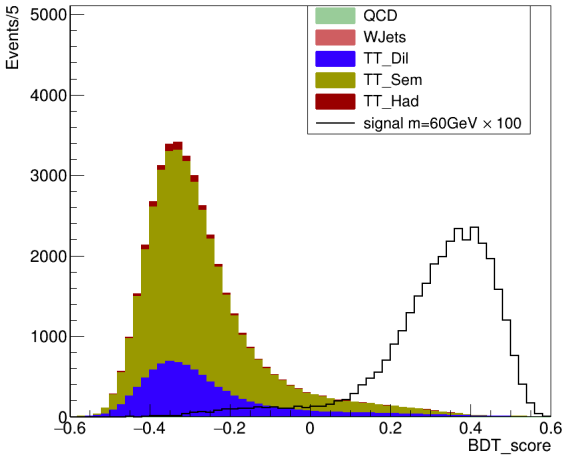

FIGURE 5.22: BDT response for all backgrounds given and signal mass $m_{\alpha} = 60\ GeV$. Distributions are normalised at the cross-section

means that the discriminator is overtrained to a certain point. Ovetraining is occurring when a machine learning problem has too few freedom degrees, because too many model parameters of an algorithm were adjusted to too few data points.[9] To avoid that there is always given a test dataset that the classifier method is applied to and it is checking if the output distributions for it are compatible with those of the training dataset.

In the next figure we see the likelihood response on the same sample. We can see that BDT responds better and that is even clearer at the ROC curve bellow at figure 5.24. ROC curve is the relation between the rejection of background and the efficiency of the signal for different separation criteria of a discriminator. So the result of the BDT application is the BDT-score variable.

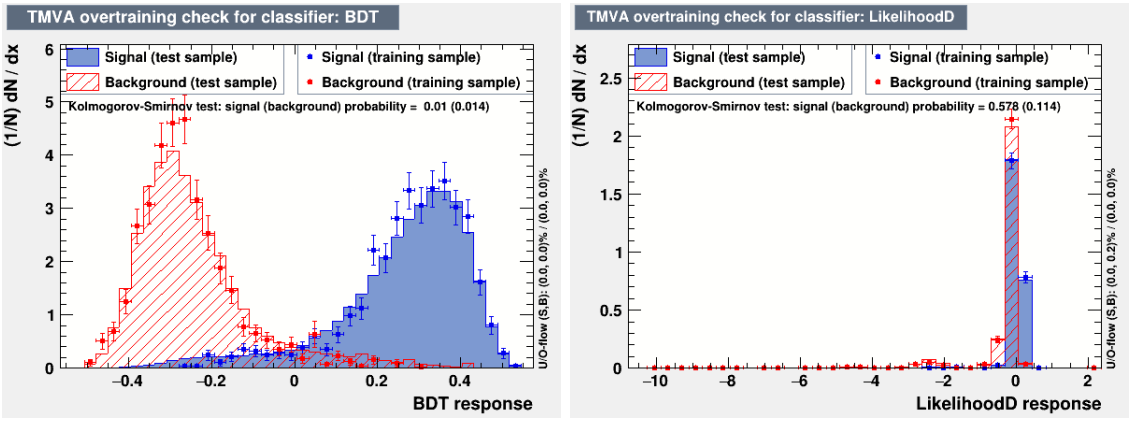

FIGURE 5.23: The BDT discriminator on the left and Likelihood discriminator on the right. In these diagrams we see the distributions of the control samples that show that over-training is low.

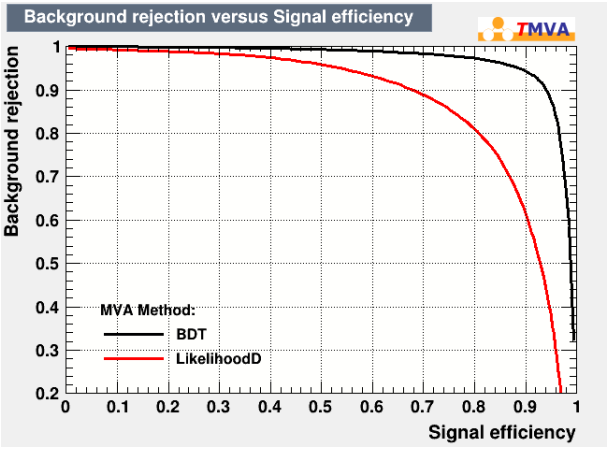

FIGURE 5.24: ROC curves of BDT and Likelihood methods. In that diagram, the more area the curve has underneath, the better signal efficiency and background rejection.

5.5 Signal Extraction

If our variables have a good separation between signal and background, we can do the maximum likelihood fit. In order to do that, we need to check for two hypotheses.

- Zero Hypothesis H_0: There are only natural procedures that are described by SM. In practice this means that we would only be able to see background procedures (B).
- Alternative Hypothesis H_1: There are additional phenomena that are BSM. In practice this means that we would be able to see signal with background (S+B).

Each hypothesis has a model. That model is then fitted upon the data in order to check the compatibility with experimental values. This data are generated from Monte Carlo toys. This

is done by generating pseudo-random numbers from the theoretical distributions. That's a very good tool to have a consistent and unbiased fit, with low statistical fluctuations.

5.5.1 Maximum likelihood fit to data

Theoretical distributions are given by the product of normalization parameters $N_{process}$ and the probability density function of the process $PDF_{process}$. So which hypothesis would have the following models

$$model_0 = \sum_{bkg} N_{bkg} \times PDF_{bkg}(x) = N_{bkg_{total}}[f_1 + PDF_1 + f_2 PDF_2 + (1 - f_1 - f_2)PDF_3], \tag{5.8}$$

$$model_1 = N_{signal} \times PDF_{signal}(x) + \sum_{bkg} N_{bkg} \times PDF_{bkg}(x) = N_{signal} \times PDF_{signal}(x) + N_{bkg_{total}}[f_1 + PDF_1 + f_2 PDF_2 + (1 - f_1 - f_2)PDF_3]. \tag{5.9}$$

These backgrounds are categorised as following

1. the sum of $t\bar{t}$ Hadronic and $t\bar{t}$ Dileptonic backgrounds, with coefficient $f_1 = 0.75$.
2. the sum of W to lepton/neutrino and QCD backgrounds, with coefficient $f_2 = 0.19$.
3. the $t\bar{t}$ Semileptonic background, with coefficient $f_3 = 0.06$.

Each coefficient represents the contribution of each background over their totality.
This strange separation came into being so fits wouldn't be biased.
The random variable x is the one that is the base over which we fit BDT scores. These scores are normalised at the cross section. Additionally the normalisation factor of each process $N_{process}$, are given by integrating these distributions. This procedure gives back the expected yields.
To proceed we need to make a value called N_{obs}, which is the observed value of the integrated distribution of the data. These data are made by us and are called pseudo-data. These data have the same magnitude as the sum of the initial yields of the model. To create that data set we take these data and add them on new pseudo-random values, which follow the theoretical distributions of the BDT score.
In these pseudo-data we apply the Maximum Likelihood fit. The likelihood function is

$$L(X \mid \theta) = \prod_{i}^{n} p(x_i \mid \theta), \tag{5.10}$$

were the function is the joint probability mass of observed data that are the parameters of the model.[29] The goal of that estimation is to find for what values of the model does the function

maximizes[30]

$$\hat{\theta} = \arg_{\theta \in \Theta} max_{\theta} L(X \mid \theta). \tag{5.11}$$

In practice, the log-likelihood function that is calculated by

$$\ln L(X \mid \theta) = \sum_{i=1}^{N} \ln(p(x_i \mid \theta)). \tag{5.12}$$

To maximize it we need to take the first derivative equal to zero

$$\frac{\partial \ln L(X \mid \theta)}{\partial \theta} \mid_{\theta} = 0. \tag{5.13}$$

The number of x_i events is N and is following a Poissonian distribution around the theoretical value (N_{exp}).
The fitting parameters are taking as initial values, the expected yields of the BDT score distributions. For the background and signal parameters, we define their range to start at zero and end when the value is doubled of the expected yield.

5.5.2 Toy Monte Carlo study

The final stages of most particle physics analyses are conducted within an interactive data analysis framework such as PAW or ROOT. These applications provide an interactive environment that supports processing via interpreted macros and includes a graphical toolkit for visualizing particle physics data. The RooFit toolkit extends the ROOT analysis environment by offering not only basic visualization and data processing tools but also a language for describing data models.[31]
The main features of RooFit include:

- A self-documenting vocabulary to build models using building blocks (e.g., exponential decay, Argus function, Gaussian resolution) and their combinations (e.g., addition, composition, convolution). A template is available for users to add specific building-block PDFs.[31]
- A data description language to specify observable quantities with descriptive titles, units, and cut ranges. Various data types are supported, including real-valued and discrete values (e.g., decay mode). Data can be read from ASCII files or ROOT ntuples.[31]
- Generic support for fitting any model to a dataset using a (weighted) unbinned or binned maximum likelihood, or χ^2 approach.[31]
- Tools for plotting data with correctly calculated errors, Poisson or binomial statistics, and superimposing normalized projections of a multidimensional model or its components.[31]

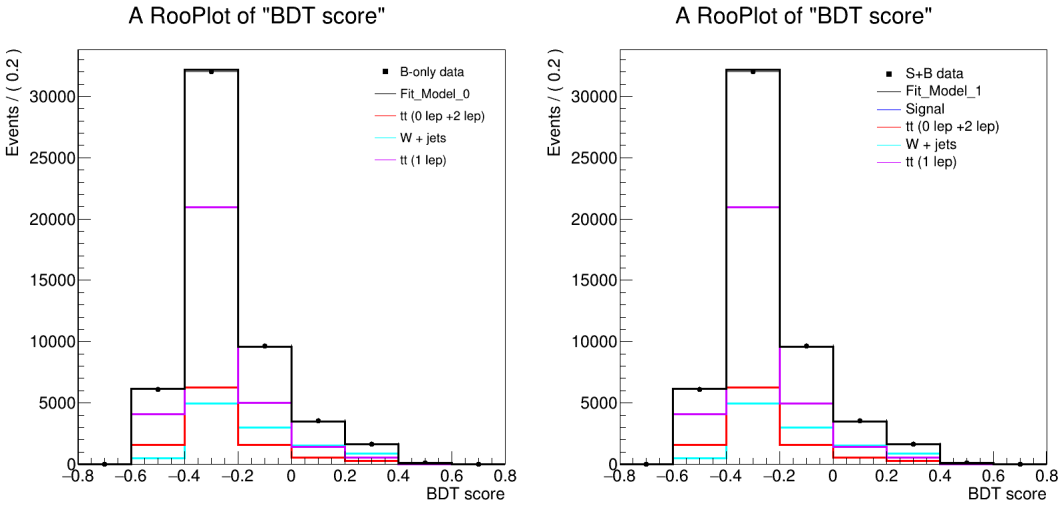

FIGURE 5.25: Maximum Likelihood fits at BDT score for a toy. Model is the black colored line, the red are $t\bar{t}$ Hadronic and $t\bar{t}$ Dileptonic backgrounds, the cyan line are W to lepton neutrino and QCD backgrounds and violet is the $t\bar{t}$ Semileptonic background. These fits have background only data (Data B).

- Tools for creating event samples from any model using Monte Carlo techniques, with some variables possibly taken from a prototype dataset to better model statistical fluctuations.[31]
- Computational efficiency, ensuring that models coded in RooFit are optimized to be as fast as, or faster than, hand-coded models. Automated optimization techniques are applied to any model without user input.[31]
- Bookkeeping tools for configuration management, automated PDF creation, and automation of routine tasks such as goodness-of-fit tests.[31]

To sum things up the steps to fit are

- from the BDT score's PDFs, we took the theoretical models,
- then we produce the pseudo-data, that we are naming Data B and Data S+B, from the theoretical models, afterwards we extract the N_{obs}
- then we execute the maximum likelihood fit of each model.

The above algorithm is a toy. The diagrams of the fits are shown in figure 5.25 In these diagrams we see the background yields. These graphs are made for alpha bosons mass $m_\alpha = 60\ GeV$ and cross section $\sigma = 1.37\ pb$. Black dots are the pseudo-data points and the black line is the applied fit.

After fitting we see the pulls of each point, which is

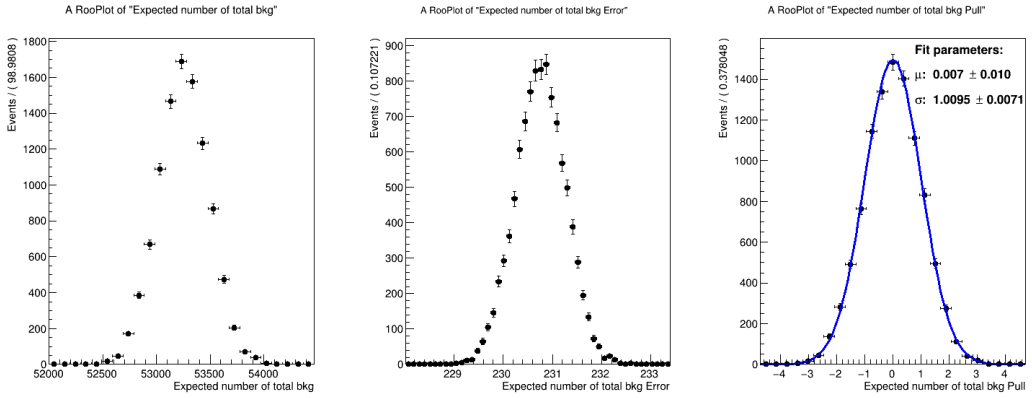

FIGURE 5.26: The left plots are representing the Expected number of total backgrounds fitted on background only data events.

$$pull = \frac{(N_{fit} - N_{in})}{\delta N_{fit}}. \tag{5.14}$$

points and the black line is the applied fit.

This procedure was repeated for masses $m_\alpha = [20, 25, 30, 40, 50, 60]\ GeV$. For each case we used 100000 toys, in order to have a statistical sample, big enough to minimize the statistical fluctuations. To check fit's effectiveness, we created the fitted yields and their corresponding pulls. And indeed these pulls were around zero each time, as seen in figure 5.27.

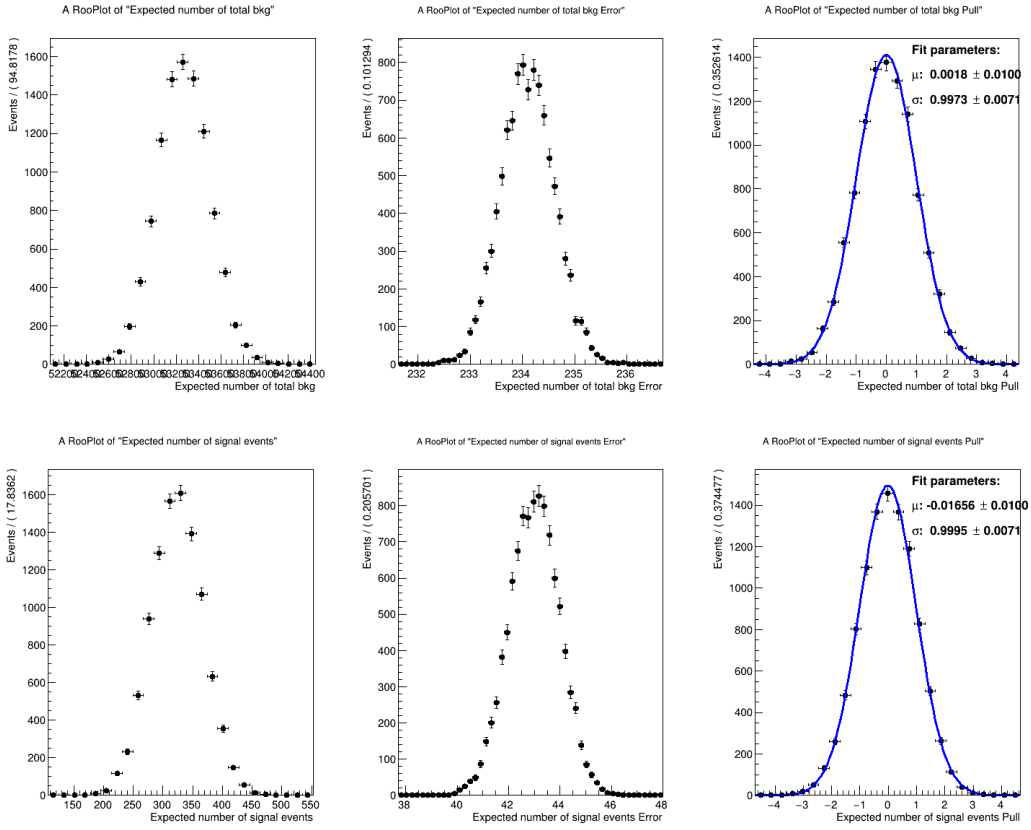

FIGURE 5.27: Pull distributions, that were produced from 100000 toys. The signal is from mass $m_\alpha = 60\ GeV$. The left plots are representing the Expected number of total backgrounds fitted on signal and background data and signal (for the bottom plot) events. The center represents the expected error and the right represents the expected pull. The pull distributions demonstrate the deviation of the observed data from the expected values, with the fit parameters indicating the mean (μ) and standard deviation (σ) of the distributions.

5.5.3 Upper limits to the signal yield using Bayesian methods

In particle physics, the search for new phenomena often involves estimating upper limits on potential signal yields. This is particularly important in scenarios where no significant signal is detected, and we need to quantify the maximum possible signal that could be consistent with the observed data. Bayesian methods offer a confident enough procedure for estimating these upper limits by taking into account prior information and systematically updating it with experimental data. This approach contrasts with frequentist methods, which focus on the probability of observing data given a true signal strength and do not directly take into account prior knowledge.[32]

Bayesian inference provides a probabilistic approach to parameter estimation. Let μ be the signal yield, a parameter we want to estimate. In Bayesian statistics, is treated as a random variable with an associated probability distribution. The key components of Bayesian inference are prior distribution that bellow is symbolized as $\pi(\mu)$ and it represents our beliefs about μ

before observing any data. This can be based on previous experiments, theoretical considerations, or our judgment. Then we need to use Likelihood Function $p(x \mid \mu)$ that represents the probability of observing the data x given the parameter μ. It is derived from the experimental model and accounts for both signal and background contributions. And finally the Posterior Distribution $p(\mu \mid x)$ that is the updated probability distribution for μ after incorporating the observed data x. It is computed using Bayes' theorem as seen in 5.15.
After applying the fit procedure to the data and take back the MC simulations, the procedure is calculating the log-likelihood. The logarithm makes calculations easier because instead of multiplying, the algorithm is adding. An additional feature is that the result is left unaltered, as in the function, because the function has the same maximum and minimum as its argument. The calculated log-likelihood function, can be done in reverse. This procedure will calculate the original likelihood function and estimate the Bayesian Upper limit.
As said above the Bayesian approach, unlike the frequentest approach, is treating the value θ as a random variable, instead of an unknown one. We label the unknown variable as μ, in the case of the analysis N_{signal} and posterior probability $p(\mu \mid x)$ are described by

$$p(\mu \mid x) = \frac{p(x \mid \mu)\pi(\mu)}{p(x)}, \tag{5.15}$$

which is known as Bayes' law. In 5.15 $\pi(\mu)$ is the prior probability, which means that it expresses any knowledge about the theoretical value known beforehand. Credibility is the range calculated, in which μ will have a certain probability level. It is seen as α.
So to calculate the upper limit μ_{up}, we need

$$L(\theta) = \frac{1}{C}\int_x p(data \mid s+b)\rho_x(x)\pi_s(s)dx, \tag{5.16}$$

where C is the normalization constant, data are the pseudo-data, ρ are the systematic uncertainties, π is the prior and $L(\theta)$ is posterior density.

$$\int_0^{ul,95\ or\ 86\% C.L.} L(\theta)d(\theta) := 0.95\ or\ 0.86. \tag{5.17}$$

In this analysis we found the upper limit via an algorithm called Markov chain Monte Carlo. We did it for all masses $m_\alpha = [20, 25, 30, 40, 50, 60]\ GeV$ and will present the $m_\alpha = 60\ GeV$ posterior distribution. The upper limit on the signal yield μ is determined by calculating the highest value of μ that is consistent with the data at a specified credibility level. This process involves integrating the posterior distribution up to a certain threshold. So the actual calculation of Bayesian upper limits will follow the steps that are presented next.
At first we define the Credibility Level that we will be symbolised as α. It is analogous to confidence level in frequentist statistics and represents the probability that the true value of μ is less than or equal to the calculated upper limit. For example, a 95% credibility level corresponds to an upper limit where there is a 95% chance that the true signal yield is below this value.

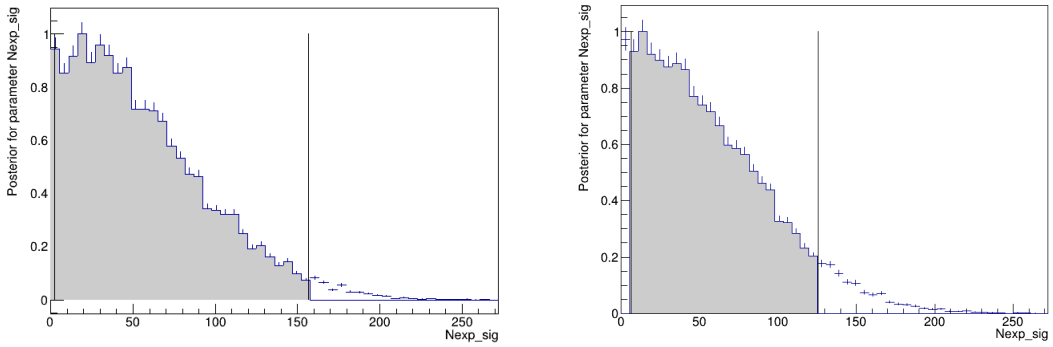

FIGURE 5.28: Posterior distribution for 95% confidence level on the left and 86% confidence level on the right for mass $m_\alpha = 20\ GeV$.

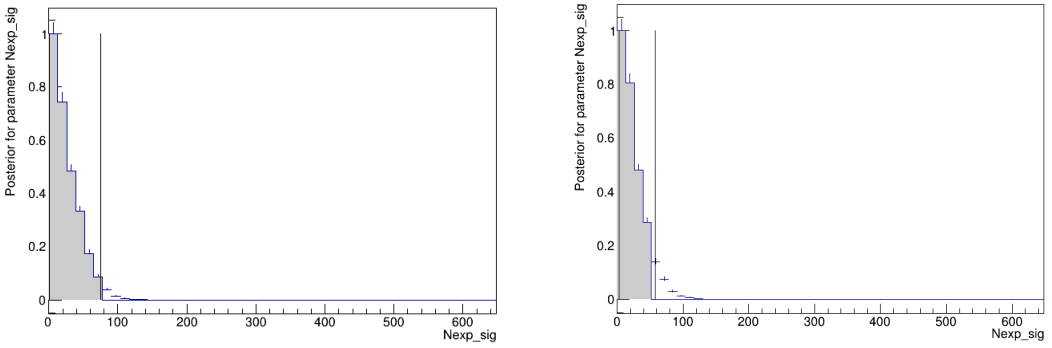

FIGURE 5.29: Posterior distribution for 95% confidence level on the left and 86% confidence level on the right for mass $m_\alpha = 60\ GeV$.

To determine the upper limit that we will say is μ_{up}, so in our case

$$\int_0^{\mu_{up}} p(\mu \mid x) d\mu = \alpha. \tag{5.18}$$

This means that the area under the posterior distribution from 0 to μ_{up} equals the credibility level α. For example, if $\alpha = 0.95$, then μ_{up} is the value where 95% of the posterior probability is below this threshold.

After that we implement Markov Chain Monte Carlo. Due to the complexity of posterior distributions in practical scenarios, analytical solutions are often infeasible. Markov Chain Monte Carlo (MCMC) methods are widely used to approximate the posterior distribution and calculate upper limits. MCMC methods generate a large number of samples from the posterior distribution, which can be used to estimate integrals and credible intervals.

The steps to do so are

1. Sampling, in which we use an MCMC algorithm (e.g., Metropolis-Hastings or Gibbs Sampling) to generate samples from the posterior distribution. These samples represent different possible values of μ given the observed data.[32]

2. Estimation in which we analyze the MCMC samples to compute the upper limit. For instance, rank the samples and find the value of μ below which 95% of the samples lie.

In the case that is presented at figure **??** we consider a particle physics experiment where we need to set an upper limit on a signal with a mass hypothesis of $m_\alpha = 60\ GeV$. Suppose we observe a data set with no significant signal. The Bayesian approach involves:

- Defining the Prior: Assume a prior distribution $\pi(\mu)$ for the signal yield μ. This could be a flat prior (uniform distribution) or a more informative prior based on previous knowledge.

- Likelihood Function: Construct the likelihood function $p(x \mid \mu)$ incorporating the signal and background contributions.

- Computing the Posterior: Use Bayes' theorem to obtain the posterior distribution $p(\mu \mid x)$.

- Finding the Upper Limit: Using MCMC samples from the posterior, determine μ_{up} by finding the value where the cumulative probability up to μ_{up} is 95% *or* 86% (or other chosen level).

So for example if $m_\alpha = 60\ GeV$, fter running MCMC simulations, let's assume the 95% upper limit is found to be $\mu_{up} = n$ events. This result implies that, given the observed data and prior information, there is a 95% probability that the true signal yield is less than or equal to n events.
In conclusion Bayesian methods provide a comprehensive approach to setting upper limits in particle physics experiments. By combining prior knowledge with experimental data and accounting for systematic uncertainties, Bayesian analysis is estimating quite precise upper limits. The use of MCMC techniques allows for practical implementation, even when analytical solutions are challenging. This methodology enhances our understanding of potential new phenomena and contributes to more accurate interpretations of experimental results.[32]

5.6 Results

The analysis results are shown at figure 5.30 bellow. The diagram we have the points of the BR, of the signal. These points are for 95% confidence level and 86%. At the table we can see

the points.

Several background processes were considered and their kinematics were analyzed, in muons

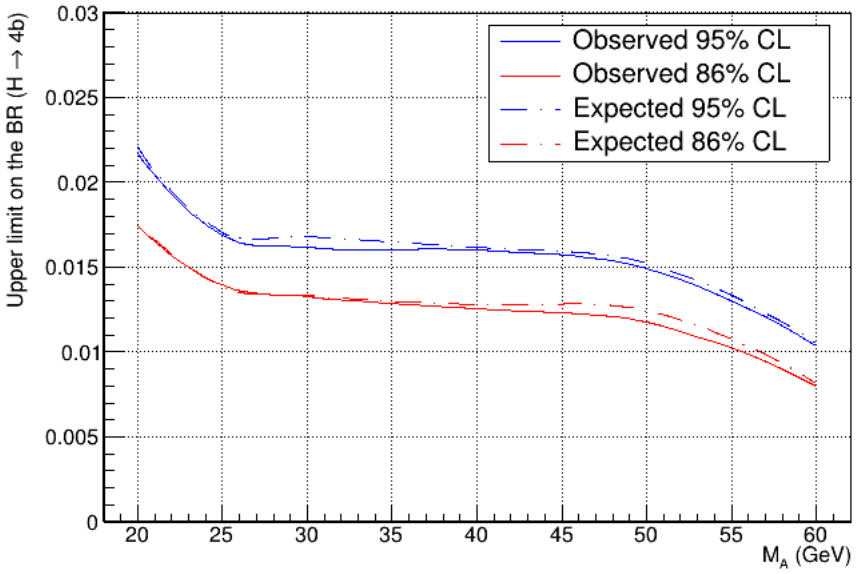

FIGURE 5.30: Upper limit on the $BR(h \rightarrow aa \rightarrow 4b)$ at 95% CL (blue) and 86% CL (orange) for the six masses hypotheses for the α boson.

signal m_α GeV	Observed 95%	Expected 95%	Observed 86%	Expected 86%
20	0.0217	0.0220	0.0174	0.0177
25	0.0169	0.0171	0.0140	0.0139
30	0.0161	0.0168	0.0132	0.0133
40	0.0160	0.0162	0.0126	0.0128
50	0.0148	0.0152	0.0117	0.0124
60	0.0103	0.0105	0.008	0.008

TABLE 5.6: The exact values of branching ratio in each mass.

and electrons the momentum has a cut on 20 GeV as seen at figures 5.6-5.7. In jet kinematics the momentum, pseudorapidity, and azimuthal angle distributions for the leading jet, second reconstructed jet, and third reconstructed jet are shown in figures 5.8-5.9-5.10 respectively. The analysis also included examining the fourth jet if it exists, with a corresponding figure showing fewer entries due to its rarity compared to the other three reconstructed jets as seen in figure 5.11.

Various kinematic variables and b-tag discriminators were used for training the BDT. The importance of each variable is ranked, with the most significant variable being the mass of the Higgs, followed by the distance between b-jets and the b-tag scores of the jets as seen in table 5.5.

The BDT score is used as the main fitting variable to simplify the analysis. Figure 5.22 shows

the BDT response for all backgrounds and a signal mass of $m_\alpha = 60\ GeV$. The signal distribution is scaled for visibility . The ROC curves in figure 5.24 demonstrate the effectiveness of the BDT in discriminating between signal and background.
To extract the signal, Maximum likelihood fits were performed to extract the signal from the data. Two hypotheses were tested:

- Zero Hypothesis (H_0): Only background processes exist, described by the Standard Model (SM).
- Alternative Hypothesis (H_1): Additional Beyond Standard Model (BSM) phenomena exist, implying the presence of signal plus background.

Monte Carlo (MC) toy simulations were used to generate data and fit models to test these hypotheses. The fits were performed using pseudo-random numbers from theoretical distributions to ensure consistency and reduce statistical fluctuations.
Figure 5.29 in the thesis presents the critical branching ratios for six different hypotheses for the α boson mass. The figure shows the upper limits of the branching ratio (BR) at 95% and 86% confidence levels for various α boson masses ranging from 20 GeV to 60 GeV.
The key points are three

1. The BR represents the fraction of the total number of Higgs decays that result in a particular final state. In this context, the BRs are for the decay of the Higgs boson into four b-quarks mediated by a hypothetical α boson.
2. The mass hypotheses, the figure includes six different mass hypotheses for the α boson: 20 GeV, 25 GeV, 30 GeV, 40 GeV, 50 GeV, and 60 GeV.
3. Confidence Levels that where
    - 95%
    - 86%

We observed a trend with mass. The upper limits of the BRs generally decrease as the mass of the α boson increases. And the implications are Constraints on New Physics, which means that the results impose stringent limits on the existence of the α boson. Specifically, if the α boson exists, its branching ratio for decaying into four b-quarks must be below the upper limits presented.
Figure 5.29 effectively summarizes the constraints on the branching ratios for different α boson masses. The decreasing trend of the upper limits with increasing mass, and the distinction between the 95% and 86% confidence levels, highlight the thoroughness of the analysis and the confidence of the constraints placed on potential new physics phenomena.

In conclusion the analysis successfully set upper limits for the signal yield using Bayesian methods and the Markov Chain Monte Carlo (MCMC) algorithm. The multivariate techniques, particularly the BDT, proved effective in distinguishing between signal and background, allowing for precise upper limit estimation on the signal yield at different mass hypotheses.
This study enhances our understanding of potential new phenomena in particle physics and contributes to the accurate interpretation of experimental results in the search for exotic Higgs decays.

Chapter 6

Conclusions

The analysis that we did in that paper was focused on an exotic Higgs decay that was $h \to 4b$. The main goal was to determine if there is evidence of BSM on this decay process. The key aspects of this analysis are

1. **Branching Ratio:** This analysis conducted calculations for 6 different hypotheses of an α boson and found the upper limit for each one using the Markov chain Monte Carlo calculator.

2. **Bayesian Methods:** Upper limits to the signal yield were calculated using Bayesian methods, as said we used the Markov Chain Monte Carlo algorithm. This approach allowed for the estimation of the posterior distributions for different masses, that aimed to see if the signal present and its significance.

3. **Signal and Background Separation:** The use of machine learning techniques, specifically the Boosted Decision Trees (BDT) method, proved effective in distinguishing between signal and background processes. The analysis demonstrated good separation capabilities, with the BDT response showing clear discrimination between the two.

4. **Monte Carlo Simulations:** The usage of Monte Carlo simulations helped in seeing the statistical behavior of the data. The toy Monte Carlo studies, with a large number of toys, ensured that statistical fluctuations were minimized.

5. **Likelihood Fits:** Maximum likelihood fits to the data were performed, comparing the zero hypothesis (only Standard Model processes) and the alternative hypothesis (BSM processes). This comparison helped in identifying any deviations that might suggest the presence of new physics.

6. **Confidence Levels:** The analysis provided results at different confidence levels (95% and 86%), so that we know if seeing the signal is possible.

In summary, this paper concluded that while the methods and analyses employed were robust, no evidence of BSM physics was observed in the $h \to 4b$ decay channel within the analyzed data. Further studies with more data and refined techniques are recommended to continue the search for new physics.

Appendix A

Appendix

A.1 Charged particle in a magnetic field

A charged particle traversing a magnetic field ($\mathbf{B}$) experiences a lateral force that is proportional to the magnetic field's strength, the velocity component orthogonal to the field, and the particle's charge. This force, known as the Lorentz force, is given by:

$$\mathbf{F} = q(\mathbf{v} \times \mathbf{B}) \tag{A.1}$$

Considering $\mathbf{v} = \mathbf{v}_\perp + \mathbf{v}_\parallel$ (with respect to ($\mathbf{B}$):

$$\mathbf{F} = q\left((\mathbf{v}_\perp + \mathbf{v}_\parallel) \times \mathbf{B}\right) \tag{A.2}$$

Thus:

$$\mathbf{F} = q(\mathbf{v}_\perp \times \mathbf{B}) \tag{A.3}$$

The Lorentz force is always orthogonal to both the particle's velocity and the magnetic field. When a charged particle moves in a static magnetic field, it traces a helical trajectory where the helix's axis is aligned with the magnetic field, and the particle's speed remains constant.

Taking:

$$\mathbf{F} = \frac{m\mathbf{v}_\perp^2}{R} \tag{A.4}$$

where R is the curvature radius in the plane orthogonal to the magnetic field, from equation A.3 we get:

$$\frac{m\mathbf{v}_\perp^2}{R} = q\mathbf{v}_\perp \cdot \mathbf{B} \tag{A.5}$$

Hence:

$$m\mathbf{v}_\perp = qR\mathbf{B} \tag{A.6}$$

Thus, the expression for transverse momentum is:

$$P_{\perp} = qR\mathbf{B} \tag{A.7}$$

The transverse momentum $P_{\perp}$ of a particle produced in this manner is conserved, making it a critical parameter. Although this derivation uses classical mechanics, the equation holds under relativistic conditions as well.

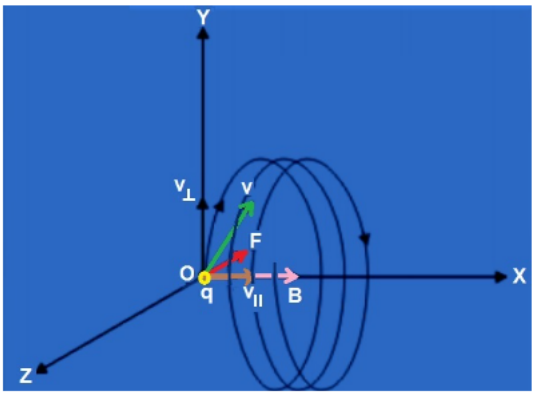

FIGURE A.1: Helical path of a charged particle in a magnetic field.

A.2 Higgs Sectors

After the Higgs boson was discovered, experimental groups at CERN intensified their search for new scalar particles, which in turn spurred further investigation into extensions of the SM. In addition to supersymmetric models, the simplest extensions of the SM's scalar sector offer an excellent framework for interpreting many searches and for inspiring new ones.[33]
It is unclear if electroweak radiative corrections significantly impact a model's phenomenology. If future measurements of the 125 GeV Higgs couplings align more precisely with SM predictions, these models will increasingly resemble their SM-like limit, making them very similar as demonstrated in this work. Only with the discovery of a new scalar can we begin to probe the various new model possibilities. In such a case, certain models exhibit highly interesting properties unique to specific scenarios.[33]
In this section, we discuss various models where the only change to the Standard Model (SM) is adding more Higgs particles.
Adding extra Higgs particles to the SM can help achieve coupling constant unification, where different force strengths become equal at high energies. For this to work naturally (with $\rho = 1$), the neutral fields of the new Higgs particles must have zero vacuum expectation value (vev). However, this method requires a lower unification scale (MU), which can be problematic for proton decay. But, if the unification doesn't involve extra gauge bosons (X and Y). The best

solution involves having two specific Higgs representations: two doublets and one triplet.[34] Complex Higgs sectors can even achieve unification at very low MU values, suitable for large extra-dimension models. Another reason to have two or more Higgs doublets is to allow for CP violation (differences between matter and antimatter) in the Higgs sector. However, with multiple Higgs doublets, the number of Higgs potential parameters increases, which must be carefully controlled to ensure all Higgs bosons have positive mass-squared values and avoid breaking electromagnetism.[34]

There are numerous well-founded possibilities for the Higgs sector that go beyond the single-doublet sector of the SM. This wide range of possibilities means that thoroughly exploring the Higgs sector could be very challenging. The diversity of models, potential unexpected decay modes [1], overlapping resonances, shared WW and ZZ coupling strengths, CP violation, the influence of extra dimensions, and Higgs-radion mixing, all underscore the need for detailed multi-channel, multi-collider analysis.

Specifically, it is important to recognize that the Higgs sector has enough complexity that discovering the Higgs at the Tevatron or LHC is not guaranteed. Even at the Linear Collider, detecting and studying the Higgs could be difficult, particularly in scenarios like general Two-Higgs-Doublet Model (2HDM), where the mass of the h_0 can be as large as 800 to $900\ GeV$ [34] without conflicting with precision electroweak data or perturbative constraints. The LHC collaborations must continually improve and explore every possible signature, and the LC design must aim for the highest achievable energy within financial and technological constraints. Additionally, research into the feasibility of a muon collider μC should continue.

The LHC's ability to demonstrate that the WW sector is perturbative could be very beneficial. Two specific examples illustrate this. First, in the Next-to-Minimal Supersymmetric Standard Model (NMSSM), it might be difficult to detect a Higgs boson using current analysis techniques, but a perturbative WW sector would suggest the existence of light CP-even Higgs bosons with significant WW coupling. This could motivate the development of new techniques to identify faint signatures. Second, consider a scenario with several heavy (around 800 to $900\ GeV$) mixed-CP Higgs bosons that share WW and ZZ coupling strengths, decay to lighter Higgs bosons (with small ZZ coupling), or produce overlapping resonance signals. In such a scenario, it would be challenging to guarantee the discovery of a Higgs boson at the LHC, LC, γC, or μC unless these machines can reach multi-TeV center-of-mass energies. The WW scattering processes at the LHC would show moderately perturbative behavior, and Giga-Z operation at the LC would confirm that the S and T values align with expectations for this scenario. These findings would indicate the need for higher center-of-mass energy at the LC to enable the production of CP-mixed Higgs boson pairs.[34]

In less extreme and more plausible scenarios where one or more Higgs bosons are relatively light, it is clear that experimentation at both the LC and the LHC is necessary to have a high

[1] such as Higgs pairs or supersymmetric (SUSY) particle

probability of discovering even one Higgs boson. Almost certainly, both machines will be required to fully study the Higgs sector. Strong motivations for the LC, γC, and μC include several factors. The LC might be essential for the NMSSM and would be necessary to detect a continuum of strongly mixed CP-even Higgs bosons. Observing the heavy H0 and A0 of the Minimal Supersymmetric Standard Model (MSSM) will require $\gamma\gamma$ collisions if the parameters [mA0, $\tan\beta$] fall within the "wedge" region. Once observed, the properties and rates of the H0 and A0 will greatly assist in determining crucial SUSY parameters, especially checking the predicted relation between their Yukawa couplings and $\tan\beta$. Exotic Higgs representations, such as the triplet motivated by the seesaw approach to neutrino masses and the Left-Right Symmetric Supersymmetric Model (LRSSM) solutions to the strong and SUSY CP problems, will result in unique collider signals that might be best explored via e^-e^- and/or $\mu^-\mu^-$ collisions. Finally, it is crucial to understand how important a γC (and eventually μC) could be for directly measuring the CP composition of a Higgs boson, particularly one with a significant CP-odd component.[34]

A.3 Proton Oscillation

Proton-proton collisions are studied at the LHC, in order to do so, LHC is equipped with magnets to manage their course. These magnets are dipole ones, so that the path is closed and circular and quadrupole ones to help with the protons beam focus[2] [1].
Protons are traveling inside the accelerator with speeds that are over 99% of the speed of light. This movement can make them "derail" [3], so to re-centralize it we use the quadrupoles. These derails are a form of oscillation [4] that is called Betatron Oscillation [1]. In the meanwhile as proton oscillates, its position is described by the displacement from the path and the angle of it [1] and we will write it as x.
Because of the oscillation we know that

$$\sum m_p\alpha = -kx \tag{A.8}$$

which describes the force (Newton's second law) of simple harmonic oscillation. If we take the oscillation constant and divide it with mass we make a new constant $K = \frac{k}{m_p}$ and take into account that acceleration is $\alpha = \frac{d^2x}{dt^2}$ then A.8 will be the differencial equation

$$\frac{d^2x}{dt^2} + Kx = 0. \tag{A.9}$$

[2] these magnets are used in the antimatter factory but this is not the subect of that thesis
[3] if we think of protons as little trains inside the tracks that is LHC
[4] proton loses the course to the right, the quadrupole magnet sifts it to the left, making it do to the left, with this procedure proton oscillates around the path

So the solutions must be

$$x = A\cos(\omega t + \phi) \tag{A.10}$$

where $\omega = \sqrt{K}$, A is oscillation's width, t is the time variable and ϕ is the phase that defines protons initial position and speed.
We also know that the velocity of the oscillation is $u = x' = \frac{dx}{dt}$ and so it will be

$$u = x' = \frac{dx}{dt} = -A\omega\sin(\omega t + \phi) \tag{A.11}$$

this speed shouldn't confuse us the lognitufal speed that is $v = \frac{distance}{time} = \frac{s}{t}$ assuming that proton is too small for the curvature of the LHC and that it has a constant velocity in very small parts, after all its boosts. So $t = \frac{s}{v}$

$$dt = \frac{ds}{v} \text{ and } \frac{dx}{dt} = v\frac{dx}{ds} \tag{A.12}$$

and the solutions are

$$x = A\cos(\frac{\omega}{v}s + \phi) \tag{A.13}$$

and

$$u = x' = \frac{dx}{dt} = -\frac{A}{v}\omega\sin(\frac{\omega}{v} + \phi). \tag{A.14}$$

Now lets try to plot the relation between x and u.

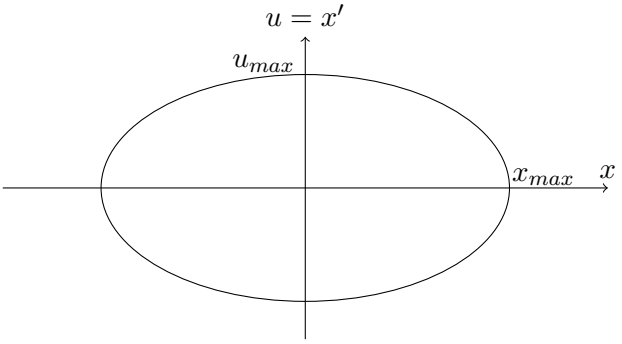

The above was a reference on one proton, but the LHC consists a great number of them [1]. These protons have different widths, phases and focus [5], so the above plot must take a more realistic turn.
To achieve that we need to make K a dynamic variable that is a function of LHC's length (s). So lets take the A.9 and put the function $K(s)$ inside

$$\frac{d^2x}{dt^2} + K(s)x = 0 \tag{A.15}$$

[5] outside the magnetic field of quaduple magnet there is no oscillation $K = 0$, and inside the LHC, K is not homogeneous [1]

and we know that $K(s)$ is the oscillating force's reset variable, and s is a dynamic variable. A.15 is Hills equation [1]. In order to solve that differential equation we must make some new parameters. These will be:

1. ϵ, is transversal emmitance [1]
2. $\beta(s)$, is the amplitude modulation [1]
3. $\psi(s)$, is the phase advance [1]

So the solution of the differential equlation is

$$x = \sqrt{\epsilon\beta(s)}\cos\left(\Psi(s) + \phi\right). \tag{A.16}$$

All these parameters are depending on the initial conditions [1]. $\Psi(s)$ is the rate that the phase is changing as it is clear on A.16 and in the theory of Betatron Oscillation it is known that [1]

$$\frac{d\Psi(s)}{ds} \sim \frac{1}{\beta(s)}. \tag{A.17}$$

So from A.16 and A.17 we take

$$u = x' = \frac{dx}{dt} = -\sqrt{\frac{\epsilon}{\beta(s)}}\sin\left(\Psi(s) + \phi\right) \tag{A.18}$$

And we plot again the phase space, so we get

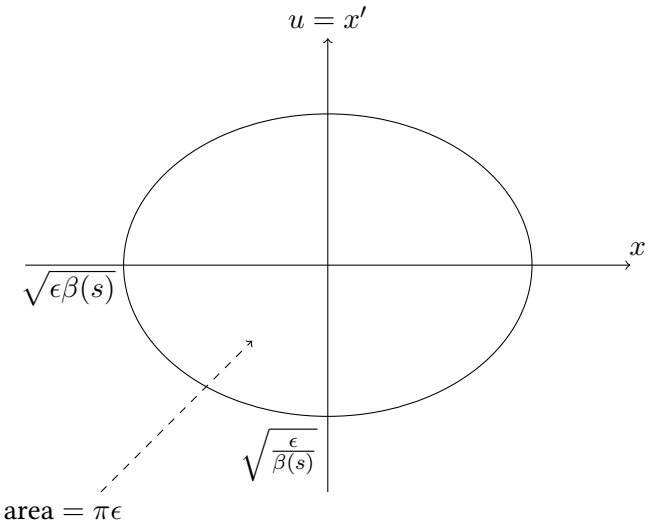

as we can see ϵ is a constant[6], and β is a function of s. If one could see all protons in one turn the plot would look more like this

[6] so the area stays the same along LHC

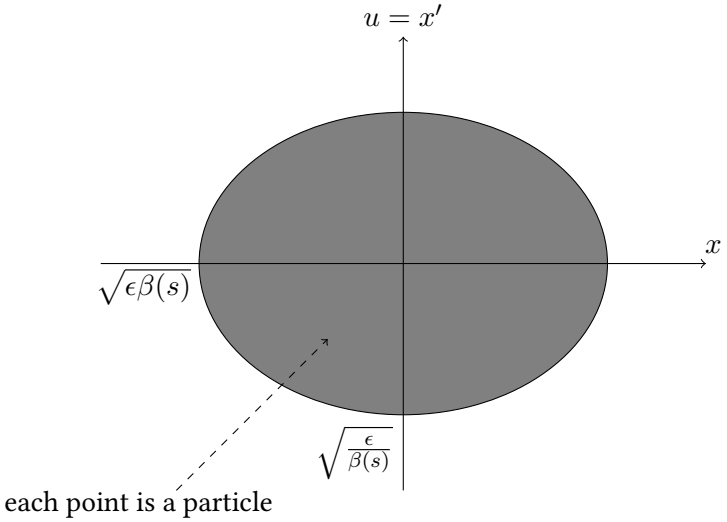

and from the above one can see that emmitance is the area of the eclipse.[1][7] The x axis has the transverse size of the protons.
The bunch cross section is the square of the beam dimension which is $2\sqrt{\epsilon\beta}$ and so[1]

$$\text{cross section} = 4\epsilon\beta \tag{A.19}$$

and its average is

$$\text{cross section} = 4\pi\sigma^2 \tag{A.20}$$

and after dividing A.19 with A.20 we got

$$1 = \frac{\cancel{4}\epsilon\beta}{\cancel{4}\pi\sigma^2} \Rightarrow \beta = \frac{\pi\sigma^2}{\epsilon}. \tag{A.21}$$

as it becomes clear this value should be the smaller it can be so the proton beam would be as focused as it can.
In addition to that beam movement, there is the longitudinal oscillation of the proton beam. This generates an oscillating voltage[1] that accelerates the proton, which cancels out as it travels in the collider.[8]
If a proton has the same oscillating frequency as the RF then we call it a synchronous proton. And because there are not single protons, the ones that are oscillating[9] around the synchronised one are called a bunch and their oscillation is the synchotron ones.[1]

[7] 12% emmitance is 12% of the cycle area
[8] these are called RF Cavities [1]
[9] longitudinally

A.4 Extended Detector Simulation

In high energy physics, colliders are tools that help us see what is happening in the microcosm. These devises need very sophisticated actions throughout all their life cycle. To do so we run a series of simulations, that make the level of detail higher by the time, which makes sense as every run on a collider generates more data.[35]
The first is the simulation of the particles with the highest energy, which is called fast simulation. In these kind of simulations we got only particles form the initial interaction, with simplified condition, so that we can generate the signal. The next simulation step is a more detailed one, the secondary particles that make up a hole new generations. With these tools, one can estimate correlations and measures on the detector.[35]
From the above, we can see that simulations are hunting the most detailed alternative reality for a collider, but there is only so much detail one can achieve without before the computational cost becomes too high. Bellow we will analyse the stages and the types of simulation ran today at LHC, with some frameworks that do it efficiently.[35]
Lets start by the stages, firstly the event is generated and simulates the initial reaction that will break into other particles that live for a short period of time, the simulation itself produces the primary tracks. The second stage is the simulation of the detection procedure, it tracks the initial particles that pass the detector, then it samples the interactions and creates secondary particles. Third stage, the simulation is looking for the hits and then estimates the signals.[35]
The most known simulation tools are

1. Detector Monte Carlo: Geant, Fluka, Geant4[35]
2. Radiation related MC: Fluka, Marks, MCNP/MCNPX[35]
3. Signal generation: Garfield[35]

A.5 Extended Background and Signal Event Tables

Background	N_{exp}^{cut1}	N_{exp}^{cut2}	N_{exp}^{cut3}	N_{exp}^{cut4}
$t\bar{t}$ Semileptonic	4.8×10^6	1.5×10^6	53948.5	32155.3
$t\bar{t}$ Dileptonic	1.2×10^6	516417	12458	8831.38
$t\bar{t}$ Hadronic	4.9×10^6	5379.65	2818	950
$W \to l\nu 70to100$	6.8×10^7	2.9×10^6	244.2	177.1
$W \to l\nu 100to200$	6.8×10^7	3.3×10^6	1517.2	701.1
$W \to l\nu 200to400$	1.8×10^7	1.2×10^7	5677.3	891.6
$W \to l\nu 400to600$	1.4×10^6	630169	599.2	364.3
$W \to l\nu 600to800$	605091	170273	213.108	139.4
$W \to l\nu 800to1200$	276233	81896.7	125.5	77.1
$W \to l\nu 1200to2500$	66735.7	20458.5	33.9	22.1
$QCD \to 80to170$	1.6×10^9	425887	3360.45	988.367
$QCD \to 170to250$	1.1×10^8	39843.8	466.529	199.941
$QCD \to 250to\infty$	3×10^7	12037.4	236.433	118.217

Table A.1: Number of expected events after each cut

α boson mass	Number of entries	Number of entries that survived	$N_{expected}$
12 GeV	954307	2357	27.2
15 GeV	938473	3160	37.0
20 GeV	958544	11851	136.1
25 GeV	934997	20998	247.0
30 GeV	934620	253140	297.9
40 GeV	955544	27714	318.9
50 GeV	938351	26779	313.9
60 GeV	953909	28097	323.9

Table A.2: Number of signal events expected after all selection criteria

A.6 Posterior Distributions

In this section we will present the posterior distribution for each α boson mass i.e. $m_\alpha = [20,\ 25,\ 30,\ 40,\ 50,\ 60]\ GeV$. The $m_\alpha = 60\ GeV$ is presented in figure 5.29

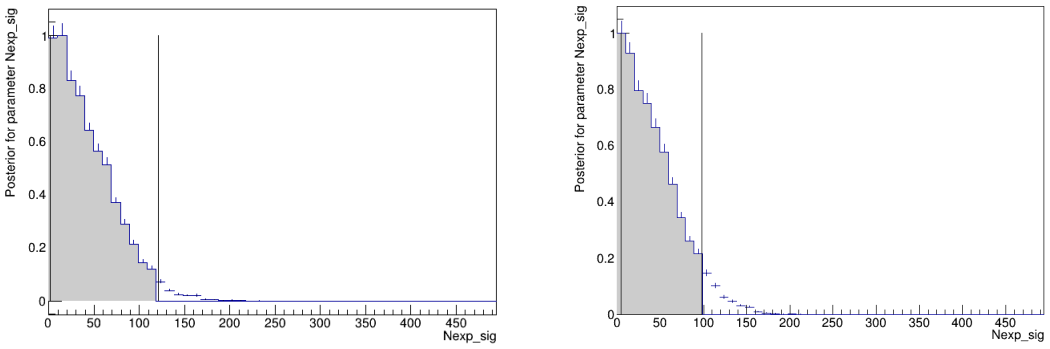

FIGURE A.2: Posterior distribution for 95% confidence level on the left and 86% confidence level on the right for mass $m_\alpha = 25\ GeV$.

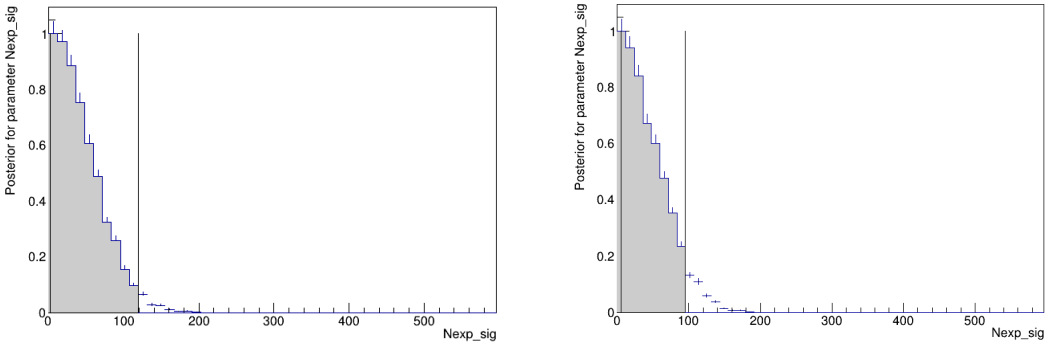

FIGURE A.3: Posterior distribution for 95% confidence level on the left and 86% confidence level on the right for mass $m_\alpha = 30\ GeV$.

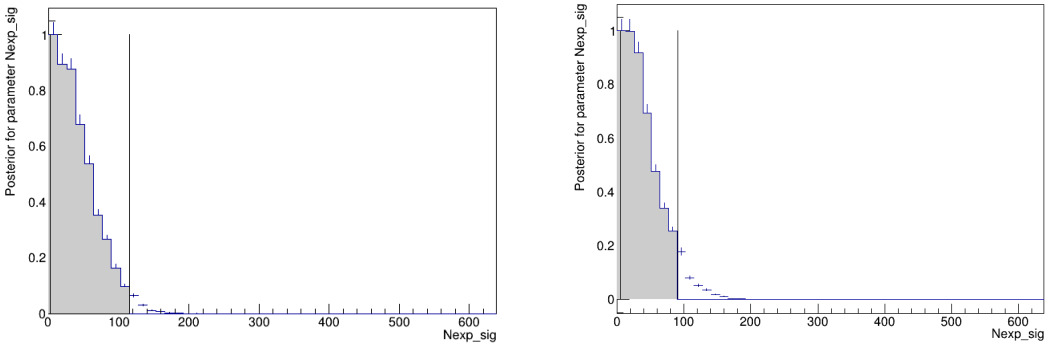

FIGURE A.4: Posterior distribution for 95% confidence level on the left and 86% confidence level on the right for mass $m_\alpha = 40\ GeV$.

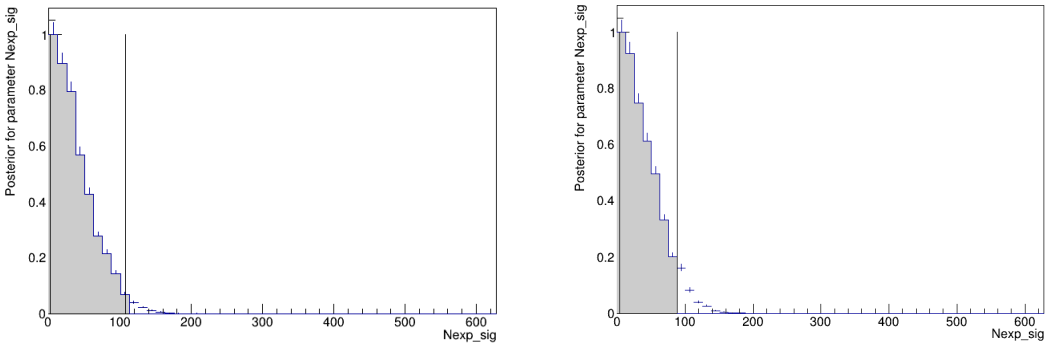

FIGURE A.5: Posterior distribution for 95% confidence level on the left and 86% confidence level on the right for mass $m_\alpha = 50\ GeV$.

A.7 Two Body Decay

To explain the results on the branching ratio, one must analyse the kinematics of the Higgs boson decaying into two α particles and then each one of them decaying to two b-quarks. Lets start by the first two body decay, that is $H \to \alpha\alpha$.

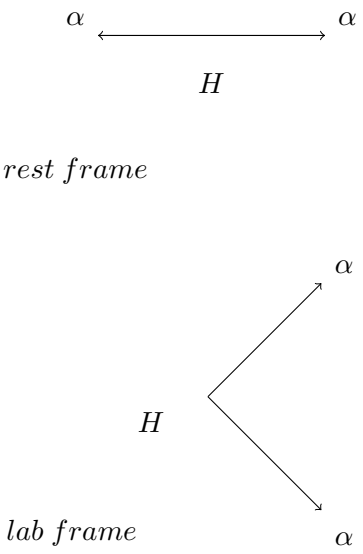

These α bosons will have masses that are smaller than half of the Higgs one, in our case masses are $m_\alpha = [12,\ 15,\ 20,\ 25,\ 30,\ 40,\ 50,\ 60]\ GeV$. Then we proceed on the second two body decay that is the α boson decaying to two b-quarks.

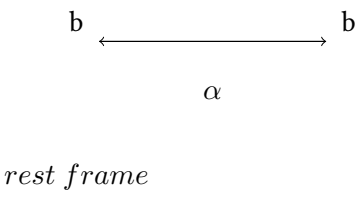

In the lab frame we know that $p^2 = m^2$, $p_x^2 = (p_1 + p_2)^2$ and $m_x^2 = p_1^2 + p_2^2 + 2p_1p_2$. After combining these we get

$$m_x^2 = m_1^2 + m_2^2 + 2|p_1||p_2| \cos\theta_{12}, \tag{A.22}$$

where $\cos\theta_{12}$ is the angle between b-quarks in the lab frame. Taking into account that the decay has a final state of two b-quarks and so $m_1 = m_2 = m$, while $m_x^2 = \sum(E^2 - |\vec{p}|^2)$, equation A.22 will be

$$m_x^2 \simeq 2E_1E_2(1 - \cos\theta). \tag{A.23}$$

Equation A.23 shows that the bigger the mass, the smaller the angle of the two outgoing b-quarks. That is the reason we did not include masses $m_\alpha = [12,\ 15]\ GeV$ because the angle is so small, we cannot impose the same strategy.

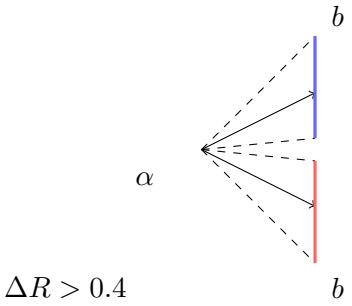

$\Delta R > 0.4$

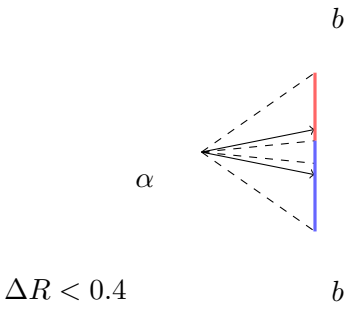

$\Delta R < 0.4$

Bibliography

[1] Ramon Cid Manzano Xabier Cid Vidal. Taking a closer look at lhc. Technical report, CERN. URL https://www.lhc-closer.es/takingacloserlookatlhc/1.home.

[2] CMS. *Compact Muon Solenoid.* URL https://cms.cern/.

[3] The CMS Collaboration. The cms experiment at the cern lhc. *Journal of Instrumentation*, 3(08):S08004, aug 2008. doi: 10.1088/1748-0221/3/08/S08004. URL https://dx.doi.org/10.1088/1748-0221/3/08/S08004.

[4] Wikipedia contributors. Proton — Wikipedia, the free encyclopedia, 2024. URL https://en.wikipedia.org/w/index.php?title=Proton&oldid=1229230406. [Online; accessed 28-June-2024].

[5] J M Campbell, J W Huston, and W J Stirling. Hard interactions of quarks and gluons: a primer for lhc physics. *Reports on Progress in Physics*, 70(1):89–193, December 2006. ISSN 1361-6633. doi: 10.1088/0034-4885/70/1/r02. URL http://dx.doi.org/10.1088/0034-4885/70/1/R02.

[6] Shyam Kumar. From detector simulation to data analysis in high energy physics experiments. In Rajendra Nath Patra, editor, *Advanced Radiation Detector and Instrumentation in Nuclear and Particle Physics*, pages 21–30, Cham, 2023. Springer International Publishing. ISBN 978-3-031-19268-5.

[7] Roberto Franceschini, Doojin Kim, Kyoungchul Kong, Konstantin T. Matchev, Myeonghun Park, and Prasanth Shyamsundar. Kinematic variables and feature engineering for particle phenomenology, 2022. URL https://arxiv.org/abs/2206.13431.

[8] Curtin, David and Essig, Rouven and Gori, Stefania and Jaiswal, Prerit and Katz, Andrey and Liu, Tao and Liu, Zhen and McKeen, David and Shelton, Jessie and Strassler, Matthew and Surujon, Ze'ev and Tweedie, Brock and Zhong, Yi-Ming. Exotic decays of the 125 gev higgs boson. *Phys. Rev. D*, 90:075004, Oct 2014. doi: 10.1103/PhysRevD.90.075004. URL https://link.aps.org/doi/10.1103/PhysRevD.90.075004.

[9] Andreas Hocker et al. TMVA - Toolkit for Multivariate Data Analysis. 3 2007.

[10] S. N. Mukherjee T.Morii, C. S. Lim. *The Physics of the Stendard Model and Beyond.* World Scientific, 2004.

[11] The CMS Collaboration. Search for light bosons in decays of the 125 GeV Higgs boson in proton-proton collisions at $\sqrt{s} = 8$ TeV. *Journal of High Energy Physics*, 2017(10), oct 2017. ISSN 1029-8479. doi: 10.1007/jhep10(2017)076. URL http://dx.doi.org/10.1007/JHEP10(2017)076.

[12] Alessandro Bettini. *Introduction to Elementary Particle Physics.* 2014. URL https://www.cambridge.org/highereducation/books/introduction-to-elementary-particle-physics/FB6ACD05BFC363374B3B74B920F45819#overview.

[13] Herwig Schopper. *Particle Physics Reference Library.* Springer Open, 2020. URL https://link.springer.com/chapter/10.1007/978-3-030-38207-03.

[14] Kien Nguyen. The higgs mechanism. *Arnold Sommerfeld Center For Theoretical Physics*, 2009.

[15] CMS Colaboration. Search for an exotic decay of the higgs boson to a pair of light pseudoscalars in the final state with two muons and two b quarks in pp collisions at 13 tev. *Physics Letters B*, 795:398–423, 2019. ISSN 0370-2693. doi: https://doi.org/10.1016/j.physletb.2019.06.021. URL https://www.sciencedirect.com/science/article/pii/S0370269319303995.

[16] Federica Primavera. Searches for exotic and rare higgs decays in cms. *EPJ Web of Conferences*, 60:12016–, 11 2013. doi: 10.1051/epjconf/20136012016.

[17] Tejinder S. Virdee. Detectors at lhc. *Physics Reports*, 403-404:401–434, 2004. ISSN 0370-1573. doi: https://doi.org/10.1016/j.physrep.2004.08.026. URL https://www.sciencedirect.com/science/article/pii/S0370157304003370.

[18] Wikipedia contributors. Luminosity (scattering theory) — Wikipedia, the free encyclopedia, 2023. URL https://en.wikipedia.org/w/index.php?title=Luminosity(scatteringtheory)&oldid=1161302723. [Online; accessed 29-June-2024].

[19] Wikipedia contributors. Underlying event — Wikipedia, the free encyclopedia, 2023. URL https://en.wikipedia.org/w/index.php?title=Underlying event&oldid=1166766034. [Online; accessed 29-June-2024].

[20] Zachary Marshall and the ATLAS Collaboration. Simulation of pile-up in the atlas experiment. *Journal of Physics: Conference Series*, 513(2):022024, jun 2014. doi: 10.1088/1742-6596/513/2/022024. URL https://dx.doi.org/10.1088/1742-6596/513/2/022024.

[21] ATLAS Collaboration. Luminosity determination in pp collisions at $\sqrt{s}$ = 8 TeV using the ATLAS detector at the LHC. *Springer Link*, 2016. URL https://doi.org/10.1140/epjc/s10052-016-4466-1.

[22] Wikipedia contributors. Jet (particle physics) — Wikipedia, the free encyclopedia, 2024. URL https://en.wikipedia.org/w/index.php?title=Jet(particlephysics)&oldid=1222946622. [Online; accessed 30-June-2024].

[23] S.D. Ellis, J. Huston, K. Hatakeyama, P. Loch, and M. Tönnesmann. Jets in hadron–hadron collisions. *Progress in Particle and Nuclear Physics*, 60(2):484–551, 2008. ISSN 0146-6410. doi: https://doi.org/10.1016/j.ppnp.2007.12.002. URL https://www.sciencedirect.com/science/article/pii/S0146641007000968.

[24] Cristina Ferro. B-tagging in cms. *EPJ Web of Conferences*, 28, 01 2012. doi: 10.1051/epjconf/20122812055.

[25] CMS Colaboration. Measurement of the differential cross sections for the associated production of a W boson and jets in proton-proton collisions at $\sqrt{(s)}$ = 13 TeV. *Physical Review D*, 96(7), October 2017. ISSN 2470-0029. doi: 10.1103/physrevd.96.072005. URL http://dx.doi.org/10.1103/PhysRevD.96.072005.

[26] Camille Beluffi. b jet identification in cms. *Nuclear and Particle Physics Proceedings*, 273-275:2491–2493, 2016. ISSN 2405-6014. doi: https://doi.org/10.1016/j.nuclphysbps.2015.09.435. URL https://www.sciencedirect.com/science/article/pii/S2405601415009244. 37th International Conference on High Energy Physics (ICHEP).

[27] CMS Colaboration. Search for the decay of the Higgs boson to a pair of light pseudoscalar bosons in the final state with four bottom quarks in proton-proton collisions at $\sqrt{s} = 13$ TeV. *Journal of High Energy Physics*, 2024(6), June 2024. ISSN 1029-8479. doi: 10.1007/jhep06(2024)097. URL http://dx.doi.org/10.1007/JHEP06(2024)097.

[28] Albertsson, Kim, An, Sitong, Gleyzer, Sergei, Moneta, Lorenzo, Niermann, Joana, Wunsch, Stefan, Zampieri, Luca, and Zapata Mesa, Omar Andres. Machine learning with root/tmva. *EPJ Web Conf.*, 245:06019, 2020. doi: 10.1051/epjconf/202024506019. URL https://doi.org/10.1051/epjconf/202024506019.

[29] Wikipedia contributors. Likelihood function — Wikipedia, the free encyclopedia, 2024. URL https://en.wikipedia.org/w/index.php?title=Likelihood function&oldid=1232415707. [Online; accessed 8-July-2024].

[30] Wikipedia contributors. Maximum likelihood estimation — Wikipedia, the free encyclopedia, 2024. URL https://en.wikipedia.org/w/index.php?title=Maximumlikelihoodestimation&oldid=1233238324. [Online; accessed 8-July-2024].

[31] Wouter Verkerke and David P. Kirkby. The RooFit toolkit for data modeling. *eConf*, C0303241:MOLT007, 2003.

[32] Particle Data Group and Workman. Review of Particle Physics. *Progress of Theoretical and Experimental Physics*, 2022(8):083C01, 08 2022. ISSN 2050-3911. doi: 10.1093/ptep/ptac097. URL https://doi.org/10.1093/ptep/ptac097.

[33] Rui Santos. Extended higgs sector beyond the mssm and the lhc, 2018. URL https://arxiv.org/abs/1809.00234.

[34] John F. Gunion. Extended higgs sectors, 2002. URL https://arxiv.org/abs/hep-ph/0212150.

[35] J. Apostolakis. *Detector Simulation*, pages 485–531. Springer International Publishing, Cham, 2020. ISBN 978-3-030-35318-6. doi: 10.1007/978-3-030-35318-6_11. URL https://doi.org/10.1007/978-3-030-35318-611.